Molecular analysis of plasmalemma vesicle-associated protein and its biological functions in the mammalian vascular endothelium

Dissertation

Zur Erlangung des Doktorgrades der Naturwissenschaften (Dr. rer. nat.)
der Fakultät der Biologie und Vorklinischen Medizin
der Universität Regensburg

Durchgeführt am Lehrstuhl für Embryologie und Humananatomie
der Universität Regensburg

vorgelegt von

Leonie Herrnberger

aus Cham

2014

Das Promotionsgesuch wurde eingereicht am: 18.02.2014

Die Arbeit wurde angeleitet von: Prof. Dr. Ernst R. Tamm

Unterschrift:

Für meine Familie und Christian

Manuscripts included in this thesis:

Herrnberger L, Seitz R, Kuespert S, Bösl MR, Fuchshofer R, Tamm ER. **Lack of endothelial diaphragms in fenestrae and caveolae of mutant *Plvap*-deficient mice**. Histochem Cell Biol. 2012, 138(5):709-724

Leonie Herrnberger, Kathrin Ebner, Benjamin Junglas, Ernst R. Tamm. **The role of plasmalemma vesicle-associated protein (PLVAP) in endothelial cells of Schlemm's canal and ocular capillaries**. Exp Eye Res. 2012, 105:27-33

Leonie Herrnberger, Robert Hennig, Werner Kremer, Claus Hellerbrand, Achim Göpferich, Hans Robert Kalbitzer, and Ernst R Tamm. **Pore formation in the endothelial wall of liver sinusoids depends on plasmalemma vesicle-associated protein (PLVAP) and is critically required for the passage of lipoproteins**. Submitted

Authors contribution:

The data submitted in this thesis are the results of my own investigation, unless stated otherwise. Experiments performed by other persons are noted in the figure legends.

_____

Leonie Herrnberger

Table of Content

Chapter 1

Chapter 2

Chapter 1

General Introduction

1 General introduction

In 1628, the English physician William Harvey published his seminal book, *Exercitatio Anatomica de Motu Cordis et Sanguinis in Animalibu*s. He could prove by a simple experiment that blood circulates throughout the body by a connected system of capillaries and is constantly pumped by the heart. His opus replaced the previous theory of the Greek physician Galen of Pergamon, who claimed that arterial blood originates in the heart and venous blood in the liver, from where it gets distributed to the rest of the body.
The functionality of the organism rests on the adequate supply of oxygen and nutrients to the different organs and parts of the body, assuming a constant flow and circulation of blood. Beyond that, the advanced understanding of blood flow, vasculature, and endothelial lining points at something far more complex than Harvey's theory.

The inner lining of blood vessels and lymphatics consists of a thin monolayer of polygonal flattened endothelial cells. In adults, the amount of endothelial cells is approximately 1 to 6 x 10^{13}. In summary they weigh 1 kg and have a total surface of 1 to 7 m^2 (Cines et al., 1998).
Endothelial cells exhibit a barrier between the blood flow and the surrounding tissue and play a crucial and active role in the maintenance of the vascular homeostasis. They regulate a variety of complex biological processes, such as hemostasis, blood coagulation, regulation of vascular smooth muscle tone, angiogenesis, immune response, and inflammatory processes including migration of leukocytes. Endothelial cell function requires the constant response to physical and chemical stimuli of circulating blood cells, and the release of a broad spectrum of paracrine and autocrine factors (Sumpio et al., 2002; Verma et al., 2003).
Another key function of vascular endothelial cells is the selective and bidirectional exchange of macromolecules, small molecules, and water between the luminal and abluminal side of capillaries (Verma et al., 2003). The size-specific selection is necessary to establish a protein gradient which is in turn essential for the maintenance of the fluid balance between blood and tissue, and depends on both the molecular radius of the transported molecules and the composition of the particular endothelial barrier (Mehta and Malik, 2006). One plasma protein turns out to be especially important in this process, namely albumin, given that this protein facilitates the co-transport of other hydrophobic molecules such as lipids and hormones across the endothelial wall due to its molecular structure and electric charge (Mehta and Malik, 2006). In general, different strategies arise for endothelial cells to accomplish such a specific transport of molecules.

1.1 Transport mechanisms across endothelial cells

1.1.1 Paracellular transport

The paracellular transport describes the passage of small molecules, water and ions between neighboring cells across the endothelial barrier (Figure 1). This restricted permeability is sustained by interendothelial junctions, such as tight junctions, gap junctions, and adherens junctions. Tight junctions and adherens junctions impede the uncontrolled penetration of large molecules by attaching neighboring cells, whereas gap junctions form paracellular channels which allow and facilitate the passage of small molecules, water and ions (Komarova and Malik, 2010).

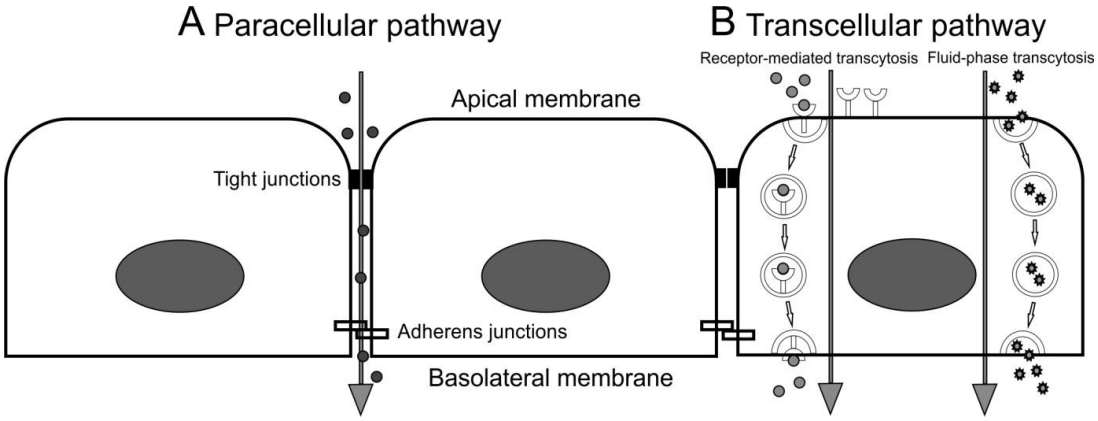

Figure 1: Paracellular and transcellular pathways to overcome the endothelial barrier. A, Small molecules, such as water and ions are transported via the paracellular route from the apical side to the basolateral side of the cell. Tight junctions and adherens junctions allow the passage of small molecules between neighboring cells. **B**, Transcellular transport involves membrane-bound vesicles which detach from the plasma membrane and transport molecules from the apical membrane to the basolateral side were they fuse again with the plasma membrane and release their cargo. This transport can be either by receptor-mediated transcytosis or by fluid-phase transcytosis.

1.1.2 Transcellular transport

The process of transcytosis was first described by Palade in the year 1950 during his studies on the permeability of blood capillaries. However, the term transcytosis was characterized by Simionescu in the year 1979 (Tuma and Hubbard, 2003). Transcytosis is defined by the process of transporting albumin from the luminal side of a capillary to the subendothelial

space (Minshall et al., 2002; Tuma and Hubbard, 2003). As already mentioned, besides albumin, other macromolecules such as albumin-binding ligands, insulin, lipids, and hormones are transported via transcytosis (Frank et al., 2003a; Minshall et al., 2002). Soluble plasma molecules can be taken up together with blood plasma, a process called fluid-phase transcytosis, or by receptor-mediated transcytosis which requires a specific binding of the molecule to a membrane-bound receptor (Tuma and Hubbard, 2003) (Figure 1). Transcytosis is an energy-dependent transport which takes place by means of membrane-bound vesicles. To transport molecules within the cell, they need to get internalized at the plasma membrane. Specialized cells, commonly referred to as phagocytes, such as macrophages, monocytes, neutrophils, and dendritic cells can internalize substances via phagocytosis, an important mechanism in terms of defense against infectious agents (i.e. bacteria and viruses). However, in most cell types the main mechanism to internalize molecules is via endocytosis. Endocytosis is defined as the process in which molecules get engulfed in coated vesicles that are formed at the plasma membrane. So far, there are three different types of coated vesicles, the Clathrin-coated, the CopI-coated, and the CopII-coated vesicles. Among those, Clathrin-coated vesicles are the best studied type so far. After formation at the plasma membrane, the vesicles detach from the membrane along with the engulfed molecules. Shortly after detaching, the clathrin-covering gets discarded and the transport vesicles migrate to their target compartment and fuse with the membrane. First they reach the early endosome than the late endosome and finally the lysosome.
Lately, the spotlight has been put on a clathrin-independent mechanism as well, namely the caveolae-mediated endocytosis (Pelkmans and Helenius, 2002).

1.1.2.1 Caveolae

In turn, the pioneering work was done by Palade and Yamada. During his observations of semithin sections from continuous lung endothelia, Palade discovered the existence of cell invaginations with a "cave-like" morphology in the early 1950s. The "cave-like" appearance gave this newly discovered cellular structure the name caveolae.
Caveolae are spherical, omega-shaped cell invaginations of the plasma membrane with a mean diameter of 50-80 nm (Figure 2A and B). They are also called non-coated or smooth-coated plasmalemmal invaginations, because they lack a cytoplasmic coat which is a typical feature of clathrin-coated pits (Gumbleton et al., 2000). Caveolae are thought to arise from lipid rafts, areas at the plasma membrane which are rich in cholesterin, glycosphingolipids, and GPI-anchoring proteins. Caveolae are very common and appear in many highly

differentiated mammalian cell types with some exceptions such as red blood cells, thrombocytes, lymphocytes, and neuronal cells (Fra et al., 1995). Caveolae tend to appear in clusters, but they are also found as single pits. Recent studies have shown that caveolae are involved in cellular transport and human diseases such as cancer, muscular dystrophy, Alzheimer's disease, and atherosclerosis (Engelman et al., 1998; Frank, 2010). A big step in the research of caveolae was the discovery of caveolin, the main structural protein of caveolae (Rothberg et al., 1992). Caveolin, now referred to as caveolin-1 is an integral membrane protein which is part of a protein family with at least three members in vertebrates: caveolin-1, caveolin-2, and caveolin-3 (Glenney, 1992; Rothberg et al., 1992; Scherer et al., 1996; Tang et al., 1996). Caveolin-1 and caveolin-2 are highly expressed in endothelial cells, adipocytes, and type I pneumocytes, Caveolin-3 is only expressed in cells of skeletal and cardiac muscle (Scherer et al., 1996, 1994; Tang et al., 1996), whereas in smooth muscle cells all protein members are present (Tang et al., 1996). Like clathrin-coated vesicles, caveolae are capable of engulfing molecules and detaching from the plasma membrane. Unlike clathrin-coated vesicles, caveolae can migrate from the luminal to the abluminal side of the cell where they release their cargo, a scenario which has been shown by perfusion with varying tracer molecules (Predescu et al., 1997; Simionescu et al., 1975). In addition, similar to phagocytes, caveolae are able to take up viruses and bacteria, and to deliver them from the cell surface to intracellular compartments for degradation (Anderson et al., 1996; Montesano et al., 1982; Shin et al., 2000). In most endothelial cells, caveolae are more common than clathrin-coated pits. The highest number of caveolae are found in endothelial cells of heart, lung and skeletal muscle (Aird, 2007a).

1.1.2.2 Transendothelial channels

Transendothelial channels (TECs) are openings which span the entire cell from the luminal to the abluminal side (Figure 2B and C). They are most likely formed either by the fusion of a caveola with the luminal and abluminal plasma membrane, or by the fusion of 2 to 4 caveolae (Stan, 2000). After application of VEGF, Chen et al. demonstrated an enrichment of caveolae in HUVEC (human umbilical vein endothelial cells), followed by the fusion of caveolae to transendothelial channels (Chen et al., 2002).

1.1.2.3 Vesiculo-vacuolar organelles (VVOs)

The term vesicular-vacuolar organelles (VVOs) represents the fusion or cluster of several caveolae (Figure 2D). VVOs are evident in endothelial cells of arterioles, capillaries, and most commonly in venular endothelium (Feng et al., 2002), are capable of spanning the entire thickness of the cell and can form groups of more than 100 single caveolae (Dvorak and Feng, 2001).

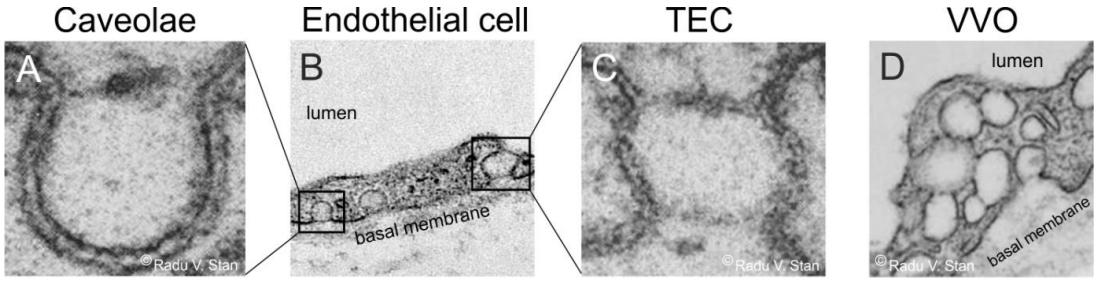

Figure 2: Endothelial cell organelles. Transmission electron micrographs of endothelial subcellular structures. **A**, Caveola with a stomatal diaphragm. **B**, Endothelial cell showing caveolae on the abluminal side of the cell (boxed area on the left) and a transendothelial channel (boxed area on the right). **C**, Electron micrograph of a transendothelial channel (TEC) with two diaphragms on both sides. **D**, Endothelial cell presenting vesiculo-vacuolar organelles. Pictures in **A**, **C** and **D** are taken from Radu V Stan, 2007.

1.2 Endothelial Heterogeneity

Vascular endothelial cells of different vascular beds are remarkably heterogeneous with respect to their structural and functional properties. This heterogeneity is based on the different needs for permeability of water and solutes in the different vascular beds (Aird, 2007a, 2007b). Endothelial cells are either discontinuous or continuous.

1.2.1 Discontinuous endothelium

Discontinuous endothelial cells are evident in vascular beds such as the bone marrow, the spleen, but most notably the liver (Figure 3B). They are characterized by large circular openings with mean diameters of 100-300nm - depending on the species - and the absence of a basal lamina (Braet and Wisse, 2002). In the liver, sinusoidal pores function as a

dynamic biofilter, which separates macromolecules of different sizes, mainly lipoproteins, between the sinusoidal lumen and space of Disse (Fraser et al., 1995).

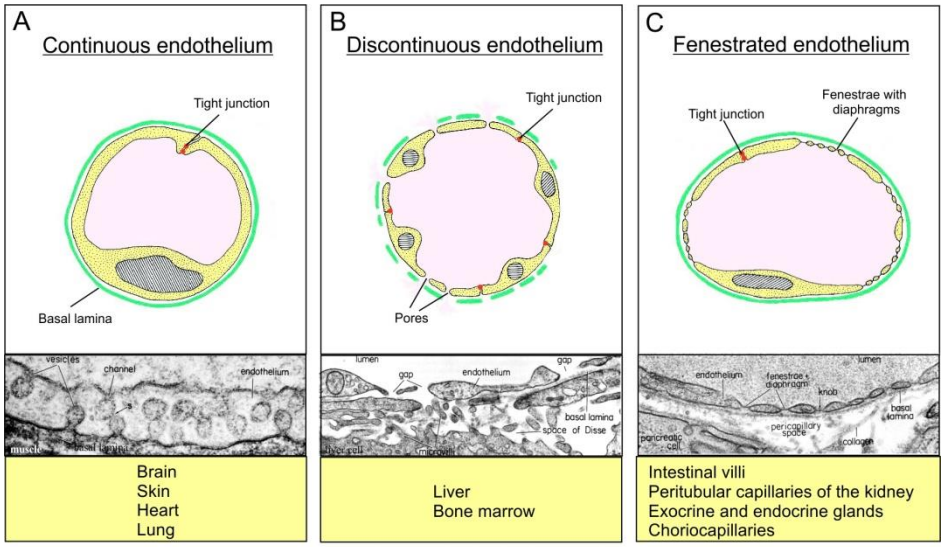

Figure 3: Endothelial heterogeneity. Schematic cross sections of the three basic types of blood capillaries. **A**, Continuous endothelium with endothelial cells linked by tight junctions and underlying continuous basal membrane. Continuous endothelial cells are found in brain tissue, skin, heart and lung and typically contain numerous caveolae. **B**, Discontinuous endothelium is characterized by the presence of large circular open pores with a mean diameter of 100-300 nm and by the absence of a basal lamina. Discontinuous endothelial cells are evident in vascular beds such as liver and bone marrow. **C**, Characteristic for fenestrated endothelial cells are transcellular pores with a mean diameter of 62-68 nm which are, depending on the vascular bed, bridged by a fenestral diaphragm. (Modified after Benninghoff and Drenckhahn, 2003).

1.2.2 Continuous endothelium

Continuous endothelial cells can be further classified into non-fenestrated or fenestrated endothelia (Tse and Stan, 2010). Non-fenestrated continuous endothelial cells are commonly found in capillaries of the brain, skin, heart, and lung (Figure 3A). The endothelial cells are connected by tight junctions and supported by an underlining continuous basal membrane.

1.2.3 Fenestrated endothelium

Fenestrated endothelial cells (Figure 3C) are also associated with a continuous basal membrane and are located in capillaries of the intestinal villi, peritubular capillaries of the

kidney, exocrine and endocrine glands, or the choriocapillaris in the eye, all organs with a substantial need for filtration and transendothelial transport. The structural hallmark is the presence of pores or fenestrae.

1.2.3.1 Fenestrae

Fenestrae are transcellular circular openings with a constant diameter of 62-68 nm which extend the entire thickness of the cells (Clementi and Palade, 1969a, 1969b; Simionescu et al., 1974). Fenestrae are arranged in so called sieve plates, large clusters of individual fenestrae. The density of fenestrae varies depending on the vascular bed. For example, in the kidney cortex 8.35 % of total endothelial surface is occupied by fenestrations, in contrast to the exocrine pancreas with only 3.68 % (Milici et al., 1985).

Depending on the particular vascular bed, caveolae, VVOs, TECs, and fenestrae are characteristically bridged by a thin 5 to 6 nm non-membranous diaphragm (Clementi and Palade, 1969c; Friederici, 1969, 1968a). Caveolae and TECs are covered by a stomatal diaphragm, fenestrae by a fenestral diaphragm (Figure 3C), both similar in regard to their structure. The diaphragm may qualify these structures with increased size and charge selectivity, allowing only small molecules and limited amounts of plasma to pass (Aird, 2007a; Palade et al., 1981; Simionescu et al., 1981b, 1981c). *In vitro* studies could show that factors like vascular endothelial growth factor (VEGF), extracellular signals (i.e. TGFβ, serotonin, retinoic acid), phorbol myristate acetate (PMA), cytochalasin B, calcium ions, or extracellular matrix components influence fenestrae formation (Carley et al., 1988; Esser et al., 1998a; Gatmaitan et al., 1996; Lombardi et al., 1988, 1986; McGuire et al., 1992; Milici et al., 1985; Steffan et al., 1987). Especially VEGF has been shown to be able to induce fenestrae formation. For instance, Roberts and Palade have shown that the topical application of VEGF to the rat cremaster muscle or subcutaneous injection in the skin induced the formation of fenestrae in these tissues, which do not contain fenestrae naturally. Furthermore, fenestrae induction was reported to appear after only 10 min exposure *in situ*, indicating that the molecular "ingredients" for the formation of diaphragms are already available, given that exposure time was too short for *de novo* protein synthesis (Roberts and Palade, 1995). However, the importance of VEGF in fenestrae formation is not generally accepted. Several studies in recent decades presented controversial results (Hofman et al., 2000; Kohn et al., 1992; Vasile et al., 1999).

Besides fenestrated vascular beds, also endothelial cells of Schlemm's canal endothelium possess fenestrae-like pores. The inner wall of Schlemm's canal (SC) shows one of the highest hydraulic conductivities throughout the body allowing the aqueous humor to exit the eye by passing the trabecular meshwork and entering the lumen of Schlemm's canal. The high hydraulic conductivity requires the formation of large intracellular (I-pores) and intercellular pores (B-pores) with diameters of 0.1 to 2 µm (Johnson, 2006). Solitary minipores which were found in SC endothelial cells of monkey and human eyes (Inomata et al., 1972; Tamm, 2009a) are very similar to diaphragmed fenestrae of fenestrated capillaries related to their size and structure, but are much more rarely formed in endothelial cells of SC endothelium than in those of fenestrated endothelia. Bill and Mäepea hypothesized that I-pores of SC develop from those minipores (Inomata et al., 1972), a scenario quite similar to that seen in liver sinusoids and glomerular capillaries during embryonic development (Bankston and Pino, 1980; Braet and Wisse, 2002; Ichimura et al., 2008).

1.3 Plasmalemma vesicle-associated protein

The only protein known so far to be localized to diaphragms of fenestral and stomatal diaphragms is plasmalemma vesicle-associated protein (PLVAP, synonyms: MECA32, PV-1) a cationic single span type II integral membrane protein which is specifically expressed in endothelial cells (Stan et al., 1999a, 1999b). PLVAP is encoded by *Plasmalemma vesicle-associated Protein* gene in humans, but the protein has also been documented in several other mammalian species including mouse, rat, chicken and bovine (Stan, 2005).

1.3.1 Ultrastructure and molecular composition of PLVAP

Protein sequences and cDNA of *Plvap* are highly conserved across species. The monomer has a calculated molecular mass of about 50 KDa in the unglycosylated form and about 60 KDa in the glycosylated form and tends to form homodimers *in situ*. The human PLVAP consists of a short N-terminal cytoplasmatic domain, a single span transmembrane domain, and a long C-terminal extracellular domain (Figure 4). The intracellular domain contains a short sequence near the transmembrane region with a putative caveolin-1 binding site (Stan, 2005). The extracellular domain holds nine cysteines, four consensus N-glycosylation sites, a proline-rich region near the C-terminus, and two coiled-coil domains. The presence of the two

coiled-coil domains suggests the secondary structure of PLVAP to be mostly alpha helical (Hallmann et al., 1995; Stan et al., 1999b).

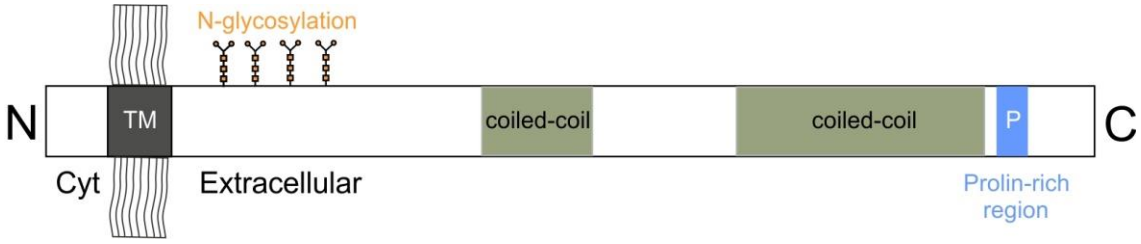

Figure 4: Schematic drawing of the PLVAP monomer. PLVAP consists of a short N-terminal cytoplasmatic domain, a single span transmembrane domain, and a long extracellular C-terminal domain. The extracellular domain holds nine cysteines, four consensus N-glycosylation sites, a proline-rich region near the C-terminus, and two coiled-coil domains. TM=transmembrane domain. Cyt=cytoplasmic (modified after Stan, 2007)

1.3.2 Localization of PLVAP and its participation in fenestrae formation

PLVAP is highly expressed in lung tissue confirmed on both mRNA and protein level, but it is also expressed in several other vascular beds such as kidney, liver, spleen, heart and skeletal muscle, but at much lower levels. Within those tissues, PLVAP is exclusively found at stomatal diaphragms of caveolae and TECs, and fenestral diaphragms of fenestrae, as shown by immunolocalization of PLVAP in rat lung (Stan et al., 1999a).

Stan and colleagues were able to show the *de novo* formation of stomatal diaphragms in caveolae and TECs, as well as fenestral diaphragms in fenestrae by upregulation of *Plvap* expression in human umbilical vein endothelial cells (HUVEC) with phorbol myristate acetate. Downregulation of *Plvap* by RNA interference resulted in the loss of diaphragms in caveolae. In addition, no fenestrae and transendothelial channels were observed (Stan et al., 2004). In turn, Ioannidou et al. found only a 70 % reduction in the amount of PLVAP in siRNA-treated cells. Furthermore, the partial reduction in PLVAP did not cause a significant reduction in the number of fenestrae. However, a population of fenestrae did not form any diaphragm and those fenestrae had enlarged and variable diameters and disorganized sieve plates, implicating that PLVAP is necessary in fenestral morphogenesis and arrangement in sieve plates (Ioannidou et al., 2006).

1.3.3 Structure of diaphragms and integration of PLVAP

Based on a quick-freeze, deep-etch study from Bearer and Orci in the year 1985 (Bearer and Orci, 1985), Radu Stan postulated a working hypothesis for the structure of stomatal and fenestral diaphragms and the integration of PLVAP in diaphragms (Stan, 2007). He assumes that both stomatal and fenestral diaphragms are built of a scaffold of radial fibrils which are on one side anchored in the rim of the pore and on the other side interweave in a central knot, resulting in a structure similar to a spoke (Figure 5). He reckons that the fibrils consist of PLVAP dimers whose C termini form the central point of the diaphragm and the intense glycosylation near the N-terminal side of the protein (Figure 4) might help to keep the dimer "afloat". Furthermore, the diaphragm could be stabilized by interactions between the C termini of neighboring PLVAP dimers or by the cooperation of an additional stabilizing extracellular protein. In general, stomatal and fenestral diaphragms are very similar with respect to their structure, but behave differently. Studies with non-specific probes such as cationic molecules (Palade et al., 1981; Simionescu et al., 1984, 1982, 1981b) or lectins (Bankston and Milici, 1983; Bankston et al., 1991) showed that stomatal diaphragms can bind lectins and lack anionic sites. In contrast, fenestral diaphragms do hardly bind lectins (Furuya, 1990) but possess multiple anionic sites instead, which are conferred by heparan sulfate proteoglycans (HSPGs) (Simionescu et al., 1981c).

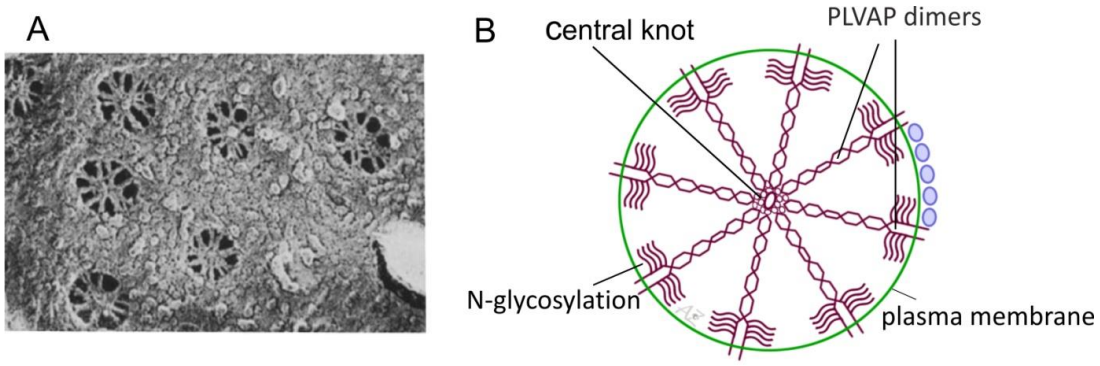

Figure 5: Molecular structure of PLVAP. **A**, Quick-freeze, deep-etch scanning electron micrograph of a peritubular capillary in the rat kidney cortex presenting numerous fenestrae with fenestral diaphragms. Many interweaving fibrils which converge in a central point are observable. **B**, Working hypothesis for the integration of PLVAP in endothelial diaphragms. Fibrils composed of PLVAP dimers are anchored in the rim of the pore (via the N-terminal domain) and meet in the midpoint in a central mesh (via the C-terminal domain). The glycosylation sites near the N-terminal side of the protein helps to keep the dimer "afloat" by preventing the collapse on the plasma membrane. Picture in **A** is taken from Bearer and Orci, 1985. Picture in **B** is modified after Stan, 2007.

1.4 Aim of the study

Since stomatal and fenestral diaphragms are thought to play a crucial role in vascular permeability and might be involved in pore formation in Schlemm's canal endothelium, the overall goal of the current study was to molecularly dissect the biological function of PLVAP. Specifically, the plan involved to find answers to some pivotal questions in endothelial cell biology.

- What happens with stomatal and fenestral diaphragms in fenestrated endothelial cells if PLVAP is absent?
- Are there any general effects on endothelial cell permeability?
- Is there any impact on Schlemm's canal physiology?

Furthermore, scientists recently gained some insight into the molecular composition and formation of caveolae (Fra et al., 1995; Stan et al., 1999a, 1999b, 1997; Vogel et al., 1998), whereas the precise mechanisms for the formation of TECs and fenestrae still need to be explored. According to a current hypothesis, fenestrae might evolve from the fusion of caveolae during endothelial thinning, followed by the approach of the membranes **(**Figure 6**)**.

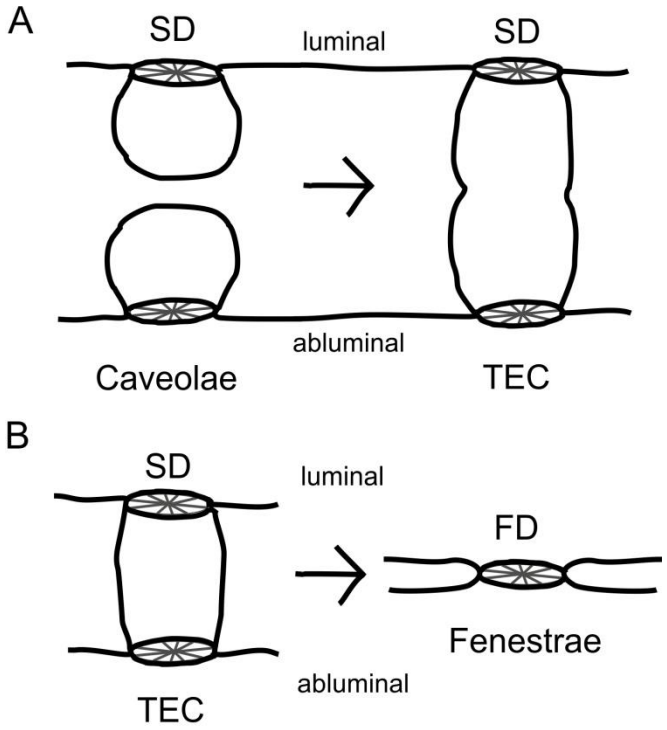

Figure 6: Theory of fenestrae formation via fusion of caveolae. Schematic drawing of the potential onset of fenestrae formation. **A**, During endothelial thinning, caveolae could get in contact and fuse to transendothelial channels with two diaphragms on both sides. **B**, Further thinning is supposed to lead to a collapse of the transendothelial channel followed by the loss of one diaphragm. Modified after Kathrin Ebner, 2008.

Still, several findings argue against this hypothesis. For instance, caveolin-1 has been shown to be absent in fenestrae of glomerular endothelial cells *in vivo* (Sörensson et al., 2002) and adrenal cortical microvascular endothelial cells in culture (Esser et al., 1998b). In addition, neither the distribution, amount or phosphorylation of caveolin-1 is altered by VEGF (Esser et al., 1998b). Furthermore, the fact that fenestrations in kidney and liver endothelial cells in caveolin-1 knockout mice (which do not form caveolae) do not show any alterations argues strongly against this hypothesis (Sörensson et al., 2002; Warren et al., 2010). These data provoked additional questions, which were followed up in this thesis:

- Is PLVAP involved during the process of caveolae, TEC, and fenestrae formation?
- Is PLVAP essential for their formation?

Due to the fact that fenestrae are bridged by diaphragms during embryonic development of liver sinusoids and glomerular capillaries (Bankston and Pino, 1980; Ichimura et al., 2008), I investigated liver sinusoidal endothelial cells in more detail.
The general concept of my work was based on the assumption that the deletion of PLVAP would provide an opportunity to answer those questions based on data obtained *in vivo.*
In particular, following goals were pursued:

1) The generation of a knockout mouse line, resulting in a complete deletion of PLVAP

2) The phenotype analysis of *Plvap*-deficient mice during embryonic and postnatal development in 2 different genetic backgrounds

3) The analysis of the general expression pattern of PLVAP in fenestrated endothelial cells of Schlemm's canal endothelium and ocular capillaries

4) The investigation of fenestrated vascular beds of *Plvap*-deficient animals in greater depth (i.e. peritubular capillaries of the kidney, capillaries of the pancreas, and Schlemm's canal endothelium)

5) The investigation of sinusoidal endothelial cells in livers of *Plvap*-deficient animals

Chapter 2

Lack of endothelial diaphragms in fenestrae and caveloae of mutant *Plvap*-deficient mice

(adapted from: Herrnberger L, Seitz R, Kuespert S, Bösl MR, Fuchshofer R, Tamm ER. **Lack of endothelial diaphragms in fenestrae and caveolae of mutant *Plvap*-deficient mice**. Histochem Cell Biol. 2012, 138(5):709-724)

2 Lack of endothelial diaphragms in fenestrae and caveloae of mutant *Plvap*-deficient mice

2.1 Abstract

Plasmalemma vesicle-associated protein (PLVAP, PV-1) is specifically expressed in endothelial cells in which it localizes to diaphragms of fenestrae, caveolae, and transendothelial channels. To learn more about its function, we generated mutant mice that lack PLVAP. In a C57BL/6N genetic background, homozygous *Plvap*-deficient embryos die before birth and suffer from subcutaneous edema, hemorrhages, and defects in the vascular wall of subcutaneous capillaries. In addition, hearts of *Plvap* $^{-/-}$ embryos show ventricular septal defects and thinner ventricular walls. In wild-type embryos, PLVAP and caveolae with a stomatal diaphragm are present in endothelial cells of subcutaneous capillaries and endocardium, while a diaphragm is missing in caveolae of *Plvap* $^{-/-}$ littermates.

Plvap $^{-/-}$ mice in a mixed C57BL/6N/FVB-N genetic background are born and survive at the most for 4 weeks. Capillaries of exocrine and endocrine pancreas and kidney peritubular interstitium were investigated in more detail as examples of fenestrated capillaries. In these vascular beds, *Plvap* $^{-/-}$ mice show a complete absence of diaphragms in fenestrae, caveloae, and transendothelial channels, findings which are associated with a substantial decrease in the number of endothelial fenestrae. The changes in the capillary phenotype correlate with a considerable retardation of postnatal growth and anemia. *Plvap* $^{-/-}$ mice provide an animal model to clarify the specific functional role of endothelial fenestrae and their contribution to passage of water and solutes in different organs.

2.2 Introduction

The inner surface of blood vessels and lymphatics are lined by endothelial cells which critically contribute to the various physiological requirements of circulation. Since the different vascular beds vary considerably with respect to their specific functions, vascular endothelial cells are remarkably heterogeneous with regard to their structural and functional properties, and their expression pattern of characteristic molecules (Aird, 2007a, 2007b). Endothelial cell heterogeneity is especially evident in capillaries in which different needs for permeability of water and solutes require different structural phenotypes of endothelial cells. As a consequence, capillary endothelia may be of a discontinuous, fenestrated, or continuous type (Tse and Stan, 2010). Discontinuous capillary endothelial cells such as in the sinusoids of the liver form large circular pores that are 100-200 nm in diameter. Such openings are missing in continuous endothelial cells which are commonly found in capillaries of the brain, skin, heart, and lung. In contrast, fenestrated endothelia are observed in capillaries of exocrine and endocrine glands, intestinal villi, peritubular interstitium of the kidney, or the choriocapillaris in the eye, all organs or tissues that have in common the need for a substantial filtration and transendothelial transport.

The structural hallmarks of endothelial cells in fenestrated capillaries are transcellular pores or fenestrae with a remarkably constant diameter of 62-68 nm, which extend through the full thickness of the endothelial cell. Fenestrae are characteristically bridged across their opening by a thin 5-6 nm non-membranous diaphragm (Clementi and Palade, 1969a; Friederici, 1969, 1968a). Results from quick-freeze deep-etch electron microscopy suggest that the diaphragm consists of radial fibrils which extend from the peripheral rim of the cellular pore to meet and interweave in a central mesh (Bearer and Orci, 1985). It has been suggested that the presence of a diaphragm may provide fenestrae with increased size and charge selectivity allowing only small molecules and limited amounts of plasma protein to pass (Aird, 2007a; Palade et al., 1981; Simionescu et al., 1981b, 1981c).

Up until now, the only protein that has been found to be directly localized to fenestral diaphragms is plasmalemma vesicle-associated protein (PLVAP, synonyms: MECA32, PV-1), a cationic, integral membrane glycoprotein that is specifically expressed in endothelial cells (Stan et al., 1999a, 1999b). In addition to its presence in diaphragms of endothelial fenestrae, PLVAP was also found to be localized in the stomatal diaphragms of caveolae and the diaphragms of transendothelial channels (Stan, 2005; Stan et al., 2004). Moreover, *in vitro* studies in cultured cells have shown that the knock-down of *Plvap* expression by RNA interference impairs the formation of diaphragms in fenestrae, caveolae, and transendothelial

channels (Ioannidou et al., 2006; Stan et al., 2004). Caveolae which are defined as spherical invaginations of the plasma membrane of regular shape and size (about 70 nm) occur in all types of endothelia as well as in most vertebrate cell types. Still, caveolae with stomatal diaphragms are only found in some selected endothelia of the continuous type (i.e., in the capillaries of the lung) and in all fenestrated and sinusoidal endothelia (Bruns and Palade, 1968; Stan, 2005). The stomatal diaphragm of caveolae appears to be quite comparable in structure to the diaphragms of fenestrae (Bearer and Orci, 1985). Transendothelial channels are pores through the entire endothelial cell provided with two diaphragms, one luminal and one abluminal, which are found predominantly in fenestrated endothelia (Milici et al., 1985). It has been hypothesized that caveolae with stomatal diaphragms fuse from luminal and abluminal sides of endothelial cells to form transendothelial channels which may then collapse to form fenestrae (Roberts and Palade, 2000). Still, the observation that in mutant *caveolin-1*-deficient mice, which do not form endothelial caveolae (Drab et al., 2001; Razani et al., 2001), the number of diaphragmed fenestrae and transendothelial channels is largely unchanged (Tkachenko et al., 2012; Zhao et al., 2002) argues against this hypothesis and leaves the functional role of the stomatal diaphragm in caveolae unresolved.

In order to shed light on the *in vivo* function of PLVAP and its role in the formation of diaphragms in fenestrae, caveolae, and transendothelial channels, we generated mutant mice that lack PLVAP. We show that in the living organism such diaphragms do not form in the absence of PLVAP. Depending on the genetic background, the lack of diaphragms interferes with cardiac morphogenesis, the integrity of embryonic vessels, and the formation of fenestrated endothelial layers. Our mouse model will provide an ideal tool to study the *in vivo* functional properties of diaphragms in capillary endothelial cells.

2.3 Materials and methods

2.3.1 Generation of *Plvap*-deficient mice

Embryonic stem cell clones (HEPD0550_4_E12) were obtained through the International Knockout Mouse Consortium (Projekt 31505) (Skarnes et al., 2011). The targeted ES cells were injected into C57Bl/6N blastocysts to generate chimeras. Chimeric males transmitted the targeted allele to their offspring. Genotyping was routinely performed by PCR analysis, using two upstream primers located in intron 1 of *Plvap* (5'-AGAGCCTTCTCTGCCAAGTG-3') or in the inserted targeting cassette (5'-TCTCATGCTGGACTTCTTCG-3'), and a downstream primer located in intron 1 downstream of the cassette (5'-GGCTAGCCTGAGCTACAGAGG-3') resulting in a 672 bp PCR fragment for the wild-type allele and a 552 bp fragment for the targeted allele. DNA was obtained from tail tips. PCR analysis was performed in 15 µl reaction volumes containing standard buffer, 0.1 µM of each primer, 1 mM dNTPs, 2.5 mM $MgCl_2$, 8% glycerol, 0.2 mM cresol red sodium salt (Sigma, Taufkirchen, Germany) and 0.25 U *Taq*-Polymerase (New England Biolabs, Taufkirchen, Germany). The cycling conditions consisted of an initial 3-min denaturing step at 94°C, followed by 34 cycles for 30 s at 94°C, for 1 min at 65°C, and for 1 min 15 s at 72°C.
Tg (TIE2GFP) 287Sato/J mice (Stock number 003658) (Motoike et al., 2000) were obtained from The Jackson Laboratory (Bar Harbor, Maine). Genotyping was routinely performed by PCR analysis, using a forward primer (5'-ATTCTCGTGGAACTGGATGG-3') and a reverse primer (5'-GGACAGGTAATGGTTGTCTGG-3'), resulting in a 567bp fragment. DNA was obtained from tail tips. PCR was performed in 15 µl reaction volumes containing standard buffer, 0.1 µM of each primer, 1 mM dNTPs, 2.5 mM $MgCl_2$, 20% glycerol, 0.2 mM cresol red sodium salt (Sigma) and 0.25 U *Taq*-Polymerase (New England Biolabs). The cycling conditions consisted of an initial 3 min denaturing step at 94°C, followed by 31 cycles for 30 s at 94°C, for 1 min at 60°C, and for 1 min at 72°C.

2.3.2 RNA analysis

Total RNA from embryos at embryonal (E) day 13.5 or postnatal (P) day 13 was extracted with peqGold Trifast (Peqlab, Erlangen, Germany) according to manufacturer`s instructions. First strand cDNA from total RNA was generated using the iScript cDNA Synthesis Kit (BioRad, München, Germany) according to the manufacturer`s recommendations. RNA that

was not reverse transcribed into cDNA served as negative control for real-time RT-PCR. Real-time RT-PCR was performed on a BioRad iQ5 Real-time PCR Detection System (BioRad) with the temperature profile as follows: 40 cycles of 10 s melting at 95°C and 40 s of annealing and extension at 60°C. Primer pairs (Table **1**) were purchased from Invitrogen (Darmstadt, Germany) and were designed to extend over exon-intron boundaries. In initial experiments, the potential housekeeping genes for real-time RT-PCR were identified for each tissue and best results were obtained for GAPDH for whole embryos at E13.5 and GNB2L for mouse tissue (P13). Quantification was performed using BioRad iQ5 Standard-Edition (Version 2.0.148.60623) software (BioRad).

Primer	Sequence
mPlvap fwd	5'-TCAACAAGACCTGCGAAGC-3'
mPlvap rev	5'-AGCACACTGCCTTCTCCTTG-3'
mGNB2L fwd	5'-TCTGCAAGTACACGGTCCAG-3'
mGNB2L rev	5'-GAGACGATGATAGGGTTGCTG-3'
mGAPDH fwd	5'-TGTCCGTCGTGGATCTGAC-3'
mGAPDH rev	5'-CCTGCTTCACCACCTTCTTG-3

Table 1. Primer used for real-time RT-PCR

2.3.3 Western blot analysis

Tissues were homogenized in RIPA buffer (150 mM NaCl, 1% NP-40, 0.5% deoxycholic acid, 0.1% SDS, and 50 mM Tris), and insoluble constituents were removed by centrifugation. For Western blot analysis of PLVAP up to 30 µg of protein was subjected to an 8% SDS-PAGE and transferred onto a PVDF membrane (Roche Diagnostics GmbH, Mannheim, Germany) by semidry blotting. After blocking with 5% low-fat milk in TBS-T, membranes were incubated overnight with rat anti-mouse pan ECA (MECA-32) IgG_{2a} antibodies (Santa Cruz Biotechnology, Santa Cruz, CA), diluted 1:500 in 0.5 % low-fat milk in TBS-T. After washing in TBS-T, membranes were hybridized with HRP-conjugated chicken anti-rat antibodies (SantaCruz), diluted 1:1000 in 0.5% low-fat milk in TBS-T. For visualization, membranes were incubated in Luminata Forte Western HRP Substrate (Millipore Corporation, Billerica,

MA) and visualized on a LAS 3000 Imager work station (Fujifilm, Düsseldorf, Germany). As loading control membranes were stained with Coomassie Blue.

2.3.4 Light microscopy

Embryos were obtained from timed mating with noon of the day of vaginal plug discovery designated as 0.5 days of gestation (E 0.5). Embryos and tissues were collected, rinsed in PBS and fixed in 4 % PFA for 4 h. After washing in 0.1 M phosphate buffer the tissue samples were processed through several graded alcohols and xylenes, and embedded in paraffin. Sections were stained with hematoxylin and eosin (H and E) and analyzed using a Zeiss Axio Imager microscope (Carl Zeiss AG, Oberkochen, Germany). Blood smears were generated with blood collected from tail veins. The slides were fixed in 100% methanol for 10 min, washed in H_2O and stained with 300 µl May-Grünwald-Giemsa solution (Fluka Chemika, Buchs, Switzerland) in 10 ml H_2O. For Immunohistochemistry, embryos and tissue samples were fixed in Carnoy's fixative (60 % methanol, 30 % chloroform, and 10 % acetic acid) for 4 h, washed in 0.1 M phosphate buffer and embedded in paraffin. For frozen sections, the tissue was equilibrated in 10, 20, and 30 % sucrose for 4 h and embedded in Tissue-Tek optimal cooling temperature (OCT) compound (Sakura Finetek Europe B.V., Zoeterwoude, NL) and cooled at -20 °C. After removal of Tissue-Tek and paraffin, the sections were blocked with 0.2 % cold water fish gelatin (Aurion, Wageningen, Netherlands), 1 % BSA and 0.1 % Triton-X (all in 0.1 M PBS) for 1 h at room temperature. After blocking, the sections were incubated with anti-pan ECA (MECA-32) IgG_{2a} (1:50, Santa Cruz) and anti-CD31/PECAM-1 IgG (1:20, R&D Systems, Wiesbaden, Germany) for double labeling. Alexa Fluor 488 (1:1000) rabbit anti-goat IgG (Invitrogen) and donkey anti-rat IgG (1:2000) conjugated to Cy3 (Jackson Immuno Research) were used as secondary antibodies and incubated for 1 h at room temperature. 4′,6-Diamidino-2-phenylindole (DAPI) was used to counterstain nuclear DNA. Slides were mounted in a medium containing DAPI (Vectashield; Vector Laboratories, Burlington, CA, USA) and analyzed under a fluorescence microscope (Zeiss Axio Imager). For negative controls, primary antibodies were omitted and the slides were incubated with secondary antibodies only.

2.3.5 Transmission electron microscopy

Tissue samples were fixed in 2.5 % glutaraldehyde in 0.1 M cacodylate buffer (pH 7.4) for 4 h. Samples were washed, postfixed with 1 % OsO_4, 0.8 % $K_4[Fe(CN)_6]$ in 0.1 M cacodylate buffer for 1.5 h, dehydrated with graded ethanol solutions and embedded in Epon (Roth, Karlsruhe, Germany). Semithin sections were stained with Richardson' stain (Richardson et al., 2009). Ultrathin sections were stained with uranyl acetate and lead citrate, and analyzed on a transmission electron microscope (Libra, Zeiss).

2.3.6 Staining for *β*-galactosidase activity

Embryos and tissues were fixed in 2.5 % glutaraldehyde in 5 mM EGTA (pH 7.3) and 2 mM $MgCl_2$ dissolved in 0.1 M PBS for 4 h on ice with shaking. After three 30 min rinses in washing buffer (2 mM $MgCl_2$, 0.01 % sodium deoxycholate, 0.02 % Nonidet-P40 in 0.1 M PBS), *β*-galactosidase activity was visualized in X-Gal staining solution (0.1 M PBS, 2 mM $MgCl_2$, 0.01 % sodium deoxycholate, 0.02 % Nonidet-P40, 5 mM potassium ferrocyanide, 5 mM potassium ferricyanide, 1 mg/ml X-Gal). Tissues were stained for 24 h at 37 °C in the dark, washed 3 times for 5 min in washing buffer and embedded in paraffin or in Tissue-Tek for frozen sections.

2.4 Results

2.4.1 Targeted removal of *Plvap* leads to embryonic death

To disrupt gene function, an IRES:lacZ trapping cassette and a promoter-driven neo cassette (Skarnes et al., 2011) were inserted between exons 1 and 2 of *Plvap* (Figure 7A). Following germ-line transmission, genotyping of newborn pups was performed by PCR. In the C57BL/6N genetic background that was used for initial breeding, only heterozygous *Plvap*-deficient mice or wild-type littermates were detected, strongly indicating that the complete deletion of *Plvap* is lethal during prenatal development. Next, heterozygous *Plvap*-deficient mice were crossed with each other to obtain embryos for genotyping. We were now able to detect homozygous *Plvap*-deficient embryos in addition to embryos with *Plvap* $^{+/-}$ or wild-type genotype when litters at embryonic (E) days E 13.5 to E 17.5 were analyzed (Figure 7B). By real-time RT-PCR, we observed in *Plvap* $^{+/-}$ embryos a reduction of approximately 50% in the amount of *Plvap* mRNA when compared with wild-type littermates, while no mRNA was detected in *Plvap* $^{-/-}$ embryos (Figure 7C).

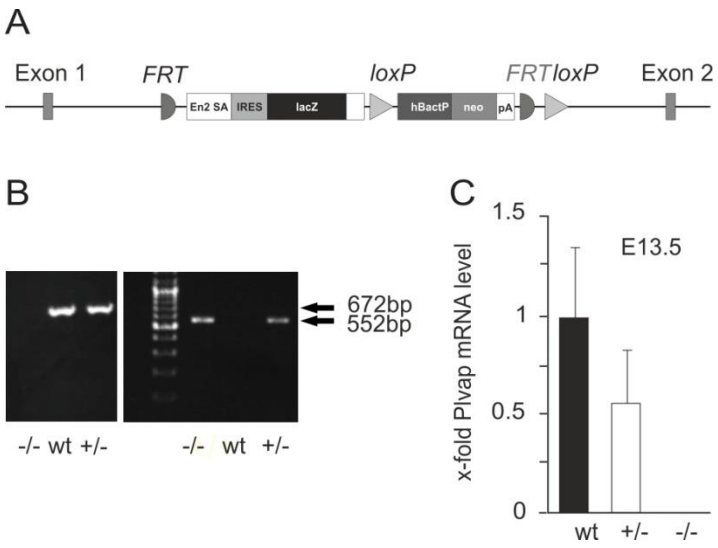

Figure 7: Generation of mutant *Plvap*-deficient mice. A, Schematic representation of the targeted allele. **B**, Genotyping by PCR using a template DNA from embryos following mating of heterozygous *Plvap*-deficient mice. A 552-bp fragment illustrates the presence of the mutated allele which replaces the wild-type locus normally represented as a 672-bp fragment. **C**, Real-time RT-PCR analysis for *Plvap* mRNA in total RNA from whole embryos at E 13.5. The mean value obtained with RNA from wild-type embryos was set to 1. GAPDH was used as a reference gene.

Lack of PLVAP was further confirmed by immunohistochemistry. In E 16.5 wild-type embryos, double immunohistochemistry with antibodies against PLVAP and the endothelial cell marker CD31 showed the presence of PLVAP in capillary endothelial cells of small intestine (Figure 8A) and lung (Figure 8B). In contrast, no labeling for PLVAP was observed in small intestine and lung of *Plvap* $^{-/-}$ littermates (Figure 8A, B).

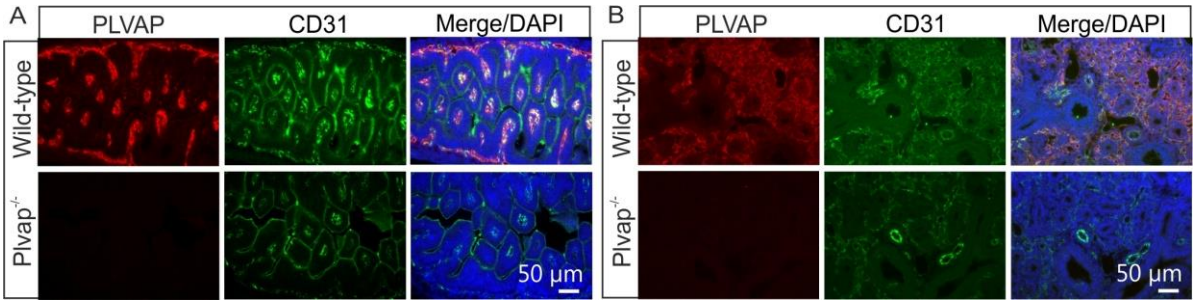

Figure 8: Generation of mutant *Plvap*-deficient mice. **A** and **B**, Double immunohistochemistry with antibodies against PLVAP and the endothelial cell marker CD31 shows the presence of PLVAP in capillary endothelial cells of small intestine (**A**) or lung (**B**) in E 16.5 wild-type animals, but not in *Plvap* $^{-/-}$ littermates.

2.4.2 *Plvap*-deficient embryos suffer from subcutaneous edemas and hemorrhages

E 16.5 *Plvap* $^{-/-}$ embryos were typically presented with a pronounced subcutaneous edema that extended from the neck to the lower back (Figure 9A, B). In addition, focal hemorrhages were present in various subcutaneous regions of trunk, extremities, head, and neck (Figure 9A, B). In areas not affected by subcutaneous hemorrhages, the skin was quite pale when compared with that of wild-type littermates indicating anemia (Figure 9A). Moreover, blood filled intact vessels that shined through the skin of body or umbilical cord in wild-type animals were not visible in *Plvap* $^{-/-}$ embryos (Figure 9A). Neither subcutaneous edemas nor hemorrhages were observed in wild-type littermates (Figure 9A). At E 17.5, homozygous *Plvap*-deficient embryos suffered from severe total body edema and extensive non-specific focal hemorrhages (Figure 9A, B). While homozygous *Plvap*-deficient embryos were still viable at E 17.5 as evidenced by cardiac pulsation and spontaneous movements, no *Plvap* $^{-/-}$ embryos were observed to be alive at later stages.

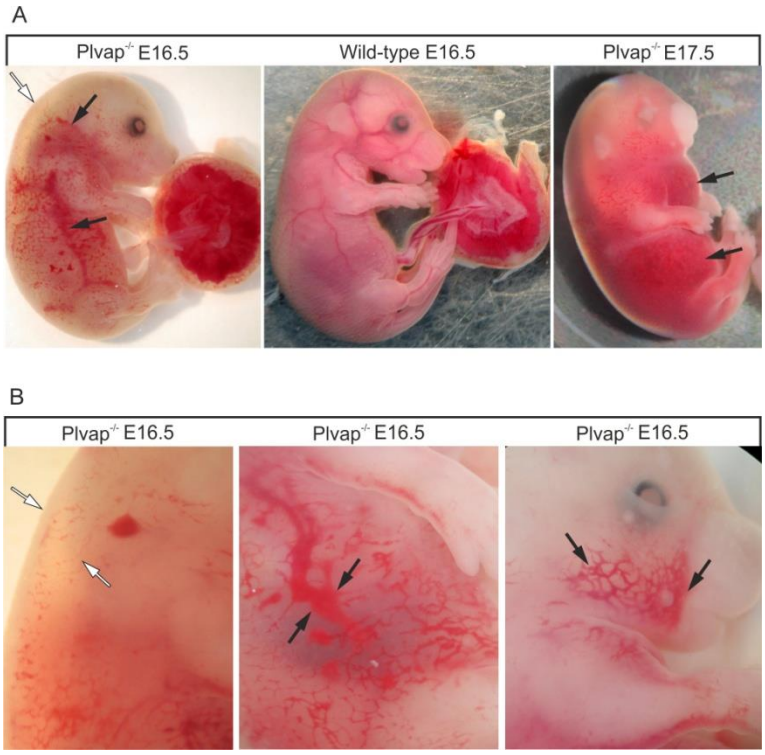

Figure 9: Phenotype of *Plvap*-deficient embryos in C57BL/6N background. A, E 16.5 *Plvap* $^{-/-}$ embryo with a pronounced subcutaneous edema that extends from the neck to the lower back (*white arrow*). In addition, focal hemorrhages are present in various subcutaneous regions of trunk, extremities, head, and neck (*black arrows*). In areas not affected by subcutaneous hemorrhages, the skin is pale when compared with that of the wild-type littermate. In addition, blood-filled intact vessels that shine through the skin of the body or umbilical cord in the wild-type animal are not visible in the *Plvap* $^{-/-}$ embryo. Neither subcutaneous edema nor hemorrhages are seen in the wild-type embryo. The E 17.5 *Plvap* $^{-/-}$ embryo shows severe total body edema and extensive non-specific focal hemorrhages (*black arrows*). **B**, Higher magnification of edema in the dorsal region of an E 16.5 *Plvap* $^{-/-}$ embryo (*white arrows*) and of subcutaneous hemorrhages (*black arrows*).

Subcutaneous edemas and hemorrhages were similarly detected in horizontal sections through E 16.5 *Plvap* $^{-/-}$ embryos, which showed accumulations of extracellular erythrocytes as well as a marked widening of the extracellular spaces beneath the skin in the anterior and dorsal regions of the trunk (Figure 10A-C). In contrast, neither subcutaneous edemas nor hemorrhages were observed in wild-type littermates (Figure 10A-C).

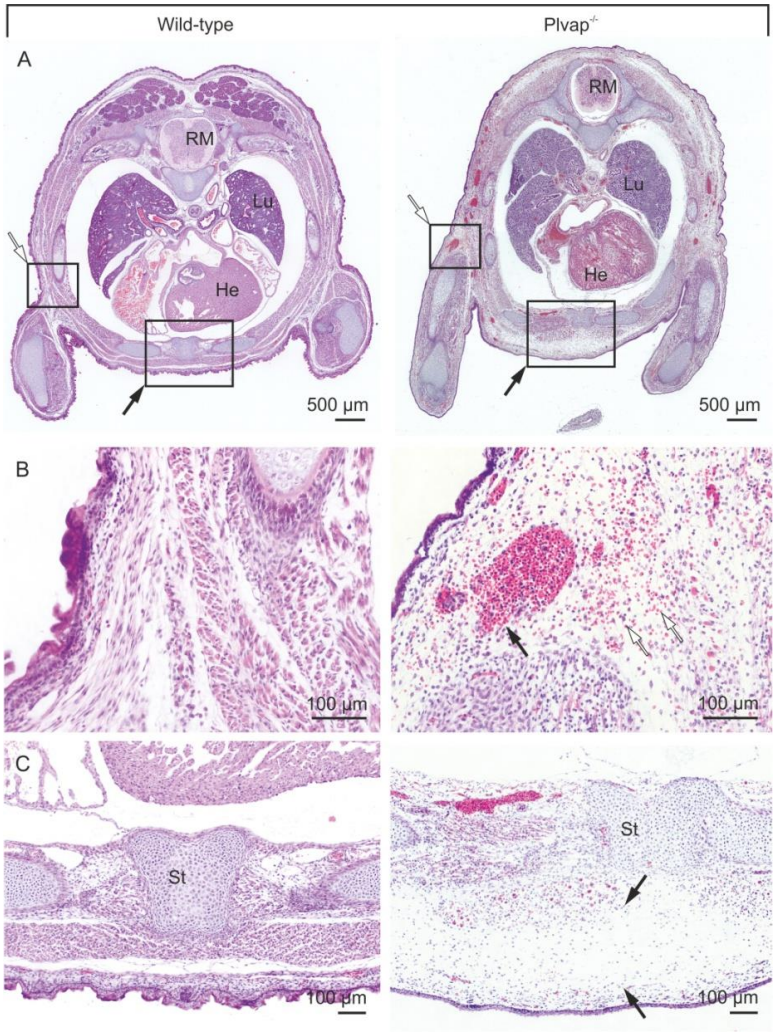

Figure 10: Histological characterization of *Plvap*-deficient embryos in C57BL/6N background. **A**, Transversal paraffin sections through the thorax of E 16.5 embryos stained with H and E. The *Plvap* $^{-/-}$ embryo displays edema in the anterior region of the trunk (*black arrow*) and hemorrhages (*white arrow*) beneath the skin, which are not seen in the wild-type littermate. **B** and **C**, Higher magnification of boxed areas in **A**. **B**, In the *Plvap* $^{-/-}$ embryo, but not in the wild-type littermate, numerous erythrocytes (*white arrows*) can be seen outside of capillaries in the surrounding tissue, indicating open blood vessels (*black arrow*). **C**, Massive widening of the *extracellular spaces* indicating subcutaneous edema in the *Plvap*-deficient (*black arrows*). *Sc* spinal cord, *Lu* lung, *He* heart, *St* sternum.

To follow up on the question, if lack of PLVAP in subcutaneous blood vessels might be responsible for subcutaneous edemas and hemorrhages, we analyzed the expression and the localization of PLVAP in this region.

When staining for *β*-galactosidase was performed at E 15.5 to detect expression of the reporter gene *lacZ* and activity of the *Plvap* promoter, positive staining was observed in endothelial cells of subcutaneous capillaries in *Plvap*-deficient embryos, but was absent throughout the entire subcutaneous region of wild-type littermates (Figure 11A). Subsequently, we performed immunostaining with antibodies against PLVAP and the

endothelial cell marker CD31 to find immunoreactivity for PLVAP in endothelial cells of the vast majority of mouse subcutaneous capillaries at E 16.5 (Figure 11B). In contrast, no specific immunoreactivity for PLVAP was observed in homozygous *Plvap*-deficient embryos (Figure 11B). Finally, we investigated endothelial cells of subcutaneous capillaries at E 17.5 by transmission electron microscopy. In both wild-type and *Plvap*-deficient embryos, the endothelium of subcutaneous capillaries was continuous without fenestrae (Figure 11C). Upon higher magnification, endothelial cells of wild-type capillaries showed numerous caveolae with stomatal diaphragms on both their luminal and abluminal surfaces. Accordingly, the neck or stroma of the caveolae was bridged by a distinct, 5- to 7-nm thick, electron-dense diaphragm (Figure 11C). Caveolae with stomatal diaphragms were invariably absent in capillaries of *Plvap* $^{-/-}$ embryos. Here, the neck of caveolae was not bridged by a diaphragm, but contained some ill-defined, fluffy electron-dense material instead (Figure 11C).

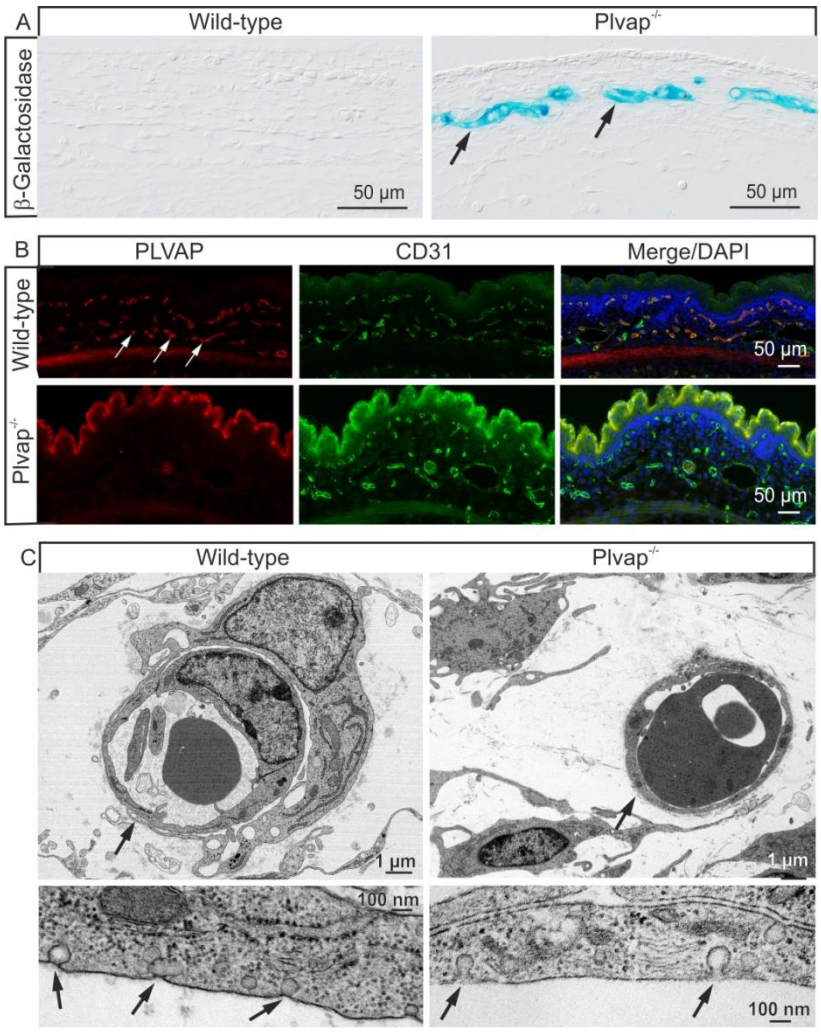

Figure 11: Expression and localization of PLVAP. **A**, *β*-galactosidase staining of sagittal frozen sections through the back skin and adjacent subcutaneous tissue of a wild-type embryo and a *Plvap* $^{-/-}$ littermate at E 15.5.

Positive staining (*arrows*) is seen in the endothelial cells of subcutaneous capillaries in the *Plvap* $^{-/-}$ embryo, whereas no staining is detectable in the wild-type littermate. **B**, Double labeling of transverse paraffin sections through the back skin and adjacent subcutaneous tissue of an E 16.5 wild-type embryo with antibodies against PLVAP (*red*) and CD31 (*green*) shows immunoreactivity for PLVAP in the majority of subcutaneous capillaries (*arrows*) and largely colocalizes with CD31 as seen in the merged picture. No specific staining for PLVAP is observed in the *Plvap*-deficient embryo. **C**, Transmission electron microscopy of subcutaneous capillaries at E 17.5. Both wild-type and *Plvap* $^{-/-}$ subcutaneous capillaries exhibit a continuous endothelium without fenestrae (*arrows*). At higher magnification, wild-type endothelial cells show numerous caveolae with a distinct 5- to 7-nm thick stomatal diaphragm (*arrows*). Caveolae are not bridged by a diaphragm in the endothelial cell membrane of the *Plvap* $^{-/-}$ embryo, but contain fluffy electron-dense material instead (*arrows*).

When areas with subcutaneous hemorrhages were more closely investigated, capillaries were observed in which the endothelial wall appeared to be incomplete (Figure 12A). Transmission electron microscopy confirmed the lack of endothelial integrity and revealed extensive defects in the endothelial lining of capillaries. In places, the defects were bridged by degranulated thrombocytes (Figure 12B, C).

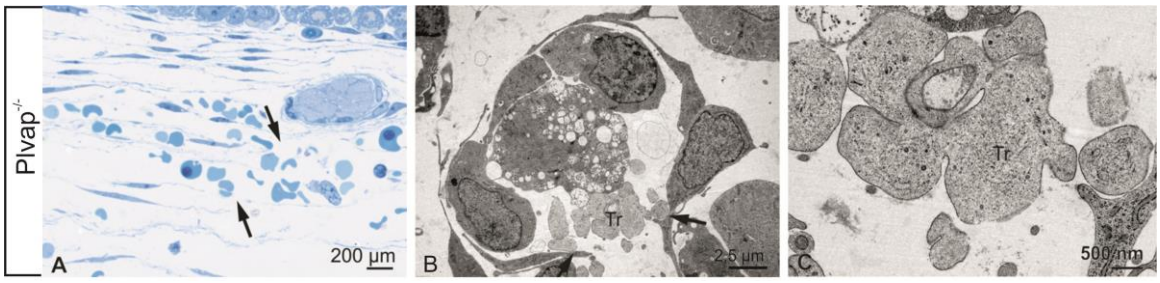

Figure 12: Loss of endothelial integrity in *Plvap* $^{-/-}$ embryos. **A**, Semithin section (Richardson's stain) through an area with subcutaneous hemorrhage in an E 16.5 *Plvap* $^{-/-}$ embryo. Erythrocytes are seen within and outside a capillary with a fragmented wall that contains large openings (*arrows*). **B** and **C**, Transmission electron microscopy of a capillary with a large opening (*arrows*) that is bridged by processes of degranulated thrombocytes (*Tr*). **C**, Higher magnification of **B**.

2.4.3 Cardiac defects in *Plvap* $^{-/-}$ embryos

Since total body edema and extensive hemorrhages in mouse embryos are very often associated with defects in cardiac morphogenesis (Clark et al., 1999; Dumont et al., 1994; Nasser et al., 2008; Patan, 1998; Peng et al., 2008; Puri et al., 1995; Ranger et al., 1998; Sato et al., 1995; Wu et al., 2000), we next investigated the hearts of *Plvap* $^{-/-}$ embryos and of their wild-type littermates. E 16.5 embryos were cut in the transverse plane and examined in serial sections from the cephalic to the caudal aspects of the specimens. In each of the three

Plvap $^{-/-}$ embryos that were investigated, histological serial sections stained with H and E showed a distinct muscular ventricular septal defect (Figure 13A). In the affected embryos, the cardiac ventricular walls were also thinner than those of the wild-type embryos (Figure 13A). By immunohistochemistry, specific immunoreactivity for PLVAP was observed in the endocardium of wild-type mice, but not in that of *Plvap* $^{-/-}$ embryos (Figure 13A). Moreover, the endocardium of cardiac ventricle and atrium as well as the endothelial cells of the associated cardiac vessels were stained for *β*-galactosidase indicating activity of the *Plvap* promoter (Figure 13B).

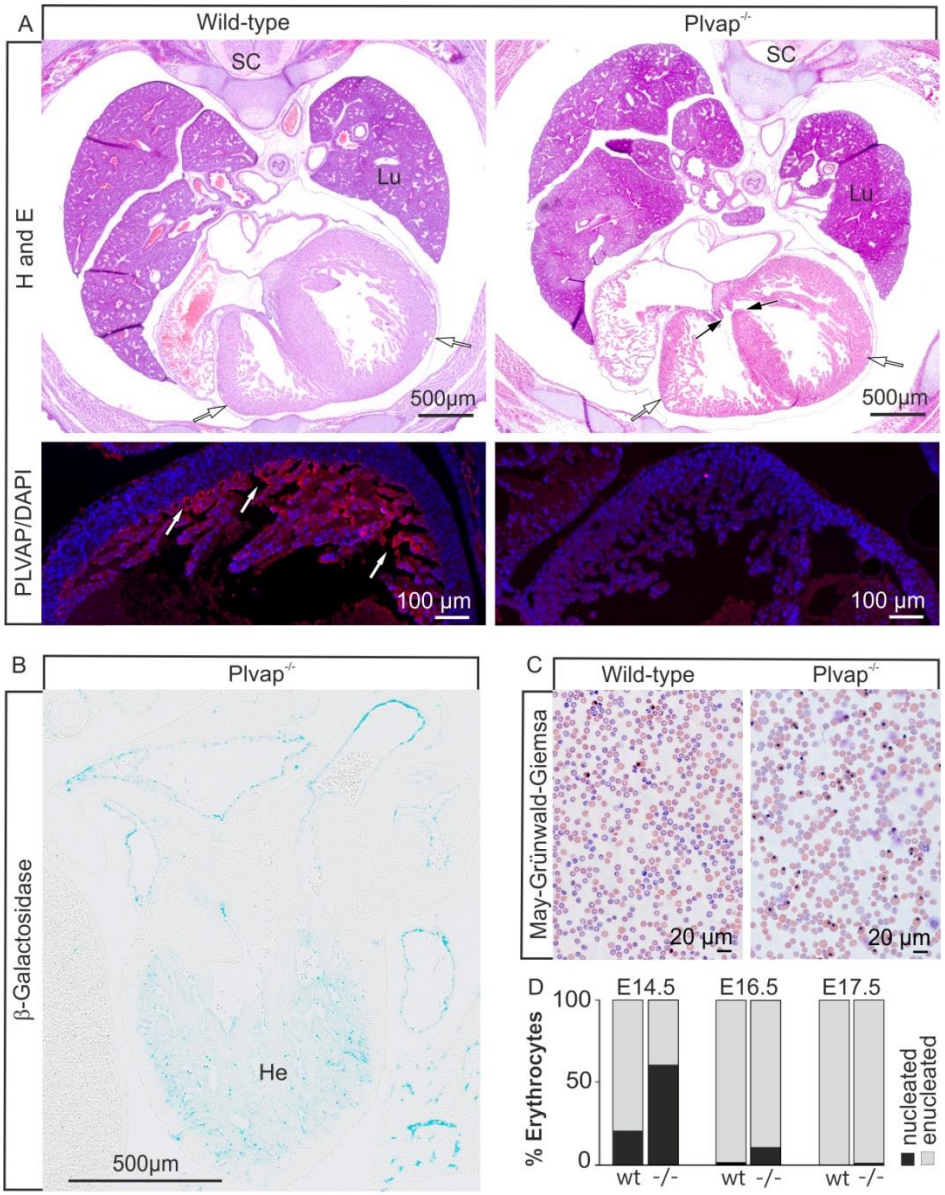

Figure 13: Cardiac and blood abnormalities in *Plvap* $^{-/-}$ embryos. **A**, H and E stained transverse paraffin sections through the thorax of wild-type and *Plvap* $^{-/-}$ embryos at E 16.5. The heart (He) of the *Plvap* $^{-/-}$ embryo shows a muscular ventricular septal defect (*black arrows*) and a thinner ventricular wall (*white arrow*) when compared with the wild-type control. Immunohistochemistry for PLVAP (*red*) shows positiv immuoreactivity in the

ventricular endocardium of the wild-type heart (*white arrows*), but not in that of the *Plvap* $^{-/-}$ embryo. Nuclear DNA is labeled with DAPI (*blue*). **B**, *β*-galactosidase staining in an E 15.5 *Plvap* $^{-/-}$ embryo shows activity of the *Plvap* promoter in ventricular and atrial endocardium, and in the endothelium of associated cardiac vessels. **C**, Smears of blood (May-Grünwald-Giemsa stain) collected from tail veins at E 16.5 show more nucleated red blood cells from the *Plvap* $^{-/-}$ embryo compared with the wild-type littermate. **D**, Ratio of nucleated erythrocytes to enucleated erythrocytes at different embryonic stages (E 14.5, E 16.5, E 17.5). *SC* spinal cord, *Lu* Lung.

Finally, we investigated the percentage of nucleated erythrocytes in blood smears from embryonic blood (Figure 13C), as we had observed in *Plvap* $^{-/-}$ embryos multiple nucleated erythrocytes in tissue sections of hemorrhages (Figure 10B, Figure 12A). In the blood smear of an E 14.5 wild-type embryo, 21 % of erythrocytes were found to be nucleated, a number that dropped to 1 % in an E 16.5 embryo, while essentially no nucleated erythrocytes were observed at E 17.5. In contrast, in *Plvap* $^{-/-}$ embryos, 61 % of erythrocytes were nucleated at E 14.5, 11 % at E 16.5 and still 2 % at E 17.5 (Figure 13D).

2.4.4 *Plvap* $^{-/-}$ mice in a mixed C57BL/6N/FVB-N background are viable and do not form fenestrae with diaphragm

In the course of our studies, we crossed *Plvap*-deficient mice that had been bred in a C57BL/6N genetic background with TIE2GFP mice that are in a FVB-N genetic background. While the initial goal was to take advantage of the GFP-labeling in endothelial cells of TIE2GFP mice, we observed that in the mixed C57BL/6N/FVB-N background, *Plvap* $^{-/-}$ animals are viable after birth and survive at the most up to an age of 4 weeks. E 17.5 embryos in the mixed background showed edema in the neck and back, but no visible hemorrhages (Figure 14A).

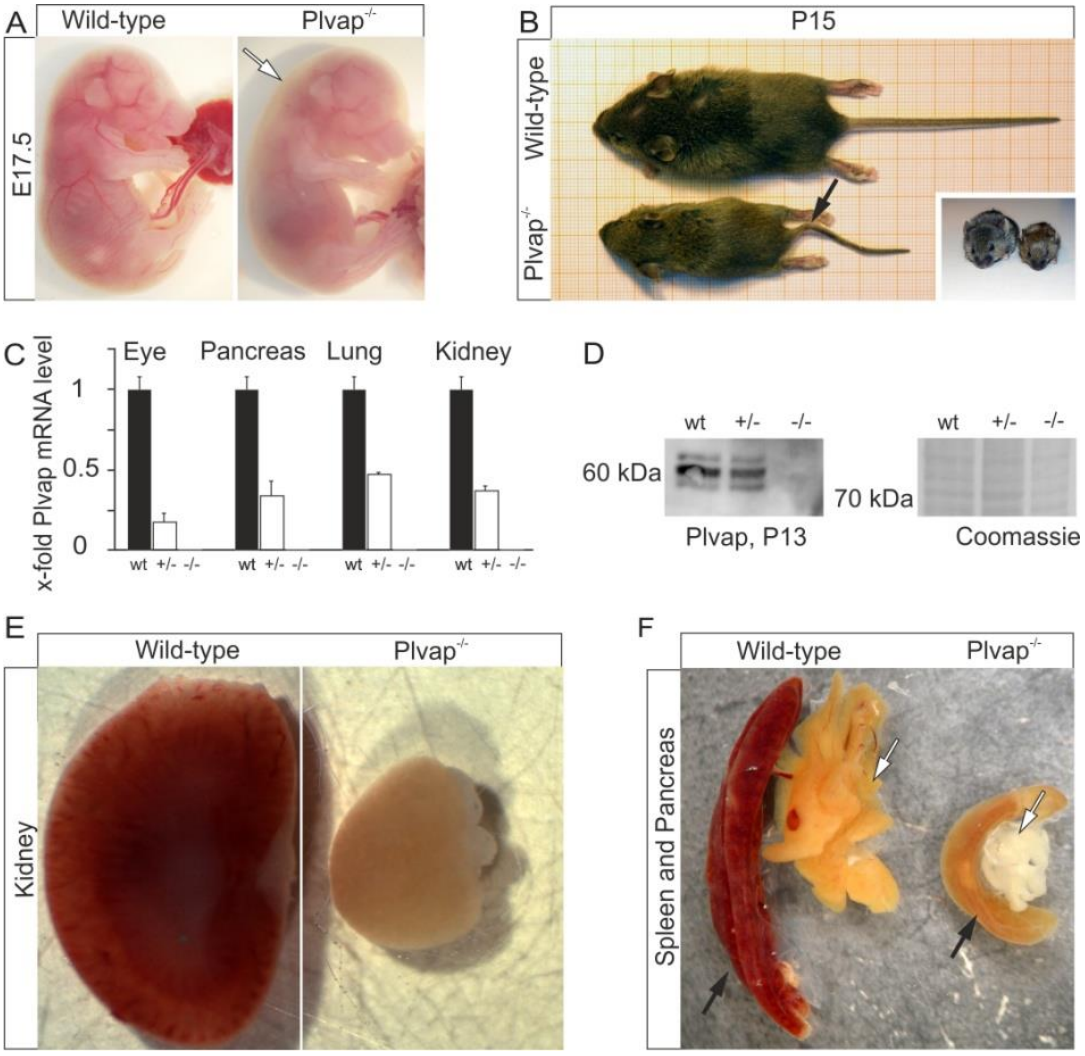

Figure 14: Phenotype of *Plvap* $^{-/-}$ animals in mixed C57BL/6N/FVB-N background. **A**, An E 17.5 *Plvap* $^{-/-}$ embryo shows edema in neck and back (*white arrow*) which is not seen in the wild-type littermate. **B**, A 15-day-old *Plvap* $^{-/-}$ animal with a kink in the tail (*arrow*) shows a marked reduction in body size when compared with its wild-type littermate. **C**, Real-time RT-PCR for *Plvap* mRNA in RNA from eye, pancreas, lung, and kidney of wild-type (wt), heterozygous (+/-) and homozygous (-/-) *Plvap*-deficient animals at 4 weeks of age. The mean value of wild-type RNA was set at 1. GNB2L was used as a reference gene. **D**, Western blot analysis for PLVAP in proteins isolated from kidneys of homozygous *Plvap*-deficient mice and their wild-type littermate at P 13. (**E**, **F**) Kidney (**E**), spleen (*black arrows*, **F**) and pancreas (*white arrows*, **F**) are smaller in a 3-week-old *Plvap* $^{-/-}$ animal when compared with the wild-type littermate and were very pale indicating anemia. Experiment in **C** performed by Sabrina Küspert. Experiment in **D** performed by Roswitha Seitz.

Postnatal, *Plvap* $^{-/-}$ mice show a marked reduction in body size when compared with wild-type littermates (Figure 14B). In addition, *Plvap* $^{-/-}$ mice typically show kinks in their tails that are not seen in wild-type littermates (Figure 14B). No ventricular septal defect was observed in tangential sections through the heart of 3-week-old mice (data not shown). When the expression of *Plvap* was analyzed by real-time RT-PCR at 4 weeks of age in organs known

to contain numerous capillaries with diaphragmed fenestrae and/or SD caveolae, we observed in eye, pancreas, lung, and kidney of *Plvap* $^{+/-}$ animals an approximately 50 % reduction in the amount of *Plvap* mRNA when compared with wild-type littermates, while no mRNA was detected in *Plvap* $^{-/-}$ animals (Figure 14C). Using Western blot analysis of proteins from kidneys of P13 *Plvap* $^{+/-}$ and wild-type embryos, three bands were observed at 55-60 KDa consisting with the presence of glycosylated and non-glycosylated forms of PLVAP (Hnasko et al., 2006). PLVAP immunoreactive bands were essentially absent in *Plvap* $^{-/-}$ animals (Figure 14D). Subsequently, the structure of two of these organs, kidney and pancreas, respectively, was investigated in more detail. Both kidney (Figure 14E) and pancreas (Figure 14F) were smaller in *Plvap* $^{-/-}$ mice when compared with the same organ from wild-type littermates and were very pale indicating anemia.

Immunostaining for PLVAP showed positive immunolabeling in interstitial capillaries of wild-type kidneys which was absent in those from *Plvap* $^{-/-}$ mice (Figure 15A). Using transmission electron microscopy of peritubular capillary endothelial cells in wild-type animals, numerous fenestrae with diaphragm were observed in areas in which the endothelial lining was thin (Figure 15B). Fenestrae were commonly arranged in rows and between neighboring fenestrae there was a regular distance of about 130 nm indicating their arrangement in typical sieve plates (Tse and Stan, 2010). In contrast, in *Plvap* $^{-/-}$ mice, the endothelial wall of interstitial peritubular capillaries was considerably thicker and fenestrae were not commonly observed (Figure 15B). In cross sections through peritubular capillaries, a considerable number of capillaries did not show fenestrae at all, while in others few endothelial openings with a diameter of 60-80 nm were observed in some parts of the circumference (Figure 15B). No diaphragms were observed in the endothelial openings of *Plvap* $^{-/-}$ peritubular capillaries (Figure 15B). In addition, SD caveolae were observed in wild-type capillaries (Figure 15B), but not in that of *Plvap* $^{-/-}$ animals.

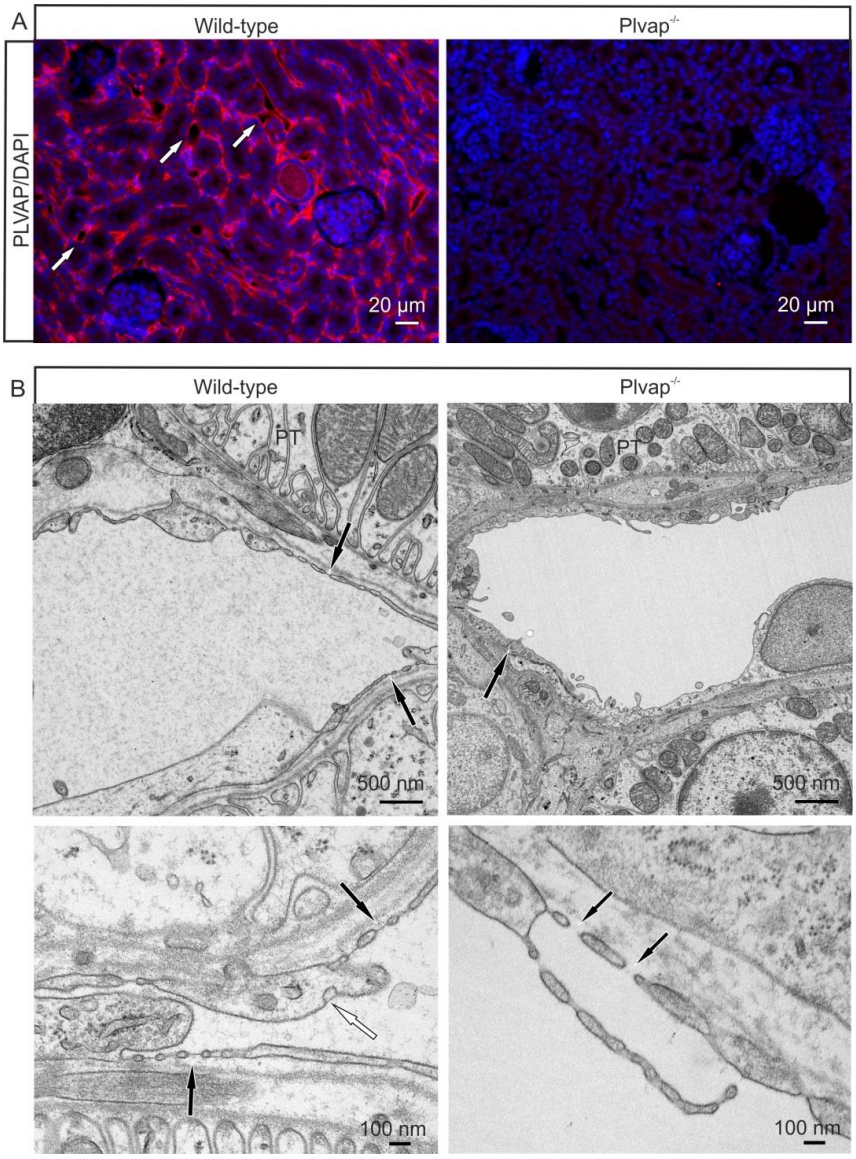

Figure 15: Peritubular capillaries in kidneys of *Plvap*-deficient animals do not form diaphragms. A, Immunolabeling for PLVAP (*red*) shows specific staining (*arrows*) in the peritubular capillaries of wild-type mice at 4 weeks of age, whereas no specific immunoreactivity is seen in kidneys of *Plvap* $^{-/-}$ littermates. Nuclear DNA is labeled with DAPI (*blue*). **B**, *Upper panels* transmission electron microscopy of a 4-week-old wild-type animal shows thin peritubular capillary endothelial cells with numerous fenestrae that are arranged in rows. In contrast, in the *Plvap* $^{-/-}$ littermate, the endothelial wall of a peritubular capillary is considerably thicker and does not form fenestrae. **B**, *Lower panels* higher magnification shows that fenestrae are bridged by a distinct diaphragm in wild-type capillaries (*black arrows*). In addition, a caveola with a stomatal diaphragm (*white arrow*) is seen. In contrast, the few endothelial openings that are formed in the *Plvap* $^{-/-}$ littermate are not bridged by a diaphragm (*black arrows*). *PT* proximal tubulus.

When pancreas was investigated, the parenchymal tissue of wild-type pancreas appeared to contain larger interstitial spaces than that of *Plvap* $^{-/-}$ littermates (Figure 16A, B). Staining for *β*-galactosidase was observed in capillaries of both the exocrine and endocrine pancreas in

Plvap $^{-/-}$ mice, but was essentially absent in wild-type littermates (Figure 16B). Quite comparable to the results obtained in peritubular kidney capillaries, endothelial cells between acini of the wild-type exocrine pancreas were thin and contained continuous rows of fenestrae (Figure 16C). Upon higher magnification, the fenestrae were bridged by diaphragms as were caveolae and transendothelial channels with stomatal diaphragms (Figure 16C). In contrast, in *Plvap* $^{-/-}$ animals, the wall of capillaries in the exocrine pancreas was considerably thicker and was continuous over large distances without any fenestrae. Some capillaries were detected that contained openings in parts of their circumference with diameters between 60 and 80 nm (Figure 16C). The openings did not contain diaphragms, but were rather filled with fluffy, electron-dense material (Figure 16C). Essentially comparable results were obtained when capillaries from the endocrine pancreas were examined (not shown).

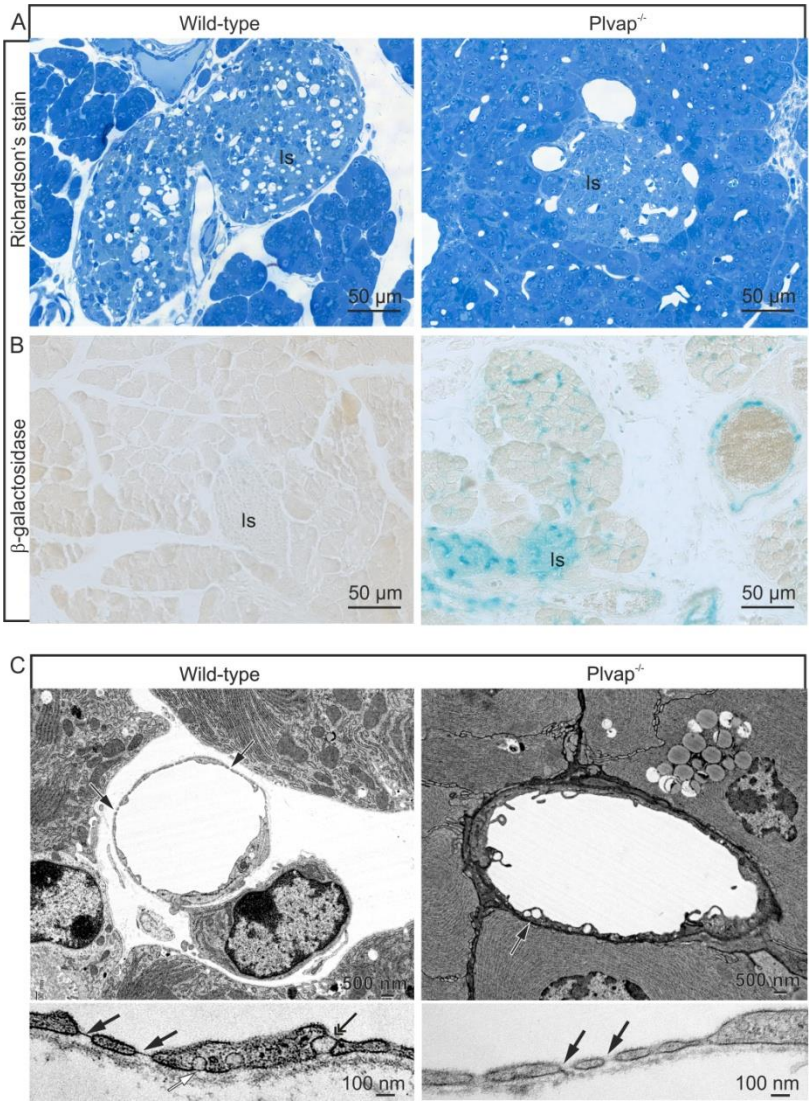

Figure 16: Capillaries in the pancreas of *Plvap*-deficient animals do not form diaphragms. **A**, *Upper panels* Semithin sections through the pancreas of 4-week-old animals. The wild-type control mouse shows larger

interstitial spaces then the *Plvap*-deficient littermate. **A**, *Lower panels* Positive staining for *β*-galactosidase is evident in capillaries of the exocrine and islets (Is) of endocrine pancreas in the *Plvap* $^{-/-}$ mouse, but not in that of the wild-type littermate. **B**, *Upper panels* Transmission electron microscopy of a wild-type capillary in the exocrine pancreas shows thin endothelial cells with numerous fenestrae (*arrows*). In contrast, in the *Plvap* $^{-/-}$ littermate, the endothelial lining (*arrow*) is considerably thicker and continuous without any fenestrae. **B**, *Lower panels* Upon higher magnification, the fenestrae of the wild-type animal are bridged by diaphragms (*black arrows*) as are caveolae (*white arrow*) and transendothelial channels (*double arrow*) with stomatal diaphragms. In contrast, the few endothelial openings that are formed in the *Plvap* $^{-/-}$ littermate are not bridged by diaphragms, but are partially filled with fluffy, electron-dense material (*arrows*). *Is* islet.

2.5 Discussion

We conclude that PLVAP is essential for the formation of diaphragms which bridge endothelial fenestrae, or the stomata of caveolae and transendothelial channels. Moreover, the lack of PLVAP and/or diaphragms causes a substantial decrease in the number of capillary openings in vascular beds that typically form fenestrated capillaries, such as the peritubular interstitium of the kidney or the exocrine and endocrine pancreas. The changes in the capillary phenotype correlate with a considerable retardation of postnatal growth and anemia. Depending on the respective genetic background, lack of PLVAP and/or diaphragms may cause embryonic lethality due to widespread hemorrhages and cardiac malformations.
The phenotype observed in *Plvap* $^{-/-}$ mice supports and extends data from previous observations of others obtained by *in vitro* assays. Stan and colleagues induced the upregulation of *Plvap* expression in cultured human umbilical vein endothelial cells (HUVEC) with phorbol myristate acetate (PMA) and observed the *de novo* formation of stomatal diaphragms in caveolae and transendothelial channels, as well as of fenestrae upon treatment (Stan et al., 2004). After applying RNA interference, none of the caveolae in siRNA-treated cells had a stomatal diaphragm present. In addition, no fenestrae or transendothelial channels were observed. Ioannidou and coworkers (Ioannidou et al., 2006) used the actin depolymerizing agent latrunculin A to induce fenestrae in the bEND5 mouse endothelioma cell line. By siRNA treatment, a 70 % reduction in the amounts of PLVAP was observed. The partial reduction in PLVAP did not cause a significant reduction in the amounts of fenestrae. Still, following treatment, a population of fenestrae did not form diaphragms. Fenestrae devoid of diaphragms had enlarged and variable diameters, whereas fenestrae that displayed regular or smaller-than-usual diameters contained diaphragms.

Clearly, our data obtained with transmission electron microscopy, showing a complete absence of diaphragms in fenestrae, caveolae, and transendothelial channels in *Plvap* $^{-/-}$ mice, strongly suggest that PLVAP is an integral molecular component of diaphragms that is critically required for their formation. Similar to the data obtained by an *in vitro* knock-down of *Plvap* (Stan et al., 2004), we did not observe an obvious reduction in the number of caveolae in endothelial cells of *Plvap* $^{-/-}$ mice. However, we did observe a substantial reduction in the number of fenestrations or endothelial openings in the two vascular beds that were investigated in detail, namely the exocrine and endocrine pancreas, and the peritubular interstitium of the kidney. In normal mice, basically all fenestrations of both these vascular beds are bridged by a diaphragm (Milici et al., 1985). Upon *Plvap* deficiency *in vivo*, the formation of endothelial openings is severely impaired, though not completely abolished, since some openings without diaphragm are still present. It is of interest to note that the few

endothelial openings in *Plvap* $^{-/-}$ mice usually appear not to be completely empty, but rather contain some fluffy electron-dense material indicating the presence of some molecules other than PLVAP. Possible candidates could be heparin sulfate proteoglycans that have been detected on the luminal surfaces of fenestrae providing distinct anionic charges (Simionescu et al., 1981b, 1981c). It appears to be more than likely that the substantial decrease in the number of endothelial fenestrae should cause a considerable reduction in transendothelial passage of water and solutes in the vascular beds affected. The almost complete absence of interstitial spaces in the pancreas of *Plvap* $^{-/-}$ mice is consistent with this assumption. Also the considerable decrease in body size of *Plvap* $^{-/-}$ animals could be the result of a functional impairment in the numerous organs that require fenestrated capillaries for normal function.

Another interesting aspect of our study is the fact that the phenotype observed upon *Plvap* deficiency critically depends on the respective genetic background. While *Plvap* $^{-/-}$ mice in a mixed C57BL/6N/FVB-N genetic background are born and survive for at least 4 weeks, a pure C57/BL/6N background results in embryonic lethality. Likely reasons for the lethal phenotype are widespread hemorrhages and failures in cardiac morphogenesis. The only endothelial structures with a diaphragm in the subcutaneous vessel that appear to be primarily affected by hemorrhages are caveolae with a stomatal diaphragm. Stomatal diaphragms may provide a mechanical stabilization for embryonic capillaries especially during the morphogenetic events during angiogenesis that require remodeling of capillary walls. Lack of diaphragms upon *Plvap* deficiency may increase the risk of breaks in the endothelial lining and cause hemorrhages. An alternative explanation could be related to the fact that caveolae are required for the proper organization of signaling pathways within endothelial cells by providing membrane domains for preformed signaling complexes (Frank et al., 2003b; Stan, 2005). Such signaling pathways might function in both angiogenesis and heart morphogenesis. As *caveolin 1*-deficient mice that form no caveolae in endothelial cells do not die during embryonic development (Drab et al., 2001; Razani et al., 2001), such a function in a signaling pathway should be specific for caveolae with stomatal diaphragms and should still be transferred by PLVAP even in the absence of caveolae. Recent studies that show rapid internalization and degradation of PLVAP in the absence of caveolae in *caveolin 1*-deficient mice argues against this hypothesis (Tkachenko et al., 2012).

An explanation for the higher number of primitive nucleated erythrocytes in *Plvap*-deficient embryos may be the higher need for oxygen carriers in the presence of multiple hemorrhages. In the mouse embryo, erythrocyte formation occurs at around E 8 in the yolk sac blood islands and results a day later in the release of primitive nucleated erythrocytes into the circulation (Brotherton et al., 1979). The nucleated cells persist in circulation until

about E 16 when they are finally replaced by mature erythrocytes originating from the liver which becomes the principal fetal hematopoietic organ (Keller et al., 1999).

In summary, functional analyses of *Plvap* $^{-/-}$ mice should help to clarify the specific role of endothelial fenestrae and their contribution to passage of water and solutes, and the relative importance of transcellular versus paracellular flow in different organs. In addition, they are expected to provide an animal model to clarify the specific function of stomatal diaphragms.

Chapter 3

The role of plasmalemma vesicle-associated protein (PLVAP) in endothelial cells of Schlemm's canal and ocular capillaries

(adapted from: Leonie Herrnberger, Kathrin Ebner, Benjamin Junglas, Ernst R. Tamm. **The role of plasmalemma vesicle-associated protein (PLVAP) in endothelial cells of Schlemm's canal and ocular capillaries**. Exp Eye Res. 2012, 105:27-33)

3 The role of plasmalemma vesicle-associated protein (PLVAP) in endothelial cells of Schlemm's canal and ocular capillaries

3.1 Abstract

Plasmalemma vesicle-associated protein (PLVAP, PV-1) is an endothelial protein that specifically localizes to diaphragms of fenestrae in fenestrated capillaries, and to stomatal diaphragms of caveolae. Here we investigated the localization of PLVAP in Schlemm's canal endothelium and ocular capillaries, and studied the structural effects of PLVAP deficiency. In mouse, pig, and human eyes, immunoreactivity for PLVAP was present in fenestrated capillaries of choroid and ciliary processes, but not in the continuous capillaries of the retina and ciliary muscle. In all three species staining for PLVAP was seen in the endothelia of the outflow vessels of aqueous humor e.g. Schlemm's canal (SC, mouse and human), aqueous plexus (AP, pig) and the scleral collector channels. Essentially comparable findings were observed when the expression of *β*-galactosidase was investigated in mutant heterozygous and homozygous *Plvap*-deficient mice with *LacZ* inserted into the *Plvap* locus. By transmission electron microscopy, the vast majority of caveolae in SC endothelial cells showed a stomatal diaphragm. In addition, solitary fenestrae or minipores with a diaphragm were occasionally observed in SC or AP of all three species. In contrast, mutant *Plvap* $^{-/-}$ mice showed a complete absence of stomatal diaphragms in SC caveolae while no SC minipores were observed. Moreover, diaphragms were absent in fenestrae of endothelial cells in the capillaries of the ciliary processes or the choriocapillaris, findings which were associated with a substantial decrease in the number of fenestrae. PLVAP is expressed in endothelial cells of Schlemm's canal and is essential for the formation of diaphragms in vascular endothelial cell of the eye.

3.2 Introduction

The structure of capillary endothelial cells is markedly dissimilar in the different vascular beds of the body (Tse and Stan, 2010). Depending on the respective needs for permeability of water and solutes, capillaries are of the discontinuous, continuous or fenestrated type. Discontinuous capillaries such as the sinusoids of the liver or the glomerular capillaries of the kidney form large, 100-200 nm wide, intracellular pores throughout their endothelial walls. Such pores are absent in the continuous capillaries of retina, brain, lung or skin. Fenestrated endothelia are present in capillaries with need for substantial filtration and transendothelial transport such as in ciliary processes and choriocapillaris of the eye, exocrine or endocrine glands, intestinal villi, or peritubular interstitium of the kidney. The characteristic hallmark of fenestrated capillaries is the presence of small transendothelial pores or fenestrae with a constant diameter of 62-68 nm, which extend through the full thickness of the endothelial cell. Fenestrae are bridged across their opening by a thin 5-6 nm non-membranous diaphragm (Clementi and Palade, 1969c; Friederici, 1969, 1968b). The presence of a diaphragm with associated basal lamina and glycocalyx may provide fenestrae with increased size and charge selectivity allowing only small molecules and limited amounts of plasma protein to pass (Levick and Smaje, 1987; Simionescu et al., 1981a, 1981b, 1981c). Accordingly, diaphragms are absent in the large pores of liver sinusoids or glomerular capillaries with substantially higher hydraulic conductivity than that of fenestrated capillaries (Renkin, 1977). Still, during development, liver sinusoids and glomerular capillaries first form fenestrae subtended by a diaphragm, which precede sinusoidal and glomerular pores (Bankston and Pino, 1980, 1980; Reeves et al., 1980).

So far, the only protein that has been identified as being part of fenestral diaphragms is plasmalemma vesicle-associated protein (PLVAP, PV-1), a cationic, integral membrane glycoprotein that is specifically expressed in endothelial cells. In addition, PLVAP is present in the stomatal diaphragms of caveolae and the diaphragms of transendothelial channels (Stan, 2005; Stan et al., 1999b). Caveolae with a stomatal diaphragm quite comparable in structure to the diaphragm of fenestrae (Bearer and Orci, 1985) are found in all fenestrated and sinusoidal endothelia (Bruns and Palade, 1968; Stan, 2005). Transendothelial channels are pores provided with two diaphragms, one luminal and one abluminal, which are predominately found in fenestrated endothelia (Milici et al., 1985). We recently generated mutant mice that lack PLVAP and observed that endothelial diaphragms do not form in the absence of PLVAP (Herrnberger et al., 2012b). Depending on the respective genetic background, lack of diaphragms in *Plvap*-deficient mice interferes with cardiac

morphogenesis, the integrity of embryonic vessels and the formation of fenestrated endothelial layers.

The endothelial lining of Schlemm's canal (SC) shows one of the highest hydraulic conductivities throughout the body allowing aqueous humor to pass from the anterior chamber via the trabecular meshwork into the lumen of SC. A specific requirement for the high hydraulic conductivity of SC appears to be the formation of large intracellular pores (I- and B-pores, respectively) with diameters of 0.1-2 µm (Johnson, 2006). In addition, solitary minipores with a diameter of about 60-65 nm and subtended by a diaphragm have been observed in the SC endothelium of monkey (Inomata et al., 1972) and human eyes (Tamm, 2009b). SC minipores are essentially similar in size and structure to the diaphragmed fenestrae of fenestrated capillaries, but are much more rarely formed in SC endothelial cells than in those of fenestrated endothelia. It has been hypothesized that the large I-pores of SC originate from those minipores (Bill and Mäepea, 1995), a scenario which would be quite similar to that seen during embryonic development of pores in liver sinusoids and glomerular capillaries. Since the molecular processes that are required for SC pore formation are completely unclear, we hypothesized that PLVAP might be an important molecular target to shed more light on the processes governing aqueous humor flow across the endothelium of SC. We therefore investigated if PLVAP is localized and expressed in SC endothelial cells.

3.3 Materials and methods

3.3.1 Tissues and animals

Pig eyes (7-8 months, post mortem time 3-4 h) were obtained from local abattoir and human eyes (64-91 years, post mortem time 6-24 h) were obtained at autopsy. Methods for securing human tissue were humane, included proper consent and approval, and complied with the Declaration of Helsinki. For immunohistochemistry of normal mouse eyes, animals from CD1 and NMR-1 genetic backgrounds were used. Mutant *Plvap*-deficient mice were established as described previously (Herrnberger et al., 2012b). Mutant *Plvap*-deficient mice in a C57BL/6N genetic background were crossed with TIE2GFP mice that are in a FVB-N genetic background. Eyes of wild-type, *Plvap* $^{+/-}$ and *Plvap* $^{-/-}$ littermates in a mixed C57BL/6N/FVB-N background (n= 6 for each genotype) were investigated.
Genotyping was routinely performed by PCR analysis, using two upstream primers located in intron 1 of *Plvap* (5'-AGAGCCTTCTCTGCCAAGTG-3') or in the inserted targeting cassette (5'-TCTCATGCTGGACTTCTTCG-3'), and a downstream primer located in intron 1 downstream of the cassette (5'-GGCTAGCCTGAGCTACAGAGG-3') resulting in a 672 bp PCR fragment for the wild-type allele and a 552 bp fragment for the targeted allele.

3.3.2 Immunohistochemistry

For immunohistochemistry, tissue samples were fixed in Carnoy's fixative (60 % methanol, 30 % chloroform, and 10 % acetic acid) for 4 h and washed in 0.1 M phosphate buffer. The samples were equilibrated in 10, 20, and 30 % sucrose for 4 h and embedded in Tissue-Tek optimal cooling temperature (OCT) compound (Sakura Finetek Europe B.V., Zoeterwoude, NL) at -20 °C. After removal of Tissue-Tek, cryosections were blocked with 0.2 % cold water fish gelatin (Aurion, Wageningen, Netherlands), 1 % BSA and 0.1 % Triton-X (all in 0.1 M PBS) for 1 h at room temperature. After blocking, sections of pig and human eyes were incubated with mouse monoclonal antibodies (clone PAL-E, IgG_{2a}, 1:50, Progen Biotechnik GmbH, Heidelberg, Germany) while sections from mouse eyes were treated with rat monoclonal antibodies pan ECA (clone MECA-32, IgG_{2a}, 1:50, Santa Cruz) both specific against PLVAP (Ioannidou et al., 2006; Niemelä et al., 2005), and with the endothelial cell marker anti-CD31/PECAM-1 IgG (1:20, R&D Systems, Wiesbaden, Germany) for double labeling. Alexa Fluor 488 (1:1000) rabbit anti-mouse IgG (Invitrogen) and donkey anti-rat IgG

(1:2000) conjugated to Cy3 (Jackson Immuno Research) were used as secondary antibodies and incubated for 1 h at room temperature. 4′,6-Diamidino-2-phenylindole (DAPI) was used to counterstain nuclear DNA. Slides were mounted in a medium containing DAPI (Vectashield; Vector Laboratories, Burlington, CA, USA) and analyzed under a fluorescence microscope (Zeiss Axio Imager). For negative controls, primary antibodies were omitted and the slides were incubated with secondary antibodies only.

3.3.3 Staining for *β* -galactosidase activity

To study promoter activity, *Plvap*-deficient mice were used in which the *Plvap* locus had been modified by insertion of an IRES:lacZ trapping cassette and a floxed promoter-driven neo cassette inserted into intron 1 of *Plvap* (Herrnberger et al., 2012b). Eyes were fixed in 2.5 % glutaraldehyde in 5 mM EGTA (pH 7.3) and 2 mM $MgCl_2$ dissolved in 0.1 M PBS for 4 h on ice with shaking. After three 30 min rinses in washing buffer (2 mM Mg Cl_2, 0.01 % sodium deoxycholate, 0.02 % Nonidet-P40 in 0.1 M PBS), *β* -galactosidase activity was visualized in X-Gal staining solution (0.1 M PBS, 2 mM $MgCl_2$, 0.01 % sodium deoxycholate, 0.02 % Nonidet-P40, 5 mM potassium ferrocyanide, 5 mM potassium ferricyanide, 1 mg/ml X-Gal). Eyes were stained for 24 h at 37 °C in the dark, washed 3 times for 5 min in washing buffer and embedded in paraffin.

3.3.4 Transmission electron microscopy

For transmission electron microscopy of mouse tissues, deeply anesthetized mice (120 mg/kg of body weight i.m. ketamine and 8 mg/kg of body weight i.m. xylazine) were fixed by intracardial perfusions with 2.5 % glutaraldehyde in 0.1 M cacodylate buffer (pH 7.4) each. Pig eyes were fixed by anterior chamber perfusion at 2 or 5 mmHg using the same fixative. After fixation, eyes were treated with 1 % OsO_4, 0.8 % $K_4[Fe(CN)_6]$ in 0.1 M cacodylate buffer for 1.5 h, dehydrated with graded ethanol solutions and embedded in Epon (Roth, Karlsruhe, Germany). Semithin sections were stained with Richardson' stain (Richardson et al., 2009)

3.3.5 Quantitative analysis

For quantitative analysis of the number of fenestrations in the choriocapillaris of *Plvap* $^{-/-}$ mice and wild-type littermates, the total number of fenestrations was counted along the side of capillaries facing the retinal pigmented epithelium (RPE) comprising a total length of 110 mm in wild-type animals and 306 mm in *Plvap* $^{-/-}$ mice. The number of fenestrations per mm capillary length was determined and expressed as mean ± SEM. Statistical analysis was done by a two-tailed Student's t-test and p values ≤ 0.05 were considered to be statistically significant.

3.4 Results

Immunostaining with antibodies against PLVAP showed strong and specific labeling in the fenestrated endothelial cells of the choriocapillaris in mouse, pig (Figure 17) and human eyes (not shown). In contrast, capillaries of the retina with a continuous endothelial layer were only immunoreactive for antibodies against the endothelial cell marker CD31, but not for PLVAP (Figure 17). In the chamber angle of the pig eye, positive immunolabeling for PLVAP was observed in the endothelial cells of the aqueous plexus, which also stained for CD31 (Figure 17). In contrast, no staining was observed in cells of the trabecular meshwork (Figure 17). Essentially comparable results were observed in sections through the human chamber angle where SC endothelial cells were labeled for both PLVAP and CD31, while TM cells were not immunoreactive for both types of antibodies (Figure 17). The capillaries of the ciliary muscle which have a continuous endothelial layer (Tamm and Lütjen-Drecoll, 1996) stained positive for CD31, but were not stained with antibodies against PLVAP (Figure 17). In the anterior mouse eye, staining for PLVAP was seen in the capillaries of the ciliary processes, which are of the fenestrated type (Tamm and Lütjen-Drecoll, 1996; Tamm, 2010). In addition, there was an intense staining of the endothelial cells of SC (Figure 17). In all three species, positive immunoreactivity for PLVAP was seen in the scleral collector channels of aqueous humor (Figure 17).

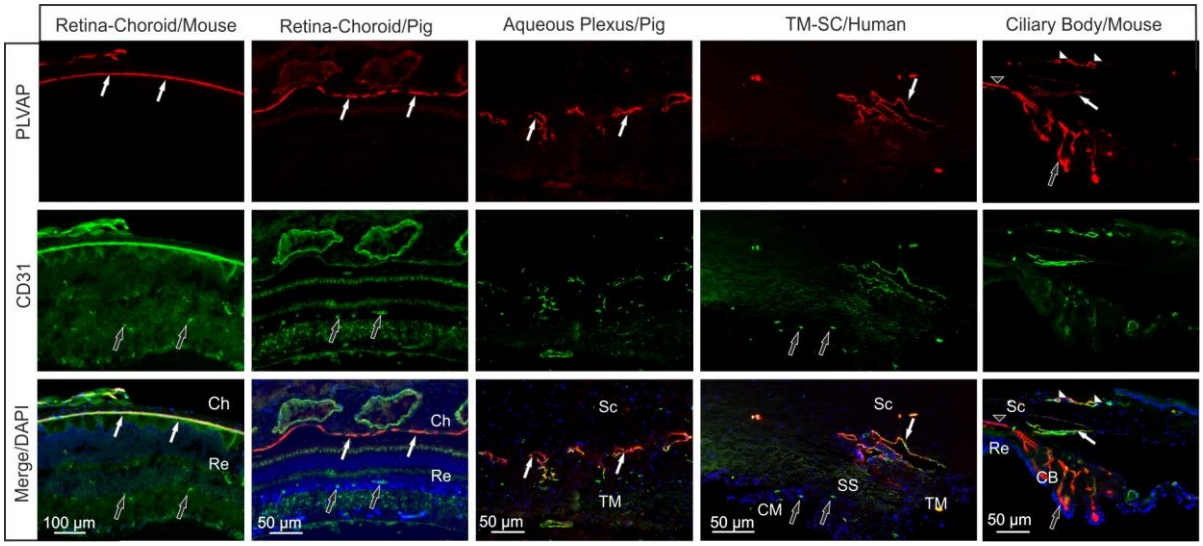

Figure 17: Double immunolabeling with antibodies against both PLVAP (*red*) and CD31 (*green*). Nuclear DNA was labeled with DAPI (*blue*). Immunostaining of retina and choroid with antibodies against PLVAP shows strong and specific labeling of the choriocapillaris in mouse and pig eye (*solid white arrows*). In contrast, capillaries of the retina are immunoreactive for antibodies against the endothelial cell marker CD31, but not for PLVAP (*black arrows*). In a frontal section through the chamber angle of a pig eye, positive immunolabeling for PLVAP is observed in the endothelial cells of the aqueous plexus (*solid white arrows*), which also stained for CD31. In a meridional section through the human chamber angle, SC endothelial cells are labeled for both

PLVAP and CD31 (*solid white arrows*). The capillaries of the ciliary muscle stain positive for CD31, but not for PLVAP (*black arrows*). In the anterior mouse eye, staining for PLVAP is seen in the capillaries of the ciliary body (*black arrows*) and the endothelial cells of SC (*solid white arrows*). Positive immunoreactivity for PLVAP is seen in the scleral collector channels (*solid white arrowheads*) and the choriocapillaris (*black arrowhead*). *Re* Retina, *Ch* Chroid, *Sc* Sclera, *TM* Trabecular meshwork, *SS* Scleral spur, *CM* Ciliary muscle, *CB* Ciliary body.

We next investigated the eyes of *Plvap*-deficient mice. By light microscopy of semithin sections from 3-week-old *Plvap* $^{-/-}$ animals and their wild-type littermates, no obvious structural defects were observed in Schlemm's canal, trabecular meshwork and ciliary body (Figure 18).

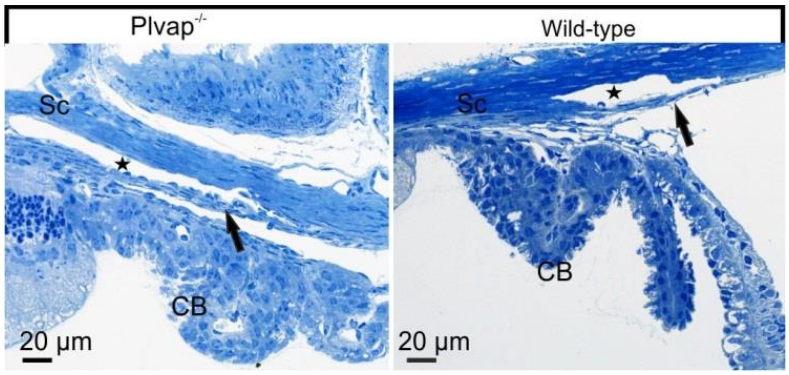

Figure 18: Semithin section (Richardson's stain) through the anterior eye of a 3-week-old *Plvap* $^{-/-}$ mouse and its wild-type littermate. Schlemm's canal (*asterisks*), trabecular meshwork (*arrows*) and ciliary body (*CB*) are visible in both eyes. *Sc*. Sclera.

Plvap promoter activity was assessed by staining for *β*-galactosidase in *Plvap* $^{+/-}$ and *Plvap* $^{-/-}$ mice with *LacZ* as a reporter gene inserted into the *Plvap* locus. Wild-type littermates did not stain for *β*-galactosidase, neither in retina and choroid of the posterior eye, nor in ciliary body, trabecular meshwork and Schlemm's canal endothelium of the anterior eye (Figure 19). In contrast, both *Plvap* $^{+/-}$ and *Plvap* $^{-/-}$ mice showed intense staining for *β*-galactosidase in the choriocapillaris essentially correlating with the results obtained by PLVAP immunohistochemistry. In the anterior eyes of *Plvap* $^{+/-}$ animals, a distinct labeling for *β*-galactosidase was observed in endothelial cells of the ciliary body capillaries (Figure 19). Staining was also seen in some, but not all, cells of Schlemm's canal endothelium (Figure 19). In contrast, in homozygous *Plvap* $^{-/-}$ mice, all endothelial cells of Schlemm's canal were labeled as were those of scleral collector channels (Figure 19). In the ciliary body of *Plvap* $^{-/-}$ animals, the entire stroma was strongly stained for *β*-galactosidase (Figure 19), a finding that

we attribute to diffusion of high amounts of reaction product from endothelial cells of ciliary body capillaries. Overall, the results obtained in mice with a knock-in of *LacZ* into the *Plvap* locus to visualize promoter activity strongly correlated with those obtained by PLVAP immunohistochemistry.

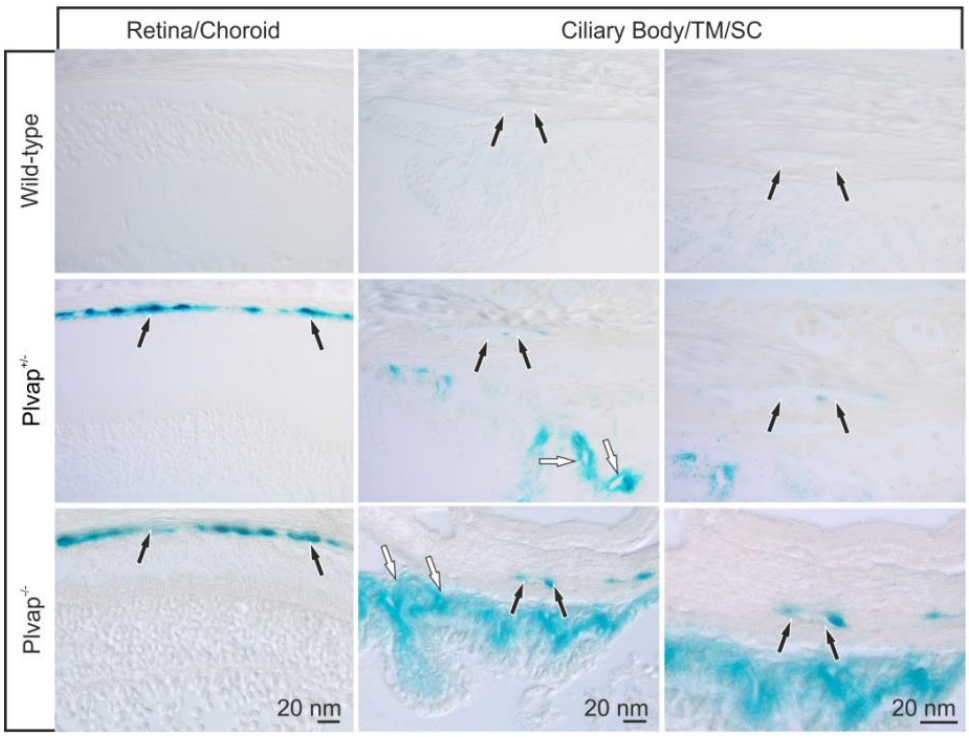

Figure 19: Promoter activity of *Plvap* visualized by staining for the reporter gene *β*-galactosidase (*blue*). Panels on right hand side are higher magnifications of panels in the middle. Wild-type mice do not stain for *β*-galactosidase, neither in retina and choroid of the posterior eye, nor in ciliary body, trabecular meshwork and Schlemm's canal endothelium (*black solid arrows*) of the anterior eye. Both *Plvap* $^{+/-}$ and *Plvap* $^{-/-}$ mice show intense staining for *β*-galactosidase in the choriocapillaris in sections through retina and choroid (*solid black arrows*), and in endothelial cells of ciliary body capillaries (*white arrows*) in sections through ciliary body, trabecular meshwork (*TM*) and Schlemm's canal (*SC*). In the ciliary body of the *Plvap* $^{-/-}$ animal, the entire stroma is strongly stained for *β*-galactosidase indicating stronger expression and diffusion of reaction product. In the *Plvap* $^{+/-}$ animal staining is also seen in some cells of Schlemm's canal endothelium (*solid black arrows*). In contrast, in the homozygous *Plvap* $^{-/-}$ mouse, all endothelial cells of Schlemm's canal are labeled (*solid black arrows*) as are those of scleral collector channels.

Immunostaining for PLVAP was absent in eyes from *Plvap* $^{-/-}$ mice (Figure 20), but was seen in endothelial cells of Schlemm's canal, ciliary process capillaries and choriocapillaris in wild-type littermates.

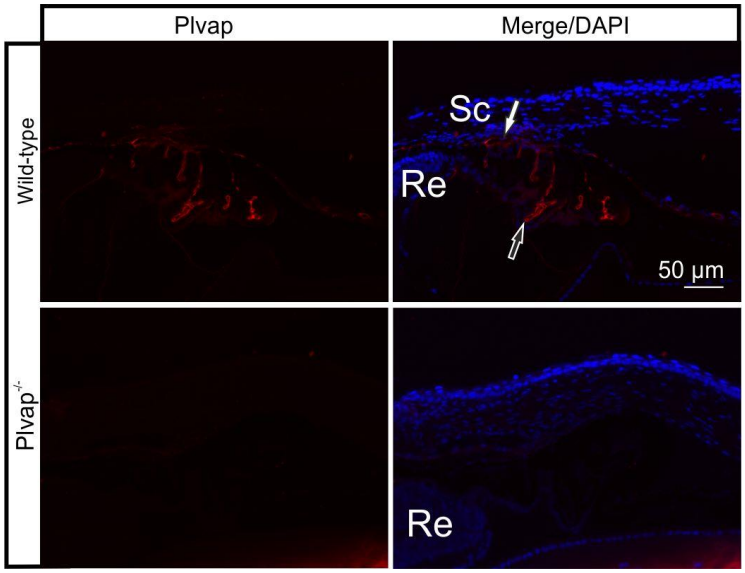

Figure 20: Immunostaining for PLVAP in the anterior eye of a 2-week-old wild-type mouse and its *Plvap*-deficient littermate. The wild-type animal shows positive immunoreactivity for PLVAP (*red*) in endothelial cells of Schlemm's canal (*solid white arrow*), ciliary body capillaries (*black arrow*) and choriocapillaris, whereas immunostaining for PLVAP is absent in the *Plvap* $^{-/-}$ littermate. Nuclear DNA was labeled with DAPI (*blue*). *Re* Retina, *Sc* Sclera.

Since localization and expression of PLVAP were seen throughout the entire circumference of SC's endothelial wall while diaphragmed SC minipores have been reported to be only rarely present, we analyzed SC endothelium for the presence of caveolae with stomatal diaphragms. By transmission electron microscopy, the vast majority of SC caveolae in mouse (Figure 21), pig and human SC (not shown) showed a distinct diaphragm. Accordingly, the neck or stoma of the caveolae was bridged by a distinct, 5-7 nm thick, electron-dense diaphragm (Figure 21). Similar to those observed in human and monkey SC, we occasionally detected solitary minipores with a diaphragm in SC endothelial cells of mouse (Figure 21) and pig eyes (not shown). Minipores were considerably rarer than caveolae with stomatal diaphragms. In our material, we did not find conclusive evidence for the presence of transendothelial channels in SC endothelium. In contrast, caveolae with stomatal diaphragms were invariably absent in SC endothelial cells of *Plvap* $^{-/-}$ mice (Figure 21). Here, the neck of caveolae was not bridged by a diaphragm, but contained some ill-defined, fluffy electron-dense material instead (Figure 21). Minipores with a diaphragm were not observed in SC endothelial cells of *Plvap* $^{-/-}$ mice.

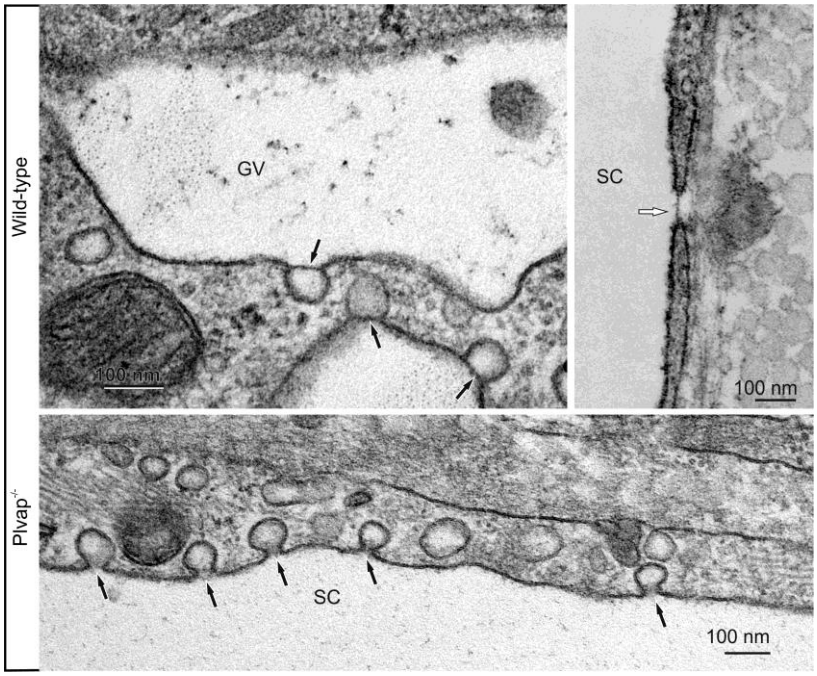

Figure 21: Transmission electron microscopy of SC endothelium in both wild-type and *Plvap* $^{-/-}$ mice. In the wild-type animal, caveolae with a stomatal diaphragm (*black arrows*) are seen in endothelial cells that form a giant vacuole (*GV*). In addition, solitary minipores with a diaphragm are observed (panel on right hand side, *white arrow*). In contrast, in the *Plvap* $^{-/-}$ mouse, the neck of caveolae is not bridged by a diaphragm, but contains some ill-defined, fluffy electron-dense material instead (*black arrow*). *SC* Schlemm's canal. Picture of fenestrae with fenestral diaphragm (upper right-handed picture) reproduced from Kathrin Ebner (Ebner, 2009), with permission.

By transmission electron microscopy of the choriocapillaris in wild-type animals, numerous fenestrae with diaphragm were observed in areas in which the endothelial lining was thin and facing the basal side of the RPE (Figure 22). Fenestrae were commonly arranged in rows indicating their arrangement in typical sieve plates (Tse and Stan, 2010). In *Plvap*-deficient animals, endothelial cells of the choriocapillaris often appeared to be bi-layered on their RPE side, as they formed long and thin cytoplasmic protrusions that reached into the vascular lumen (Figure 22). Fenestrae were observed both on the endothelial side of the capillaries facing the RPE and in their luminal protrusions. None of the fenestrae was bridged by a diaphragm, but rather contained some fluffy and ill-defined electron-dense material (Figure 22).

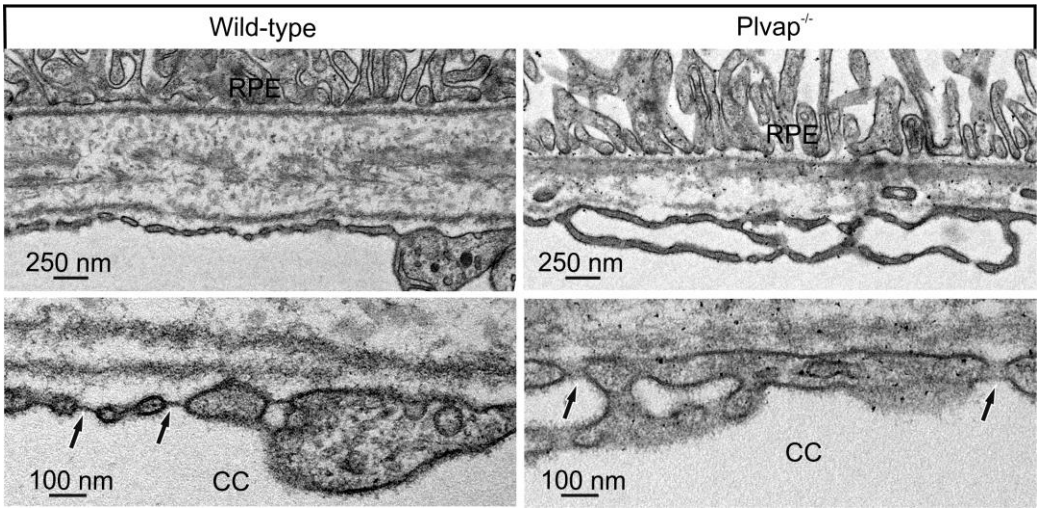

Figure 22: Transmission electron microscopy of choriocapillaris in 4-week-old wild-type and *Plvap* $^{-/-}$ mice. In the wild-type animal, numerous fenestrae arranged in rows and covered by a diaphragm (*black arrows*) are seen in the endothelial cells adjacent to the retinal pigmented epithelium (*RPE*). In the *Plvap* $^{-/-}$ littermate endothelial cells form long and thin cytoplasmic protrusions that reach into the vascular lumen. Fenestrae are not bridged by a diaphragm, but are filled with fluffy, electron-dense material instead (*black arrows*). *CC* Choriocapillaris.

In addition, the number of fenestrae was significantly reduced by about one third when compared to that of wild-types littermates (Figure 23). Essentially comparable structural changes were observed for the fenestrated capillaries of the ciliary processes (not shown).

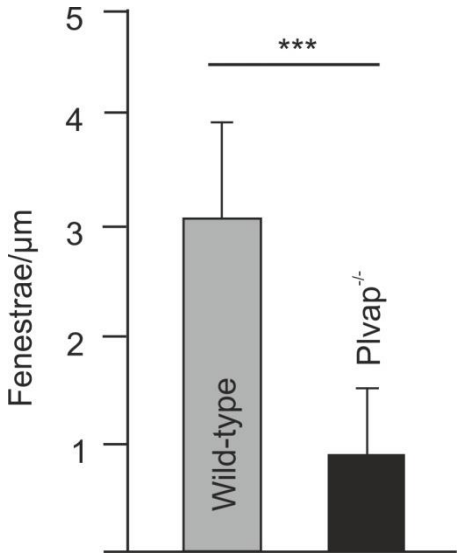

Figure 23: Quantitative analysis of the number of fenestrae per µm endothelial length in the choriocapillaris of wild-type and *Plvap* $^{-/-}$ mice. N = 2 each, mean ± SD, ***p ≤ 0.001.

3.5 Discussion

We conclude that PLVAP is expressed and localized in endothelia of aqueous humor outflow vessels, and is essential for the formation of endothelial diaphragms in the eye. The conclusions rest upon (1) the finding of specific immunoreactivity for PLVAP in endothelial cells of SC and aqueous plexus in mouse, pig and human eyes, (2) the expression of the reporter gene *LacZ* under the control of the *Plvap* promoter in SC endothelial cells of mutant *Plvap* $^{+/-}$ and *Plvap* $^{-/-}$ mouse eyes, (3) the observation of diaphragmed caveolae and minipores in SC endothelial cells, and (4) the absence of diaphragms in endothelia of SC, ciliary process capillaries and choriocapillaris in *Plvap* $^{-/-}$ mice.

The deletion of PLVAP did not only cause the absence of diaphragms in vascular endothelial cells of the eye, but also led to a significant reduction in the number of fenestrae in fenestrated ocular capillaries. We recently reported quite comparable findings for the fenestrated capillaries in the pancreas or the peritubular interstitium of the kidney (Herrnberger et al., 2012b). While our findings indicate that PLVAP is essential for the formation of proper diaphragms in vascular endothelia, they also strongly indicate that PLVAP and/or diaphragms are important, although not essential, for the development of transendothelial pores. It is reasonable to assume that the fenestrae in the capillaries of the ciliary processes or the choriocapillaris play an important role in facilitating flow of water and solutes from the capillary lumen to the interstitium and *vice versa*. *Plvap*-deficient mice appear to be an ideal model to study if lack of fenestrae and absence of diaphragms cause changes in ciliary process and choroidal fluid dynamics, and if those changes impair the secretion of aqueous humor or retinal function.

Since SC caveolae with diaphragm are considerably more numerous than SC diaphragmed minipores it is more than likely that they are the primary site of PLVAP immunolabeling. The specific function of caveolae with stomatal diaphragms is essentially unclear. It has been hypothesized that caveolae with stomatal diaphragms may fuse from luminal and abluminal sides of endothelial cells to form transendothelial channels which may then collapse to form diaphragmed fenestrae (Roberts and Palade, 2000). Diaphragmed fenestrae are very likely identical with the solitary diaphragmed minipores of SC (Inomata et al., 1972; Tamm, 2009a) which may burst in response to aqueous flow and open to the large size transient intracellular I-pores that are typical for this kind of endothelial layer. We did not observe any minipores in SC endothelial cells of *Plvap*-deficient mice, a finding which appears to indicate that their number has been substantially reduced, quite comparable to the number of endothelial fenestrae in the choriocapillaris. Still, SC minipores are also rare in wild-type animals, a fact that has precluded a quantitative analysis so far comparable to that we performed in the choriocapillaris. On the other hand, to test the functional role of PLVAP

and/or SC minipores in I-pore formation, it seems feasible to visualize I-pores by scanning electron microscopy and to quantify the number of I-pores, a study which is currently performed in our laboratory. *Plvap*-deficient mice appear to be an important model to study the biology of pore formation in SC endothelium.

Chapter 4

Pore formation in the endothelial wall of liver sinusoids depends on plasmalemma vesicle-associated protein (PLVAP) and is critically required for the passage of lipoproteins

(adapted from: Leonie Herrnberger, Robert Hennig, Werner Kremer, Claus Hellerbrand, Achim Göpferich, Hans Robert Kalbitzer, and Ernst R Tamm.
Pore formation in the endothelial wall of liver sinusoids depends on plasmalemma vesicle-associated protein (PLVAP) and is critically required for the passage of lipoproteins. Submitted)

4 Pore formation in the endothelial wall of liver sinusoids depends on plasmalemma vesicle-associated protein (PLVAP) and is critically required for the passage of lipoproteins

4.1 Abstract

Hepatic sinusoidal endothelial cells are characterized by the presence of fenestrations. The molecular mechanisms that control the formation of the fenestrations are unclear. Here we report that mice deficient in plasmalemma vesicle-associated protein (PLVAP) develop a distinct phenotype that is caused by the lack of sinusoidal fenestrations. PLVAP was expressed in endothelial cells of the liver in wild-type mice, but not in *Plvap*-deficient littermates. *Plvap*$^{-/-}$ mice suffered from a pronounced and highly significant reduction in the number of sinusoidal fenestrations which was seen by transmission and scanning electron microscopy. The lack of fenestrations was associated with an impaired passage of macromolecules such as FITC-dextran and quantum dot nanoparticles from the sinusoidal lumen into Disse's space. *Plvap*-deficient mice showed a pronounced hyperlipoproteinemia as evidenced by milky plasma and the presence of lipid granules that occluded kidney and liver capillaries. By NMR spectroscopy of plasma, the nature of hyperlipoproteinemia was identified as massive accumulation of chylomicron remnants, while the amounts of low density and high density lipoproteins were reduced. At around three weeks of life, *Plvap*-deficient livers developed extensive multivesicular steatosis, steatohepatitis, and fibrosis. PLVAP is critically required for the formation of fenestrations in sinusoidal endothelial cells. Lack of fenestrations caused by PLVAP deficiency substantially impairs the passage of chylomicron remnants between liver sinusoids and hepatocytes, and finally leads to liver damage.

4.2 Introduction

Endothelial cells of liver sinusoids differ from that of other capillaries because of the presence of open fenestrations and the absence of a basal lamina (Aird, 2007b; Braet and Wisse, 2002; McCuskey, 2008; Wisse et al., 1996). The diameter of the sinusoidal fenestrations varies between different species and measures 107 ± 1.5 nm (mean ± SEM) in the human liver (Wisse et al., 2008), while for the mouse liver diameters of 141 ± 5.4 nm (mean ± SEM) (Wisse et al., 2008), 99 ± 18 nm (mean ± SD) (Steffan et al., 1987) or 78 ± 12 (mean ± SEM) (Warren et al., 2010) have been reported. A specific function of liver sinusoids is the filtration of particles that are exchanged between the sinusoidal lumen and the space of Disse, allowing only particles smaller than the fenestrae to reach the hepatocytes or to leave the space of Disse (Wisse et al., 1985). Such a filter function appears to be especially important for the passage of lipoproteins. In support of this are observations of numerous chylomicron remnants with a size smaller than the diameter of fenestrations in the space of Disse of breastfeeded rat pups (Naito and Wisse, 1978). Moreover, multiple studies found evidence for a negative correlation between fenestration size and number, and the plasma concentration of larger lipoproteins (Braet and Wisse, 2002; Carpenter et al., 2005).

The proliferation and survival of sinusoidal endothelial cells (Gerber et al., 1999), as well as their capability to form fenestrations (Carpenter et al., 2005), depend on vascular endothelial growth factor (VEGF) that is secreted from hepatocytes (Carpenter et al., 2005). Otherwise very little is known about the signaling mechanisms that modulate the maintenance and turnover of fenestrations in liver sinusoids. Multiple agents have been shown to modulate size and numbers of fenestrations (Braet and Wisse, 2002). Still, a common theme indicating a specific molecule that is part of the biological process which is required to form a pore in the wall of a sinusoidal endothelial cell in the liver has not been identified.

Capillary endothelial cells of other organs with high demands for the passages of fluids and solutes differ from sinusoidal endothelial cells of the liver as they form fenestrae that are covered by a thin 5-6 nm non-membranous diaphragm (Aird, 2007a, 2007b). The only protein that has been identified to be a component of endothelial diaphragms is plasmalemma vesicle-associated protein (PLVAP, synonyms: MECA32, PV-1), an endothelial-specific, cationic, integral membrane glycoprotein (Stan et al., 1999a, 1999b). We and others recently showed that PLVAP is critically required for the formation of endothelial diaphragms which are completely absent in endothelia of *Plvap*-deficient mice (Herrnberger et al., 2012b; Stan et al., 2012).

Here we report that the absence of PLVAP in *Plvap*-deficient mice causes a pronounced reduction in the number of fenestrations in sinusoidal endothelial cells of the liver. Our results indicate that PLVAP is not only required for the formation of endothelial diaphragms, but also for the formation of endothelial fenestrae, even of those without diaphragms. The lack of sinusoidal fenestrations impairs the passage of macromolecules between the sinusoidal lumen and Disse's space. A direct result is the presence of severe hyperlipoproteinemia caused by accumulation of chylomicron remnants in the plasma of *Plvap*-deficient animals. The phenotype provides clear molecular evidence for the assumption that open fenestrae in liver sinusoidal cells are critically required for the passage of lipoproteins.

4.3 Materials and Methods

4.3.1 Animals

All procedures conformed to the tenets of the National Institutes of Health Guidelines on the Care and Use of Animals in Research, the EU Directive 2010/63/E, institutional guidelines and the Uniform Requirements for Manuscripts Submitted to Biomedical Journals. *Plvap*$^{-/-}$ mice were used as described previously (Herrnberger et al., 2012b). Mice were kept in a mixed C57BL/6N/FVB-N background. All experiments were performed in mice of either sex. Genotyping was routinely performed by PCR analysis, using two upper primers located in intron 1 of *Plvap* (5'-AGAGCCTTCTCTGCCAAGTG-3') and in the inserted cassette (5'-TCTCATGCTGGACTTCTTCG-3') and a lower primer located in intron 1 downstream of the cassette (5'-GGCTAGCCTGAGCTACAGAGG-3') resulting in a 672 bp PCR fragment for the wild-type allele and a 552 bp fragment for the targeted allele. DNA was obtained from tail tips. PCR was performed in 15 µl reaction volumes containing standard buffer, 0.1 µM of each primer, 1 mM dNTPs, 2.5 mM $MgCl_2$, 8% glycerol, 0.2 mM cresol red sodium salt (Sigma, Taufkirchen, Germany) and 0.25 U Taq-Polymerase (New England Biolabs, Taufkirchen, Germany). The cycling conditions consisted of an initial 3 min denaturing step at 94°C, followed by 34 cycles for 30 s at 94°C, for 1 min at 65°C, and for 1 min 15 s at 72°C.

4.3.2 Electron microscopy

For transmission electron microscopy of mouse livers, deeply anesthetized mice (120 mg/kg body weight i.m. ketamine and 8 mg/kg body weight i.m. xylazine) were either fixed by intracardial perfusion with 2.5% glutaraldehyde in 0.1 M cacodylate buffer (pH 7.4) followed by immersion fixation in 2.5% glutaraldehyde in 0.1 M cacodylate buffer (pH 7.4) overnight, or by immersion fixation alone. Afterwards, livers were treated with 1% OsO_4, 0.8% $K_4[Fe(CN)_6]$ in 0.1 M cacodylate buffer for 1.5 h, dehydrated with graded ethanol solutions and embedded in Epon (Roth, Karlsruhe, Germany). Semithin sections were stained with Richardson' stain (Richardson et al., 2009). Ultrathin sections were stained with uranyl acetate and lead citrate, and analyzed on a transmission electron microscope (Libra, Zeiss). For scanning electron microscopy of mouse livers, deeply anesthetized mice (120 mg/kg body weight i.m. ketamine and 8 mg/kg of body weight i.m. xylazine) were fixed by intracardial perfusion with 2.5% glutaraldehyde in 0.1 M cacodylate buffer (pH 7.4). Liver samples were isolated and further fixed by immersion in 2.5% glutaraldehyde in 0.1 M

cacodylate buffer (pH 7.4) overnight. After treatment with 1% OsO_4, 0.8% $K_4[Fe(CN)_6]$ in 0.1 M cacodylate buffer for 1.5 h, the sample were rinsed in four changes of 0.1 M cacodylate buffer and immersed in 30% DMF dissolved in 0.1 M cacodylate buffer for 30 min. The liver samples were frozen with liquid nitrogen and were crushed into randomized pieces which were placed again in 30% DMF for 30 min, then rinsed twice with buffer and three changes of distilled water. The specimens were dehydrated in ascending acetone solutions and critical point dried using a CP drying apparatus E 3000 (Quorum Technologies Ltd, East Sussex, United Kingdom) with CO_2 substitution (Anderson, 1951). Dried samples were sputter-coated with platinum and examined with a field-emission scanning electron microscope (LEO 1530, Zeiss).

4.3.3 Perfusion studies

For liver perfusion via the portal vein, mice were deeply anesthetized (120 mg/kg of body weight i.m. ketamine and 8 mg/kg body weight i.m. xylazine). The abdomen was opened and the portal vein was cannulated using a 27 gauge needle (Henry Schein, Melville, NY, USA). The needle was attached via disposable Mallinckrodt pressure tubing with an inner diameter of 0.050" and 24" length (Tyco Healthcare, Pleasanton, CA, USA) to a 3-way-stopcock (Fresenius Kabi AG, Bad Homburg, Germany). Two additional pressure tubes which are connected to two 10 ml syringes (Henry Schein, Melville, NY, USA) were attached to the 3-way stopcock. For perfusion, an infusion pump (PHD 2000, Harvard Apparatus, Holliston, MA, USA) was used. Fluorescein isothiocyanate-dextran (FITC-dextran, FD70, Sigma, Taufkirchen, Germany) was dissolved at a concentration of 50 mg/ml in PBS. Qdot® 655 ITK™ Amino (PEG) quantum dots (Life Technologies GmbH, Darmstadt, Germany) were perfused at a total amount of 20 pmol for each liver, with an infusion rate of 1 ml/min, and an infusion volume of 1 ml. After start of the perfusion, the inferior vena cava was cut open. To fix the tissue after perfusion, the 3-way-stopcock was switched to the syringe filled with 4% PFA and perfusion was restarted with an infusion rate of 1 ml/min and an infusion volume of 1 ml. Finally, right liver lobes were collected and further processed for histology and immunohistochemistry.

4.3.4 Light microscopy

Embryos were obtained from timed matings with noon of the day of vaginal plug discovery designated as 0.5 days of gestation (E0.5). Embryos and tissues were collected and fixed in 4% PFA for 4 h. After fixation, embryos and tissue samples were washed in 0.1 M phosphate buffer, processed through several graded alcohol and xylenes, and embedded in paraffin. For frozen sections, the embryos and tissues were equilibrated in 10, 20, and 30% sucrose for 4 h and embedded in Tissue Tek optimal cooling temperature (OCT) compound (Sakura Finetek Europe B.V., Zoeterwoude, NL) and cooled at -20°C. After removal of paraffin, the sections were stained with hematoxylin and eosin (H&E) and analyzed using a Zeiss Axio Imager microscope (Carl Zeiss AG, Oberkochen, Germany). For sirius red staining, de-waxed sections were stained with Weigert's hematoxylin (1% Hematoxylin, pH 5.0-7.2 in 96% isopropyl alcohol) for 8 min and then washed for 10 min in running tap water. Afterwards the sections were stained with 0.1% Picro-sirius in saturated aqueous solution (Waldeck GmbH & Co., Division Chroma, Münster, Germany) for 1 h. After two washing steps in acidified water (0.5% acetic acid diluted in distilled water), the water was physically removed from the slides and the sections were dehydrated through three steps of 100% ethanol for 10 min. Afterwards the sections were cleared in two steps of 100% xylenes for 10 min, mounted with DePeX (Serva Feinbiochemica, Heidelberg, Germany) and examined using a Zeiss Axio Imager microscope (Carl Zeiss AG, Oberkochen, Germany). For staining for periodic acid schiff (PAS), de-waxed paraffin sections were oxidized by 1 % periodic acid dissolved in 70 % ethanol for 10 min and washed 3 times in distilled water for 1min. Afterwards, the aldehyde groups are detected by Schiff reagent and counterstained with Weigert's hematoxylin (1% Hematoxylin, pH 5.0-7.2 in 96% isopropyl alcohol). Sections were processed through several graded alcohol and xylenes and mounted with DePeX (Serva Feinbiochemica, Heidelberg, Germany). For staining for β-galactosidase activity, embryos were fixed in 2% glutaraldehyde in 5 mM EGTA (pH 7.3) and 2 mM MgCl2 dissolved in 0.1 M PBS for 4 h on ice with shaking. After three 30 min rinses in washing buffer (2 mM $MgCl_2$, 0.01% sodium deoxycholate, 0.02% Nonidet-P40 in 0.1 M PBS), β-galactosidase activity was visualized in X-Gal staining solution (0.1 M PBS, 2 mM $MgCl_2$, 0.01% sodium deoxycholate, 0.02% Nonidet-P40, 5 mM potassium ferrocyanide, 5 mM potassium ferricyanide, 1 mg/ml X-Gal). Tissues were stained for 24 h at 37°C in the dark, washed three times for 5 min in washing buffer, and embedded in Tissue-Tek for frozen sections. P-phenylendiamine (PPD, Carl Roth, Karlsruhe, Germany) staining was performed on semithin sections of liver and kidney. Sections were stained with 1% PPD solution (10 mg/ml PPD in 98% ethanol) for 30 min at room temperature in the dark. Afterwards the sections were differentiated with 100% ethanol and counterstained with methylene blue.

4.3.5 Immunohistochemistry

Tissue samples were fixed in 4% PFA or Carnoy's fixative (60% methanol, 30% chloroform and 10% acetic acid) for 4 h, washed in 0.1 M phosphate buffer, and embedded in either paraffin or Tissue-Tek optimal cooling temperature compound (Sakura Finetek Europe B.V., Zoeterwoude, the Netherlands). For detection of PLVAP, CD31, and α-smooth muscle-actin, sections were blocked with 1% BSA, 0.2% cold water fish gelatin (Aurion, Wageningen, Netherlands), and 0.1% Triton-X (all in 0.1 M PBS) for 1 h at room temperature. After blocking, the sections were incubated with rat anti-panECA (MECA-32) IgG_{2a} (1:50, Santa Cruz), goat anti-CD31/PECAM-1 IgG (1:20, R&D systems, Wiesbaden, Germany) or goat anti-α-smooth muscle-actin IgG (α-SMA) (1:200; GeneTex, Irvine, CA, USA). Donkey anti-rat IgG (1:2500) or rabbit anti-goat IgG (1:1000) conjugated to Alexa Fluor 488 (Life Technologies GmbH, Darmstadt, Germany) were used as secondary antibodies. For fibronectin staining, sections were blocked with 2% BSA and 0.1 M Triton-X in 0.1 M PBS for 1 h. After blocking, sections were incubated with rabbit anti-fibronectin (1:500, Dako, Hamburg, Germany). Goat anti-rabbit IgG (1:1000) conjugated to Alexa 488 (Life Technologies GmbH, Darmstadt, Germany) were used as secondary antibodies. For IBA-1 staining sections were pretreated with 0.05 M ammonium chloride for 30 min and with 0.5% Triton-X for 5 min. Afterwards, sections were blocked with 1% BSA, 0.2% cold water fish gelatin (Aurion, Wageningen, Netherlands), and 0.1% Triton-X (all in 0.1 M PBS) for 1 h at room temperature. After blocking, sections were incubated with rabbit anti IBA-1(1:100, Wako, Neuss, Germany). Goat anti-rabbit IgG (1:1000) conjugated to Alexa 488 (Life Technologies GmbH, Darmstadt, Germany) were used as secondary antibodies. Primary antibodies were always incubated overnight at 4°C and secondary antibodies were incubated for 1 h at room temperature in the dark. Slides were mounted with a medium containing 4',6-Diamidino-2-phenylindole (DAPI, Vectashield; Vector Laboratories, Burlington, CA, USA) and analyzed under a fluorescence microscope (Zeiss, Axio Imager). For negative controls, primary antibodies were omitted and the sections were incubated with secondary antibodies only.

4.3.6 TUNEL staining

Apoptotic liver cells were detected by terminal deoxynucleotidyl transferase-mediated dUTP nick end labeling using the Deadend Fluorometric TUNEL system (Promega, Mannheim, Germany). Tissues were fixed in 4% PFA for 4 h. After removal of paraffin, TUNEL staining

was performed according to the manufacturer's instructions. Slides were analyzed under a fluorescence microscope (Zeiss, Axio Imager).

4.3.7 Plasma analysis

For collection of blood plasma for lipoprotein analysis, mice were euthanized with isoflurane and rapidly killed by decapitation to collect trunk blood. Blood samples were centrifuged at 4000 g for 15 min and plasma was stored at - 20 °C. Hematocrit was evaluated by collecting trunk blood which was separated by standard laboratory methods using heparinized micro hematocrit tubes (Brand GmbH, Wertheim, Germany). Serum aspartate transaminase (AST), alanine transaminase (ALT), cholesterol, albumin and total protein levels were measured applying standard procedures.

4.3.8 NMR spectroscopy

NMR spectra were recorded on Avance 800 and 600 NMR spectrometers (Bruker Biospin Karlsruhe, Germany) operating at 800.2 and 600.2 MHz proton resonance frequencies, respectively. Both spectrometers were equipped with a cryoprobe for obtaining a higher sensitivity. Spectra were recorded from blood plasma of individual mice at 310 K. If the sample volume was smaller than 500 μL, an appropriate amount of physiological extracellular buffer (Freund and Kalbitzer, 1995) was added up to 500 μL. Quantification of the plasma lipoproteins was obtained from NOESY-type 1D spectra (Beckonert et al., 2007) and a set of Oneshot (Pelta et al., 2002) diffusion weighted ^{1}H NMR spectra. The concentrations of the different lipoprotein subclasses defined by the hydrodynamic radii r_H was calculated according to methods published previously (Huber et al., 2005; Pelta et al., 2002). Chemical shifts δ and hydrodynamic radii r_H were referenced to the methyl signal of lactate used as internal standard. The chemical shift of lactate was set to 1.365 ppm, since it is known that the usual reference compound DSS interacts with the lipoproteins. The hydrodynamic radius of Tris-buffer was experimentally determined as 0.307 nm in a separate set of experiments and used for the calibration of the hydrodynamic radii of the triplet signal in the lipoproteins. The obtained r_H-values were associated with different types of lipoproteins from the data published for human lipoprotein subclasses (Petersen et al., 2012). The relative concentration changes of the different lipoproteins were calculated for 3 samples each of wild-type and *Plvap*$^{-/-}$ littermates.

4.3.9 Quantitative analysis

For quantitative analysis of the number of fenestrations in liver sinusoids, the total number of fenestrations was counted along the endothelium comprising a total length of 2.5 mm in both wild-type and *Plvap*$^{-/-}$ littermates. The number of fenestrations per µm capillary length was determined and expressed as mean ± SEM. Statistical analysis was done by a two-tailed Student's t-test and *p* values ≤ 0.05 were considered to be statistically significant.

4.4 Results

4.4.1 The loss of PLVAP in sinusoidal endothelial cells is associated with a lack of fenestrations

To analyze the expression of *Plvap* in the developing liver, we stained for β-galactosidase to detect the expression of the reporter gene *lacZ*. At embryonic day (E) 15.5, a time when fenestrations have been formed in the sinusoids of the mouse liver, we detected a positive staining in the sinusoidal endothelial cells of *Plvap*-deficient embryos (Figure 24A). In contrast, staining was essentially absent in wild-type littermates (Figure 24A). The β-galactosidase staining in the liver sinusoidal endothelium was patchy and considerably weaker than the more homogenous staining in the capillaries of the immediately adjacent small intestine or skin (Figure 24A) which show strong *Plvap* expression (Herrnberger et al., 2012b). Comparable results were obtained when localization of PLVAP was investigated by immunohistochemistry. At E16.5, liver sinusoidal cells of wild-type embryos showed a distinct immunoreactivity for PLVAP, a finding that was not observed in *Plvap*$^{-/-}$ embryos (Figure 24B). The immunoreactivity was patchy and weaker than in the capillaries of the adjacent small intestine or pancreas (Figure 24B). In three-week-old mice the immunoreactivity for PLVAP in the sinusoidal endothelial cells of wild-type animals was of similar intensity than in embryos, but more homogenous (Figure 24C). Again, no immunoreactivity for PLVAP was observed in *Plvap*$^{-/-}$ littermates (Figure 24C).

PLVAP is a component of the diaphragms covering endothelial fenestrae, transendothelial channels, and caveolae (Stan, 2005; Stan et al., 1999a). Since the formation of fenestrae with diaphragms precedes that of open fenestrae during development of the sinusoidal endothelium in rat embryos (Bankston and Pino, 1980), we assumed that the PLVAP staining in the mouse embryos was associated with the formation of diaphragmed fenestrae. Indeed, we observed fenestrae with a diaphragm in the sinusoidal endothelium of mouse embryos starting from E12.5 (Figure 24D). As expected, fenestrae of sinusoidal endothelial cells in three-week-old mice were open while fenestrae or transendothelial channels covered by diaphragms were not observed (Figure 25A). Also caveolae which were only rarely observed in sinusoidal endothelial cells of wild-type pups after birth did not form stomatal diaphragms (Figure 24E), a finding that was corroborating results from a previous report (Ghitescu and Fixman, 1984). Overall, our data did not support the concept that the presence of PLVAP in sinusoidal endothelial cells of the postnatal mouse liver is associated with the presence of endothelial diaphragms.

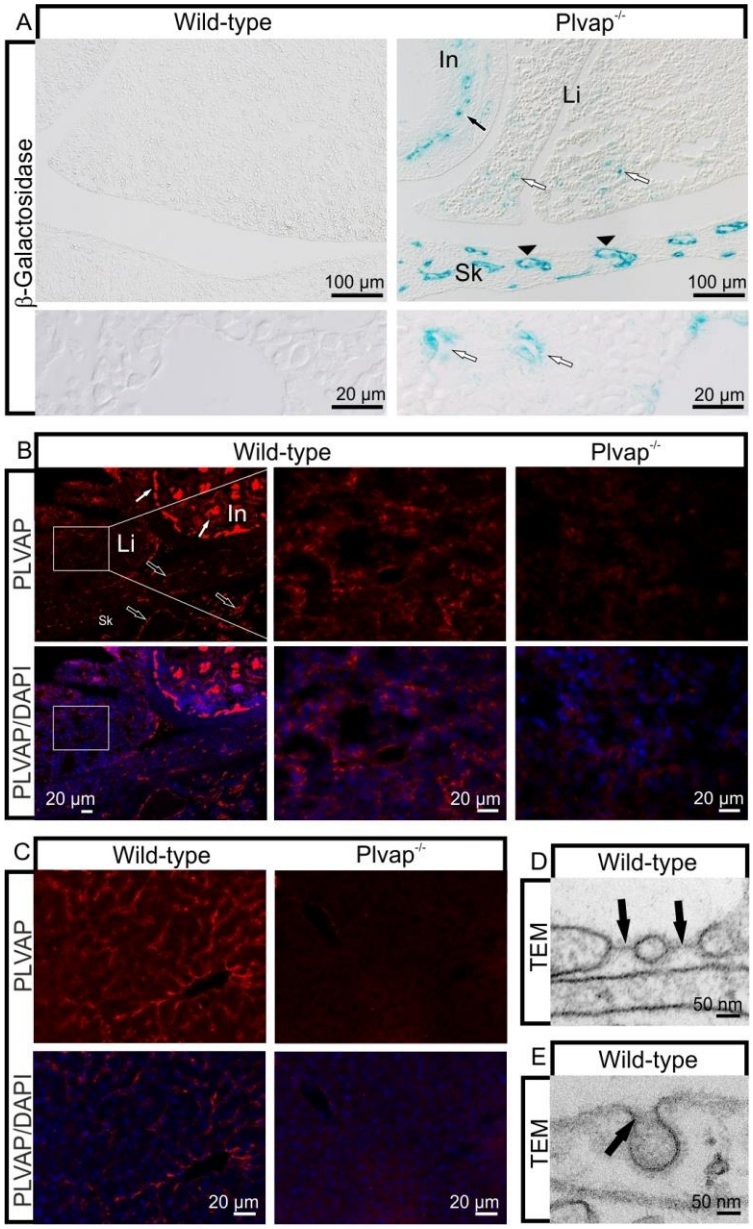

Figure 24: PLVAP in the liver. A, β-galactosidase stained sections through the liver of a *Plvap*$^{-/-}$ animal and its wild-type littermate at E15.5. Staining is seen in the sinusoidal endothelium of the *Plvap*-deficient embryo (*white arrows*), but not in the wild-type. Staining in the liver is patchy and weaker than the homogenous staining of capillaries in the small intestine (*In, black arrows*) or skin (*Sk, arrowheads*). Lower panels show magnification of the staining in liver sinusoids (*white arrows*). **B**, Immunolabeling for PLVAP *(red)* shows staining in the sinusoidal endothelium of a wild-type embryo at E16.5 (boxed areas in the left panel). Stronger immunostaining for PLVAP is seen in capillaries of the small intestine (*white arrow*) and the pancreas (*black arrow*). No staining is seen in the *Plvap*-deficient littermate (right panel). Middle panel shows magnification of the boxed panel. **C**, Liver staining for PLVAP (*red*) at P11 shows positive immunoreactivity in wild-type sinusoidal endothelium, but not in the *Plvap*$^{-/-}$ littermate. Nuclear DNA is labeled with DAPI (*blue*). **D** and **E**, TEM. Fenestrations bridged by 5- 7 nm thick diaphragms (*black arrows*) are seen in wild-type sinusoidal endothelium at E12.5 (**D**). Caveolae of wild-type sinusoidal endothelium at P20 are not bridged by stomatal diaphragms (*black arrow*, **E**).

We next analyzed whether sinusoidal endothelial cells of *Plvap*-deficient mice show ultrastructural changes when compared to wild-type littermates. By TEM, numerous fenestrae were observed in sinusoidal endothelial cells of wild-type animals at three weeks of age (Figure 25A). In contrast, fenestrae were only very rarely observed in the sinusoidal endothelium of *Plvap*-deficient littermates (Figure 25A). Moreover, in *Plvap*$^{-/-}$ mice the space of Disse was compressed and filled with fine granular electron-dense material which was observed adjacent to the hepatocyte microvilli and was not present in wild-type littermates (Figure 25A). The lack of fenestrae in sinusoidal endothelial cells of *Plvap*-deficient mice was confirmed by SEM. Sinusoidal endothelial cells in wild-type mice displayed numerous fenestrae that were arranged in sieve plates (Figure 25B). In contrast, sinusoidal endothelial cells of *Plvap*-deficient mice showed only very few fenestrations which formed individual openings instead of being arranged in clusters (Figure 25B). The diminished porosity of the sinusoidal endothelium was verified by quantification which showed a highly significant ($p \leq 0.001$) and approximately 6.2-fold reduction in the number of fenestrae in *Plvap*-deficient mice (Figure 25C).

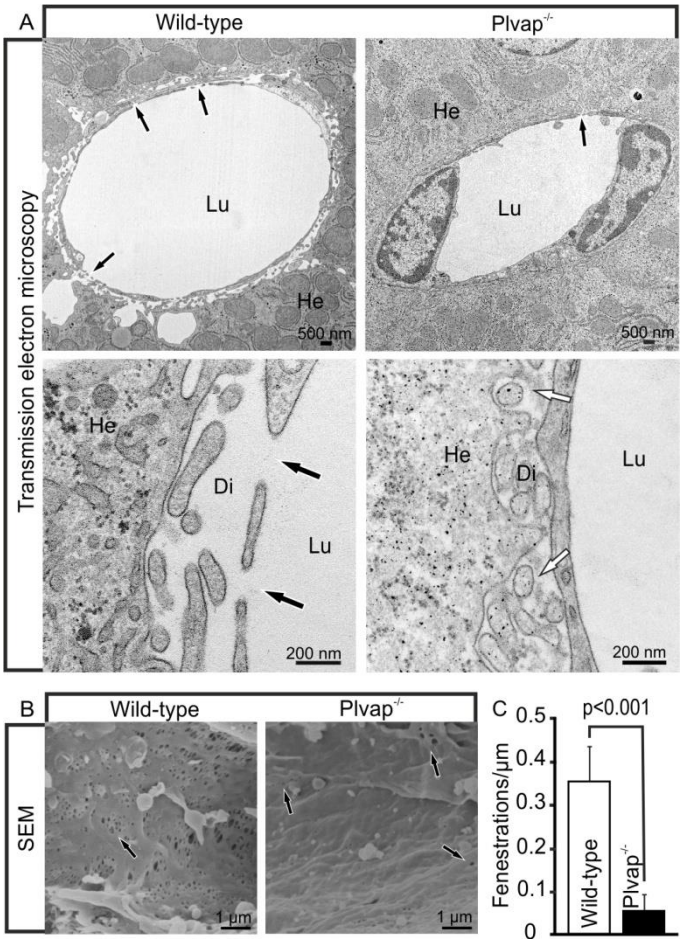

Figure 25: Ultrastructure of *Plvap*-deficient sinusoids. A, TEM of a 3-week-old wild-type animal shows numerous fenestrations in sinusoidal endothelial cells (*black arrows*). In contrast, fenestrations are very rare in the

Plvap$^{-/-}$ littermate (*black arrow*). Lower panels show magnification. While in the wild-type animal Disse's space (*Di*) is open, it is compressed and filled with fine granular electron-dense material in the *Plvap*-deficient littermate (*white arrows*). *He*, hepatocyte, *Lu*, sinusoidal lumen. **B**, SEM of a 3-week-old wild-type animal shows the arrangement of fenestrations (*arrows*) in sieve plates. In contrast, sinusoidal endothelial cells of a *Plvap*-deficient littermate show only few fenestrations (*arrows*) which form individual openings. **C**, Quantitative analysis of fenestrations per µm endothelial length in sinusoids of wild-type and *Plvap*$^{-/-}$ animals. N = 5, mean ± SEM, $^{***}p$ = 0.00069.

4.4.2 The lack of fenestrations leads to a decrease in the permeability of sinusoidal endothelial cells

We next analyzed if the absence of PLVAP and the decrease in the number of fenestrations in sinusoidal endothelial cells was associated with major changes in sinusoid architecture. To this end we labeled the vascular endothelial cells of the liver with antibodies against CD31 and detected no obvious differences between *Plvap*$^{-/-}$ mice and wild-type littermates with regards to orientation and density of positively-labeled vascular endothelial cells (Figure 26A). No obvious structural differences in the architecture of liver sinusoids were observed when semithin sections were studied (Figure 26B). A distinct difference though between the sinusoids of *Plvap*-deficient mice and that of wild-type littermates was the higher number of mononuclear cells (presumably Kupffer cells) in the lumen of the *Plvap*$^{-/-}$ sinusoids (Figure 26B). In addition, livers of *Plvap*$^{-/-}$ mice showed areas with accumulations of mononuclear cells in Disse's space (Figure 26B). We next tested the permeability of the sinusoids for macromolecules by perfusion with 70 KDa FITC-dextran possessing a hydrodynamic diameter of approx. 10 nm *via* the portal vein. After perfusion of wild-type animals, a strong FITC-signal was detected throughout the entire liver. Immunolabeling with CD31 strongly suggested that numerous FITC-dextran molecules had passed the endothelial cells via their fenestrae and had accumulated in the space of Disse (Figure 26C). In contrast, in *Plvap*-deficient littermates a signal for FITC-dextran was barely detectable (Figure 26C). In a parallel approach, we used 25 nm diameter quantum dots[18] holding a CdSe-containing core for portal vein perfusion (quantum dots were provided by Prof. Dr. Achim Göpferich and confocal microscopy (data not shown) was done with the help of Robert Hennig). The core allowed us to measure the amount of cadmium per kg liver tissue by inductively coupled plasma mass spectrometry (ICP-MS), which correlates with the amount of quantum dots in the tissue after perfusion. Only 0.05 mg/kg cadmium were detected in the liver homogenate from a *Plvap*-deficient mouse while the liver of the wild-type littermate contained 1.2 mg/kg cadmium (ICP-MS was conducted by Firma Friedle, Regensburg, Germany). Overall, our

experiments strongly supported the assumption of a constrained passage of macromolecules and nanoparticles through the hepatic sinusoidal endothelium of *Plvap*-deficient mice.

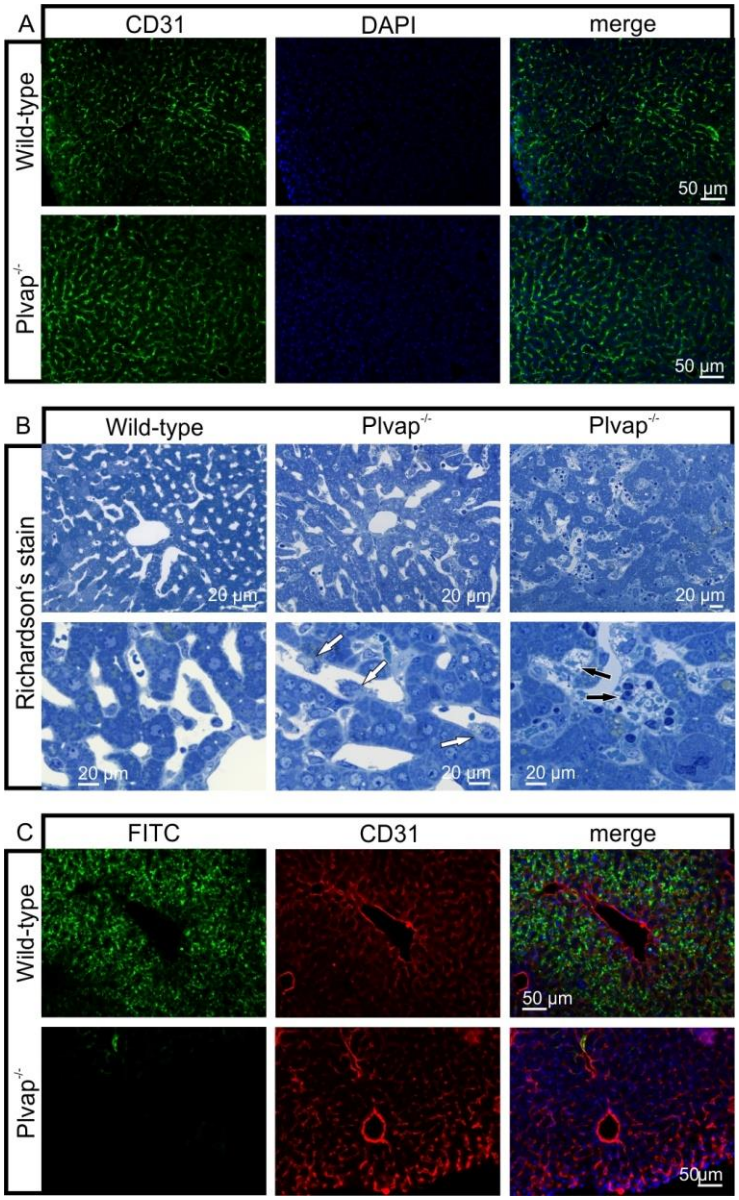

Figure 26: Diminished permeability of liver sinusoids in *Plvap*-deficient mice. Neither by immunohistochemistry with antibodies against CD31 (**A**) nor light microscopy of 1 µm semithin sections (**B**, Richardson's stain) obvious differences are detected with regards to the overall orientation and the density of liver sinusoids between 3-week-old *Plvap*$^{-/-}$ mice and wild-type littermates. Sinusoids of *Plvap*-deficient mice show a higher number of macrophages in their lumen (*white arrows*) and focal areas with accumulations of mononuclear cells in Disse's space (*black arrows*). Lower panels in **B** show higher magnifications. **C**, After perfusion of a wild-type animal with FITC-dextran, a strong FITC-signal (*green*) throughout the liver is detected. Immunolabeling with CD31 (*red*) suggests that FITC-dextran molecules have accumulated in the space of Disse. In contrast, in the *Plvap*-deficient littermate, the signal for FITC-dextran is much weaker and barely detectable. Nuclear DNA is labeled with DAPI (*blue*).

4.4.3 The lack of sinusoidal fenestrae in *Plvap*-deficient mice causes hyperlipoproteinemia and steatosis

We next hypothesized that the loss of sinusoidal fenestrations in *Plvap*$^{-/-}$ mice should impair the passage of chylomicron remnants to hepatocytes, and analyzed the animals for signs of hyperlipoproteinemia. Plasma isolated from 10-day-old breastfeeding *Plvap*-deficient pups was whitish, milky and thus strongly indicative of hyperlipoproteinemia (Figure 27A). In contrast, plasma from wild-type littermates appeared clear. Upon macroscopic analysis of 2- to 3-week-old *Plvap*$^{-/-}$ animals, the blood in the vessels supplying the small intestine or the kidneys had a milky color, while that of wild-type animals was red (Figure 27B). In contrast to the kidneys of wild-type animals, which had an intense reddish color, those of *Plvap*-deficient littermates were pale (Figure 27B). A similar difference in color was observed upon macroscopic analysis of the livers (Figure 27B). The differences in color were not caused by anemia, as no obvious differences in hematocrit readings were observed between *Plvap*$^{-/-}$ animals and their wild-type littermates (Figure 27A).

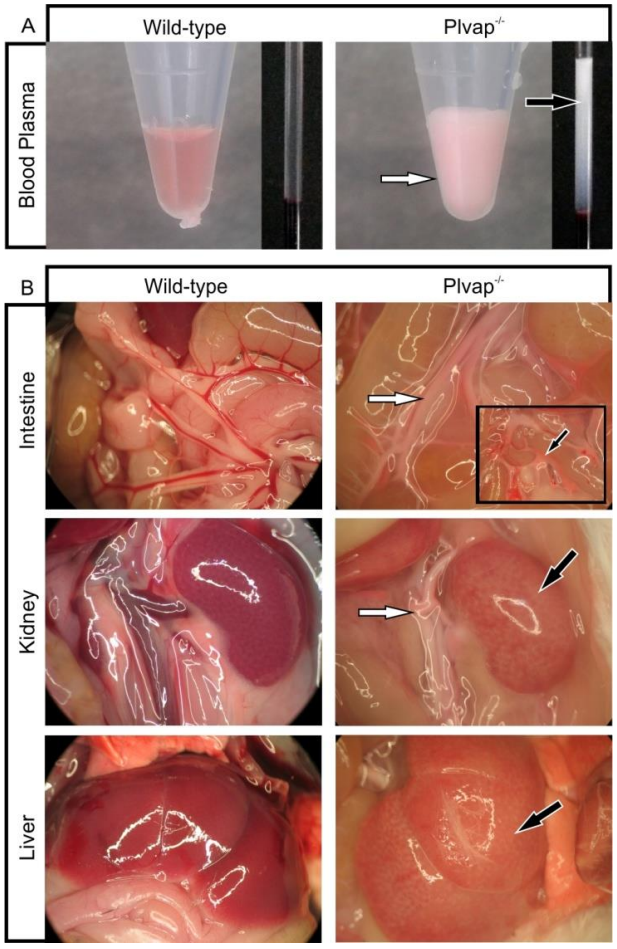

Figure 27: Hyperlipoproteinemia in *Plvap*-deficient mice. A, Plasma of a P10 *Plvap*-deficient pup looks milky (*arrows*), while that from a wild-type littermate is clear. No obvious differences in hematocrit readings are

observed between a *Plvap*$^{-/-}$ pup and its wild-type littermate (right-handed panel). **B**, The blood in the mesenterial or kidney vessels of a 3-week-old *Plvap*-deficient animal is milky (*white arrows*), while that of wild-type animals is red. Boxed area displays a magnification of mesenteric capillaries that are cut open to show milky blood (*black arrow*). Kidneys and livers of wild-type animals are of reddish color (*black arrows*), while those of *Plvap*-deficient littermates are pale.

To clarify, if the differences in kidney or liver colors were caused by hyperlipoproteinemia, we analyzed semithin sections of mice at three weeks of age, which is close to the maximal life span of our *Plvap*-deficient animals. When kidney sections of *Plvap*$^{-/-}$ mice were labeled with the lipid stain PPD, abundant granular structures were identified that filled the peritubular and glomerular capillaries (Figure 28A). In contrast, in kidneys of wild-type littermates only erythrocytes were seen in the capillary lumen (Figure 28A). By TEM, the granular structures in the lumen of *Plvap*-deficient capillaries were identified as homogenously electron-dense particles with diameters between 50 to 500 nm (Figure 28B). The particles were surrounded by extracellular fibrils with the ultrastructural characteristics of fibrin indicating thrombus formation. When semithin sections through the livers of *Plvap*-deficient animals were stained, PPD-labeled granular structures were identified in the lumen of liver sinusoids and in Kupffer cells (Figure 28B). The cytoplasm of the vast majority of hepatocytes was densely filled with PPD-labeled granules (Figure 28B). Similar granules were only occasionally observed in hepatocytes of wild-type littermates (Figure 28B). By TEM, the cytoplasmic granules were identified as liposomes indicating a pronounced microvesicular steatosis in *Plvap*-deficient livers (Figure 28B). Hepatocytes of wild-type animals contained large aggregates of glycogen, which were absent in *Plvap*-deficient littermates (Figure 28B). Similar to the findings in kidney capillaries, the lumen of liver sinusoids in *Plvap*$^{-/-}$ animals was frequently occluded by aggregates of fibrillar fibrin suggestive of thrombus formation (Figure 28B).

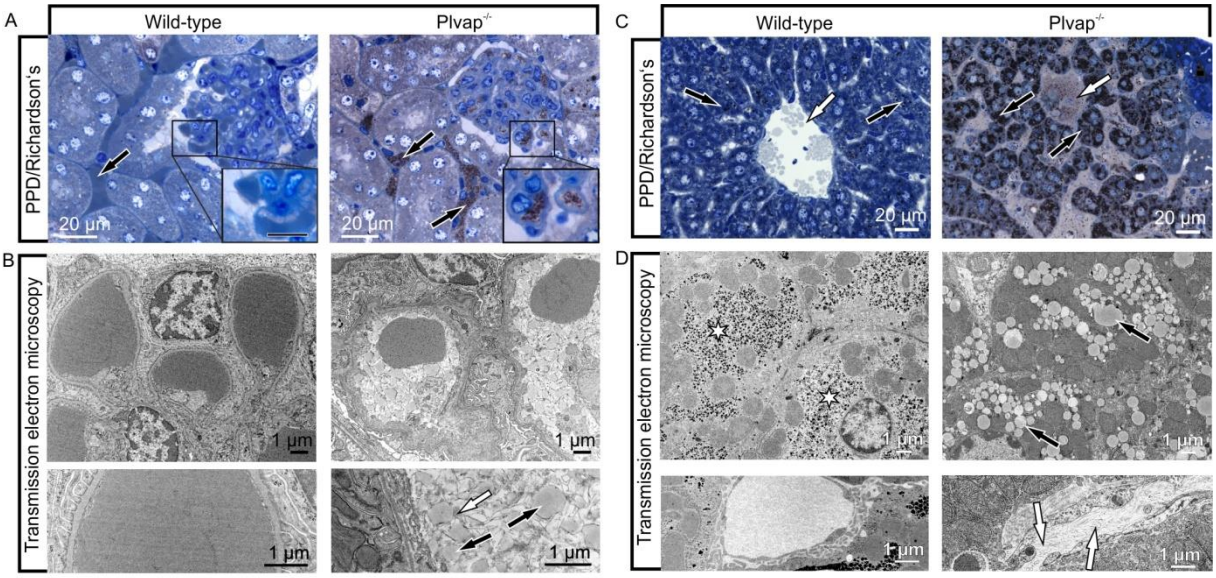

Figure 28: Lipoproteins in capillaries and hepatocytes of *Plvap*-deficient animals. **A**, PPD-labeled granular structures fill the lumen of kidney capillaries in a 3-week-old *Plvap*$^{-/-}$ mouse (*arrows*, *boxed area*, counterstain: Richardson's stain), while only erythrocytes are seen in the wild-type littermate (*arrow, boxed area*). **B**, The granular structures (*black arrows*) in the lumen of *Plvap*-deficient capillaries have diameters between 50 to 500 nm and are homogenously electron-dense. The particles are surrounded by extracellular fibrils with the ultrastructural characteristics of fibrin (*white arrow*) (TEM, lower panel shows higher magnification). **C**, PPD-labeled granular structures are seen in the lumen of liver sinusoids in a *Plvap*$^{-/-}$ mouse but not in a wild-type littermate (*white arrows*). The cytoplasm of the vast majority of *Plvap*$^{-/-}$ hepatocytes is densely filled with PPD-labeled granules (*black arrows*) which are rare in hepatocytes of wild-type littermates (*black arrows*). **D**, By TEM, numerous liposomes (*black arrows*) are seen in the *Plvap*-deficient liver indicating a pronounced microvascular steatosis. Hepatocytes of the wild-type animal contain large aggregates of glycogen (*asterisks*), which are absent in hepatocytes of the *Plvap*-deficient littermates. The lumen of *Plvap*$^{-/-}$ liver sinusoids is occluded by fibrillar fibrin (*white arrows*) suggestive of thrombus formation (Figure 28D).

4.4.4 Increase in plasma chylomicron remnants in *Plvap*-deficient mice

To obtain molecular information on the nature of the particles that caused hyperlipoproteinemia in *Plvap*-deficient mice, we performed pulsed gradient stimulated echo NMR experiments and analyzed lipoprotein size and concentration changes between wild-type and *Plvap*-deficient mice (Figure 29). The data were evaluated analogously to a well-established method for analysis of human lipoproteins by NMR spectroscopy (Huber et al., 2005; Petersen et al., 2012). For the analysis of the nature of the respective lipoproteins, the nomenclature used for human lipoproteins which are defined by their hydrodynamic radii was used (Huber et al., 2005; Petersen et al., 2012). Peaks labeled with CH3 containing the signals of the methyl groups of fatty acids of complex lipids and some cholesterol signals

were analyzed. Evidently, the shape and intensity of the peaks were different between wild-type and *Plvap*$^{-/-}$ mice (Figure 29A). A triplet signal for lipoproteins with a hydrodynamic radius of 80-100 nm (subclass 13) and largely corresponding to the sizes of chylomicron remnants was increased dramatically in *Plvap*-deficient mice (Figure 29A, B). A much smaller increase was observed for lipoproteins with sizes between 40 and 80 nm (subclasses 12, 11). Within the limits of error, lipoproteins with sizes between 25 and 40 nm were unchanged, but all smaller lipoproteins (subclasses 8-1) corresponding to low-density lipoproteins (LDL) and high-density lipoproteins (HDL) were almost completely abolished in *Plvap*$^{-/-}$ mice. The relative concentration of large chylomicrons with diameters > 150 nm (subclass 15) was somewhat decreased in the plasma of *Plvap*-deficient mice.

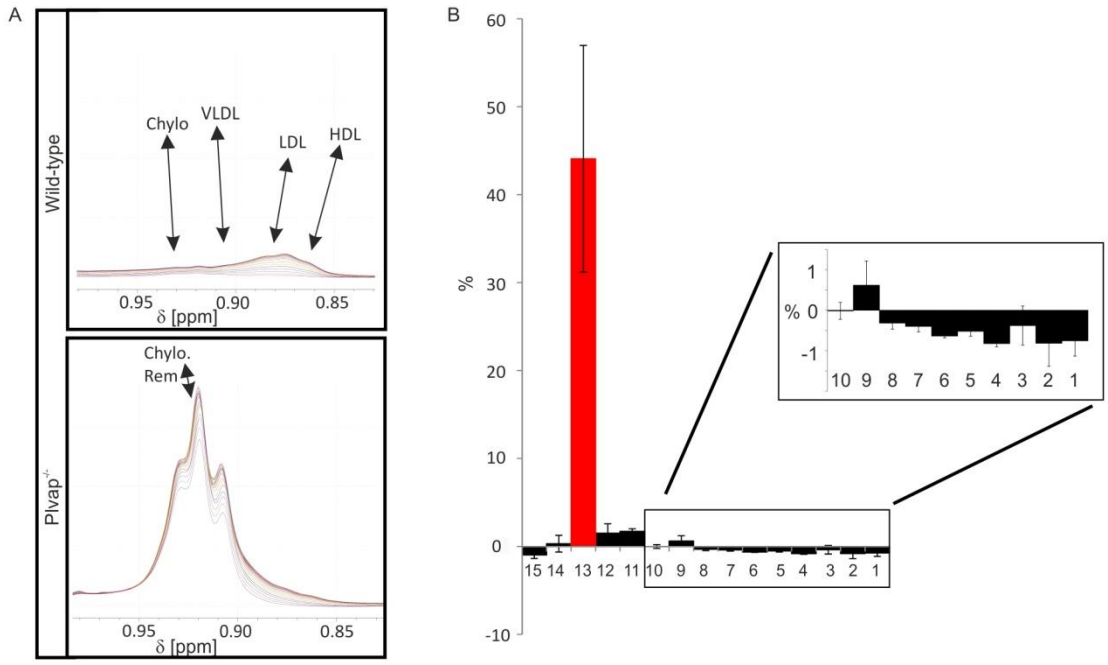

Figure 29: NMR spectroscopy of wild-type and *Plvap*-deficient plasma. A, Part of 600 MHz 1H NMR spectra of wild-type and *Plvap*$^{-/-}$ mice at different gradient strengths displaying the (CH3) signals from the methyl groups of the lipids of lipoproteins with maximum gradient strength of 0.535 T/m ± 0.01 T/m determined with a water reference sample, the different colors represent different gradient strengths. A strong decrease of the signal intensity corresponds to a small hydrodynamic radius. **B**, Average difference (*black bars*) of the relative particle numbers ΔN_{rel} in the lipoprotein subclasses L15 to L1 (Huber et al., 2005; Petersen et al., 2012) between wild-type and *Plvap*$^{-/-}$ mice. The red bar indicates the signal intensity difference of the triplet signal visible in the *Plvap*$^{-/-}$ mice shown in A. Experiments performed by Prof. Dr. Werner Kremer and Prof. Dr. Dr. Hans Robert Kalbitzer, Institut für Biophysik und Physikalische Biochemie, Lehrstuhl für Biophysik, Universität Regensburg.

4.4.5 Steatosis in *Plvap*-deficient mice progresses to necrosis and fibrosis

Since hepatic steatosis potentially progresses to severe liver disease, we analyzed the livers of three-week-old *Plvap*-deficient mice and observed that the surface of wild-type livers was smooth while that of *Plvap*$^{-/-}$ mice showed scar tissue (Figure 30A). By light microscopy of *Plvap*$^{-/-}$ livers at postnatal day (P) 18, we consistently observed focal necrotic areas (Figure 30B) containing numerous TUNEL-positive nuclei (Figure 30C). Immunostaining for IBA-1 at P18 identified a pronounced increase in the number of macrophages in *Plvap*$^{-/-}$ livers when compared to wild-type littermates (Figure 30D). By staining with sirius red numerous intensely stained focal areas were detected indicating a pronounced focal increase in the amounts of extracellular matrix (Figure 30E). In contrast, in wild-type littermates positive staining for sirius red was only seen around larger hepatic vessels (Figure 30E). Intense staining for PAS was seen in the cytoplasm of wild-type hepatocytes (Figure 30F) and correlated with the presence of glycogen aggregates that were identified by TEM (Figure 28D). Hepatocytes were not reactive for PAS in livers of *Plvap*$^{-/-}$ littermates (Figure 30F). In contrast, numerous focal areas of positive extracellular PAS-labeling were observed (Figure 30F). By immunohistochemistry of P18 *Plvap*$^{-/-}$ livers, we regularly observed foci with accumulations of α-smooth muscle actin-positive cells (α-SMA) (Figure 30G). In the liver, α-SMA is a specific marker for activated hepatic stellate cells (HSC), which are the cellular source of increased extracellular matrix (ECM) formation and deposition in response to hepatic injury (Hellerbrand, 2013). Similar areas showed an increase in immunoreactivity for fibronectin (Figure 30H). Focal areas that stained for fibronectin or α-smooth muscle positive cells were essentially absent in the livers of wild-type littermates (Figure 30G, H). Together, these data indicate HSC activation and enhanced fibrogenesis in P18 *Plvap*$^{-/-}$ livers.

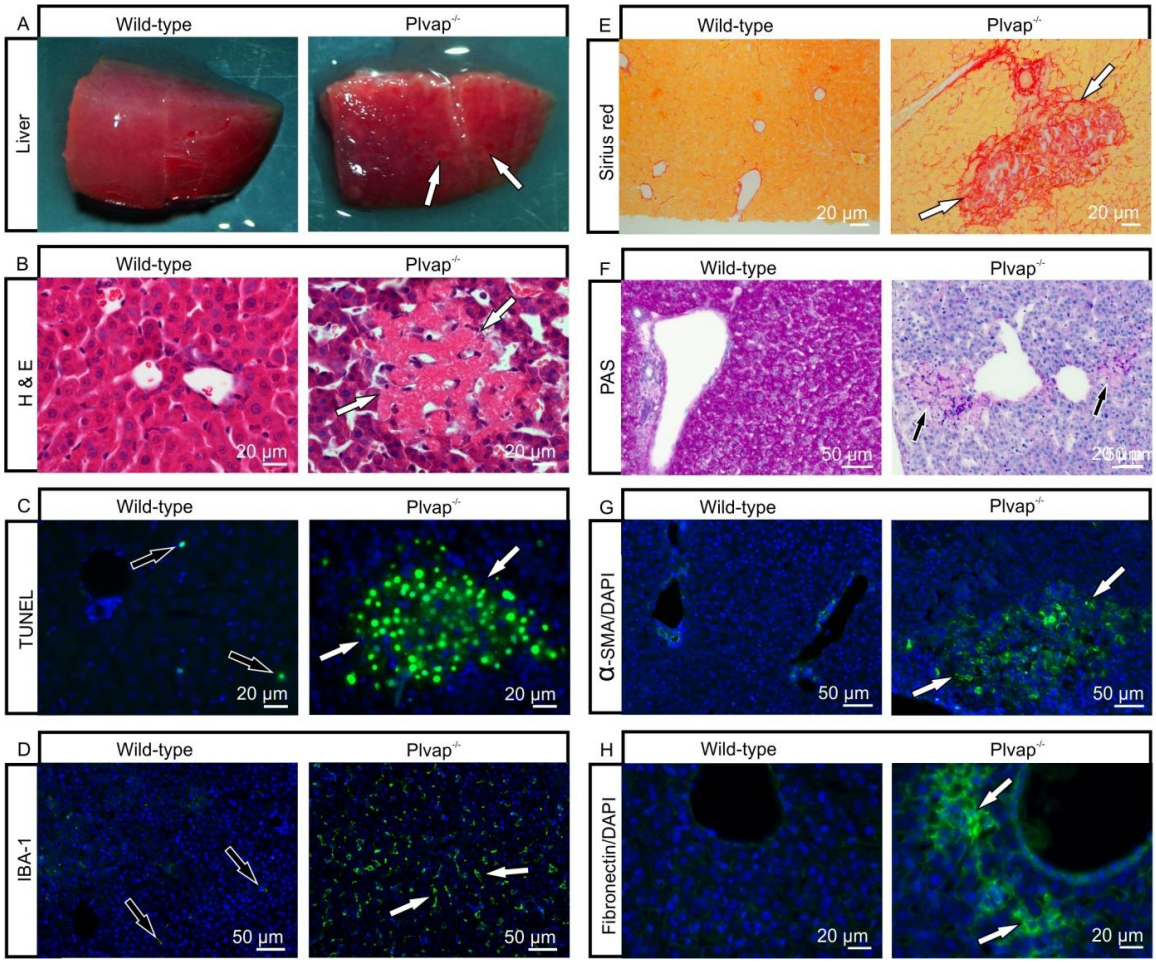

Figure 30: Liver fibrosis and necrosis in *Plvap*-deficient mice. A, The surface of a wild-type liver at three weeks of age is smooth while that of a Plvap$^{-/-}$ mouse shows scars (*white arrows*). **B**, H&E stained paraffin section through the liver of a P18 *Plvap*$^{-/-}$ animal shows a focal necrotic area (*white arrows*). Similar areas are not seen in the wild-type littermate. **C**, Numerous TUNEL-positive nuclei (*white arrows*) accumulate in a focal necrotic area of the P18 *Plvap*$^{-/-}$ animal shown in B. In contrast, only individual TUNEL-positive cells are rarely seen in the wild-type littermate (*black arrows*). **D**, Immunostaining for IBA-1 (*green*) at P18 shows a higher number of macrophages (*white arrows*) in the *Plvap*$^{-/-}$ liver when compared to the wild-type littermate. **E**, A sirius red stained focal area in the liver of an P17 *Plvap*$^{-/-}$ mouse indicates focal fibrosis (*white arrows*). In the wild-type littermate positive staining for sirius red is only seen around larger hepatic vessels. **F**, Intense staining for PAS is seen in the cytoplasm of wild-type hepatocytes. In contrast, hepatocytes are not reactive for PAS in the liver of a *Plvap*$^{-/-}$ littermate with focal areas of positive extracellular PAS-labeling (*black arrows*). **G**, α-SMA-positive cells accumulate in the liver parenchyma of a *Plvap*$^{-/-}$ mouse (*white arrows*), but are only seen in the walls of blood vessels in the wild-type littermate. **H**, A similar area as in G shows immunoreactivity for fibronectin in the liver of a *Plvap*$^{-/-}$ mouse (*white arrows*). Staining for fibronectin is essentially absent in the liver of the wild-type littermate. Nuclear DNA is labeled with DAPI (*blue*).

To assess functional parameters of the liver, we performed chemical plasma analysis and observed a decrease in the amounts of total protein and albumin in the plasma of *Plvap*$^{-/-}$

mice (Figure 31). Cholesterol was highly increased consistent with the accumulation of relative cholesterol-rich chylomicron remnants. In some, but not all *Plvap*$^{-/-}$ animals, the amounts of AST and ALT were increased.

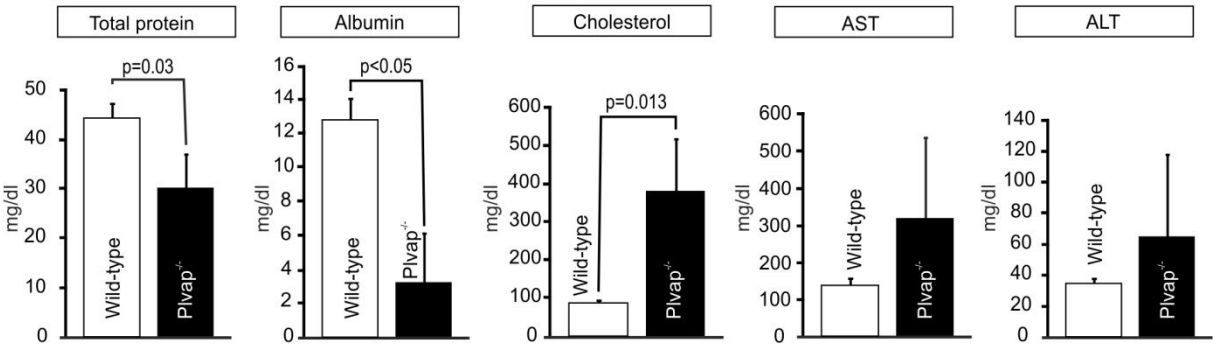

Figure 31: Plasma analysis of wild-type and *Plvap*$^{-/-}$ mice. mean ± SD. Analysis was performed by the Klinische Chemie, Universitätsklinikum Regensburg.

Finally, we investigated Disse's space by TEM. Here we regularly observed bundles of collagen fibrils with the typical 67 nm periodicity of collagen types I or III in *Plvap*-deficient animals at three weeks of age (Figure 32). In contrast, no fibrillar extracellular matrix was seen in Disse's space of wild-type littermates (Figure 32).

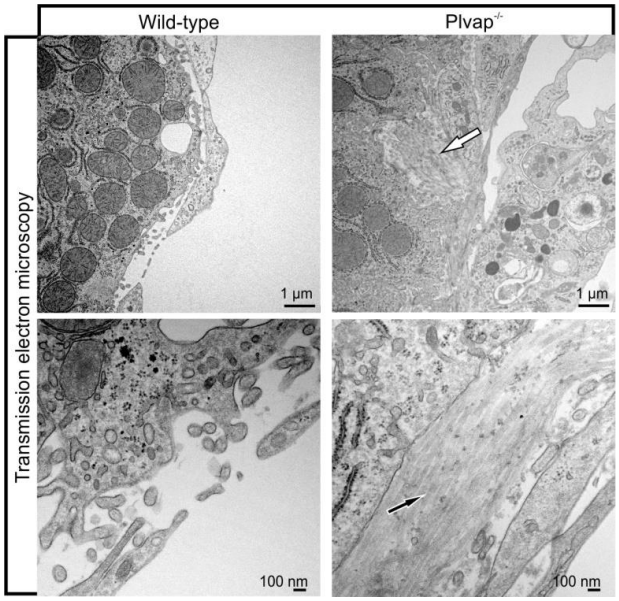

Figure 32: Accumulation of collagen in livers of *Plvap*-deficient mice. By TEM of a *Plvap*-deficient animal at three weeks of age, bundles of collagen fibrils with the typical 67 nm periodicity are seen in Disse's space (*arrows*). No fibrillar extracellular matrix is present in Disse's space of the wild-type littermate. Lower panels show higher magnification.

4.5 Discussion

We conclude that PLVAP is required for the formation of fenestrations in liver sinusoidal endothelial cells. The reduced permeability impairs the passage of chylomicron remnants and other lipoproteins between the lumen of liver sinusoids and hepatocytes, a scenario that causes hyperlipoproteinemia and results in liver injury. The conclusions rest upon (1) the finding of a substantial reduction in the number of fenestrations (2) the observation of an impaired passage of macromolecules and nanoparticles between sinusoids and Disse's space (3) the presence of a massive accumulation of plasma chylomicron remnants (4) the reduction in plasma LDL and HDL, and finally (5) the development of multivesicular steatosis, steatohepatitis, focal liver necrosis, and fibrosis in *Plvap*-deficient animals.

The important role of PLVAP in transcellular pore formation appears not to be restricted to the formation of fenestrations in the liver. When transcellular pores are generated by vascular endothelial cells to allow leukocyte migration, PLVAP forms a ring that surrounds the migrating lymphocytes and which is supported by vimentin filaments which physically interact with PLVAP (Keuschnigg et al., 2009). Moreover, blocking of PLVAP by antibodies resulted in a decrease in the number of migrating leukocytes (Keuschnigg et al., 2009). Studies on the mechanism of fenestration formation in liver sinusoids identified cytoskeletal rings around the fenestrations (Braet et al., 1998, 1996). The formation of fenestrations was significantly induced following experimental disruption of the cortical actin fibers (Braet et al., 1998, 1996; Svistounov et al., 2012) and originated from a distinct focal area that was termed "fenestrae-forming center" (Braet et al., 1998). The entire process occurred rapidly and likely required no *de novo* protein synthesis (Braet et al., 1998, 1996).
It is tempting to speculate that PLVAP molecules in or close to the plasma membrane are required to facilitate local actin disruption and pore formation, processes that are significantly less likely to occur in the absence of PLVAP. PLVAP is essential for the formation of endothelial diaphragms (Herrnberger et al., 2012b; Stan et al., 2012) and in recent studies we observed a reduction in the number of diaphragmed fenestrations in the *Plvap*$^{-/-}$ pancreas (Herrnberger et al., 2012b) or the choroid (Herrnberger et al., 2012a). In the liver, we found endothelial diaphragms in wild-type fetal sinusoids, but not after birth and regard it as unlikely that the formation of an endothelial diaphragm by PLVAP is a prerequisite for the formation of fenestrations in liver sinusoids. Data from *in vitro* studies are consistent with this assumption Braet et al., 1998, 1996).

The accumulation of chylomicron remnants in the plasma of *Plvap*$^{-/-}$ mice supports the concept that the structural characteristics of liver sinusoidal endothelial cells, like the

presence of open fenestrations and the absence of a basal lamina, have developed in evolution to allow passage of lipoproteins that are small enough in size (Braet and Wisse, 2002; Fraser et al., 1995a). Dietary lipids are absorbed by enterocytes and packaged into triglyceride-rich chylomicrons (Mansbach and Siddiqi, 2010). Chylomicrons have diameters between 75 nm and 1200 nm (Jonas and Phillips, 2008; Petersen et al., 2012) and cannot pass the endothelial wall of the diaphragmed fenestrated capillaries in the intestine which allow passage of particles with sizes between 6 and 12 nm (Sarin, 2010). Instead, chylomicrons enter the lymphatic capillaries which have a discontinuous endothelial layer (Lee et al., 2010). Chylomicrons reach the blood via the thoracic duct where most of their triglycerides are rapidly removed by lipoprotein lipase (LPL), an enzyme localized at the surface of capillaries in adipose and muscular tissues. Cholesterol-rich chylomicron remnants are finally taken up in the liver, a process that requires passage across the sinusoids and binding to both LDL receptor (LDLR) and LDL receptor-related protein (LRP) on hepatocytes (Willnow, 1997; Willnow et al., 1995). Mice that are deficient in LDLR and LRP show a comparable plasma increase in the amounts of chylomicron remnants and total cholesterol as *Plvap*$^{-/-}$ mice (Willnow et al., 1995).

It is tempting to speculate that the reduced number of fenestrations in *Plvap*$^{-/-}$ mice hinders not only the passage of chylomicron remnants, but also that of hepatocyte-derived lipoproteins towards the sinusoidal lumen. Our methods do not allow specifically assessing the amounts of plasma very low density lipoproteins (VLDL), since the hydrodynamic radii of chylomicron remnants and VLDL overlap, and chylomicron remnants trapped in the plasma are further reduced in their diameters by the activity of LPL.

Still, the markedly reduced amounts of LDL and HDL indicate that lack of fenestrations in sinusoidal endothelia does not only interfere with the passage of lipoproteins from the sinusoidal lumen to Disse's space, but also *vice versa*. VLDL are assembled in hepatocytes and converted to LDL in the plasma, while HDL are formed at the surface of hepatocytes (Cohen and Fisher, 2013; Fisher et al., 2012). Liver-derived lipoproteins which are not capable of passing the endothelial layer of *Plvap*$^{-/-}$ sinusoids would not accumulate in Disse's space, but be drained by the liver lymphatics to the abdominal lymph nodes (Chung and Iwakiri, 2013). A reduced protein synthesis in *Plvap*$^{-/-}$ hepatocytes compromised by steatosis and steatohepatitis provides an alternative explanation for the reduced plasma amounts of LDL and HDL. In support of this possibility are the reduced plasma amounts of total protein and albumin in *Plvap*$^{-/-}$ animals.

Finally, the loss of endothelial diaphragms in capillaries outside the liver might be a contributing factor to hypoproteinemia and low plasma levels of small size lipoproteins such

as LDL and HDL which might increasingly pass through fenestrations that are normally bridged by a diaphragm, but are more permeable in *Plvap*$^{-/-}$ mice.
Stan and colleagues reported recently on the phenotype of *Plvap*-deficient mice that were bred in a genetic background (hybrid intercrosses containing a mix of Balb/c, C57Bl/6J and 129Sv/J) different from our animals (Stan et al., 2012). The authors observed similar plasma changes as reported here. Accordingly, *Plvap*$^{-/-}$ (Balb/c, C57Bl/6J, 129Sv/J) mice showed a comparable increase in the plasma amounts of larger lipoproteins and cholesterol, and a decrease in LDL, HDL, total protein and albumin. The authors argued that the increase in larger lipoproteins might be a sequel to hypoproteinemia, which may cause depletion of endothelial LPL in animals (Shearer and Kaysen, 2006). We regard this possibility as unlikely, as our data clearly show a specific increase in the amounts of chylomicron remnants, while the amounts of chylomicrons were unchanged or decreased in the plasma of *Plvap*$^{-/-}$ mice. We suggest that an analysis of the number of fenestrations and their permeability to macromolecules in the sinusoids of *Plvap*$^{-/-}$ (Balb/c, C57Bl/6J, 129Sv/J) mice might show similar changes as seen in our study.

For the synthesis of VLDL, hepatocytes require triglycerides which derive from chylomicron remnants, from *de novo* lipogenesis or from albumin-bound fatty acids (Donnelly et al., 2005). It seems reasonable to assume that the reduced availability of chylomicron remnants stimulates *Plvap*$^{-/-}$ hepatocytes to increase fatty acid synthesis from carbohydrates. Our observation of a decrease in the amounts of hepatocyte glycogen supports this assumption. A chronic increase in lipogenesis is a contributing factor for non-alcoholic fatty liver disease (Kawano and Cohen, 2013) and may well cause or contribute to steatosis in *Plvap*$^{-/-}$ mice. The release of proinflammatory signals from reactive Kupffer cells that ingested chylomicron remnants trapped in the sinusoidal lumen are likely to induce steatohepatitis. Consequently, hepatocytes of *Plvap*$^{-/-}$ mice might undergo by apoptosis while HSC might get activated and transdifferentiate to activated myofibroblasts, a key event in the pathogenesis of liver fibrosis (Guo and Friedman, 2007; Schuppan and Kim, 2013). The number of sinusoidal fenestrations decreases significantly in fibrosis (Guo and Friedman, 2007; McGuire et al., 1992), a process that occurs with the formation of a continuous basal lamina and is termed “capillarization” (Schaffner and Poper, 1963). Sinusoidal capillarization may precede liver fibrosis, but it is unclear if it has the potential to initiate fibrosis (DeLeve, 2007). Our results answer this question since in *Plvap*$^{-/-}$ mice the targeted null-mutation of an endothelial-specific molecule primarily induces the lack of sinusoidal fenestrations and only secondarily leads to liver fibrosis.

Chapter 5

General Discussion

5 General discussion

One of the most important functions of endothelial cells is to allow directed passage of molecules and solutes across the endothelial barrier. Despite intensive research efforts over the recent years, the molecular requirements for transendothelial transport have not been clarified conclusively. Here we present results from studies that focused on plasmalemma vesicle-associated protein (PLVAP) which is the only known protein so far to be localized to diaphragms, thin structures which cover fenestrae and the stomata of caveolae and transendothelial channels. The general concept was to investigate the impact of the deletion of PLVAP in fenestrated vascular beds in vivo. We expected to obtain more insights into the process of fenestrae formation and the function of fenestrae, and additionally to clarify the specific function of fenestral diaphragms in transendothelial passage.

Passage of molecules across endothelial cells may involve transport via cellular vesicles. In this context, caveolae and their main structural protein caveolin-1 have been thought to play a role in transcytosis and transendothelial transport, along with other functional properties involving vascular permeability, tightness of the blood-brain barrier, vascular tone, angiogenesis, tumor growth, and atherosclerosis (Bauer et al., 2005; Frank et al., 2003b; Hehlgans and Cordes, 2011; Pavlides et al., 2012; Senetta et al., 2013; Sonveaux et al., 2004).

Indeed, caveolin-1-deficient mice (Drab et al., 2001; Razani et al., 2001) which lack any plasmalemmal caveolae in fibroblasts, endothelial cells, and adipocytes show impaired transport of albumin across lung endothelial cells (Schubert et al., 2001). Moreover, the mice suffer from other defects in vascular function, from lung abnormalities (i.e. hypercellularity, thickened alveolar septa), and decreased vascular tone due to endothelial nitric oxide synthase (eNOS) activation. Still, caveolin-1 deficient mice are viable and do not show any gross abnormalities neither during embryonic development nor during adulthood (Drab et al., 2001; Razani et al., 2001).

Besides the transport of molecules by means of vesicles, specific endothelial cells may increase their permeability by the formation of open transcellular pores which span the entire thickness of the cell, such as transendothelial pores or fenestrae present in fenestrated endothelial cells. Recently, several studies have shown that immune cells, such as lymphocytes, can pass across the vascular endothelium by migrating through transcelluar pores, a process termed diapedesis (Carman and Springer, 2004; Engelhardt and Wolburg, 2004; Muller, 2011). Still more common is passage through paracellular pores and several proteins are thought to be involved in paracellular leukocyte migration, such as vascular endothelial cadherin (VE-cadherin), platelet/endothelial-cell adhesion molecule 1 (PECAM-1), intercellular adhesion molecule 2 (ICAM2) and CD99 (Ley et al., 2007). During

transcellular migration, translocation of intercellular adhesion molecule 1 (ICAM1) expressed on the surface of endothelial cells to regions rich in F-actin and caveolin-1 near the cell borders, induces the association of several caveolae to form vesiculo-vacuolar organelles (VVOs) (Ley et al., 2007; Millán et al., 2006). The VVOs are capable of spanning the entire cell, therefore providing channels for leukocytes to migrate to the subendothelial space. Indeed, downregulation of caveolin-1 using RNA interference resulted in decreased transcellular migration of T-lymphocytes, whereas paracellular migration was unaffected (Millán et al., 2006). In the liver, immune cells do not migrate across newly formed transcellular pores, but rather use the fenestrae of sinusoids through which they extend cytoplasmatic projections into the space of Disse to respond to signals from hepatocytes (Jenne and Kubes, 2013).

In 2009, Keuschnigg and colleagues presented data that linked PLVAP to transcellular leukocyte migration across vascular endothelial cells. By studying the process *in vitro* and *in vivo* the authors observed that PLVAP forms a ring around the transendothelial pore. Moreover, PLVAP associates with vimentin, an intermediate filament known to be involved in leukocyte migration. PLVAP is redistributed during lymphocyte transmigration and the inhibition of PLVAP attenuates inflammation *in vivo* (Keuschnigg et al., 2009).

5.1 PLVAP is required for the formation of diaphragms

The results of our studies clearly show that PLVAP is required for the formation of diaphragms covering fenestrae, caveolae, and transendothelial channels. Accordingly, diaphragms are completely absent in *Plvap*$^{-/-}$ mice. Our data were corroborated by a recent contribution from Stan and coworkers (Stan et al., 2012). Moreover, Stan and coworkers could rescue the phenotype observed in *Plvap*$^{-/-}$ mice by transgenic complementation. After reconstitution, PLVAP was expressed throughout all organs and diaphragms were restored in lung, kidney, adrenal gland, pancreas, thyroid, and pancreas (Stan et al., 2012).

5.2 Lack of PLVAP leads to embryonic or perinatal lethality

Depending on the genetic background, the deletion of PLVAP in our mouse model leads to embryonic lethality. In a pure C57BL/6N background, *Plvap*-deficient animals die *in utero* due to cardiac malformations, widespread hemorrhages, and edema. Presumable reasons for the

lethal phenotype are the hemorrhages and malformations in cardiac morphogenesis. Since caveolae with a stomatal diaphragm are the only structures in subcutaneous capillaries with an endothelial diaphragm, it is quite likely that those structures are primarily affected. Stomatal diaphragms may provide mechanical stability for embryonic capillaries especially during the morphogenetic events of angiogenesis including remodeling of capillary walls. The absence of stomatal diaphragms upon *Plvap* deficiency may increase the risk for breaks in the endothelial lining, thereby causing hemorrhages and edema. In fact, it has been shown that caveolae/caveolin-1 play an important role in cell migration and angiogenesis by interacting with VEGF and eNOS (Liu et al., 2002; Maniatis et al., 2006; Navarro et al., 2004; Sonveaux et al., 2004). The requirement of caveolae for the proper organization of signaling pathways in endothelial cells by providing membrane domains for preformed signaling complexes, could be another explanation (Frank et al., 2003b; Lisanti et al., 1994). Those pathways could function in both angiogenesis and heart morphogenesis. The fact that the deletion of caveolin-1 in mice is not lethal leads to the assumption that the proposed function of caveolae in signaling pathways ought to be specific for caveolae with stomatal diaphragms and should still be transferred by PLVAP even in the absence of caveolae. Recent data argue against this hypothesis as PLVAP is rapidly internalized and degraded in the absence of caveolae in *caveolin-1*-deficient mice (Tkachenko et al., 2012).

Another interesting aspect of my studies is the discovery that *Plvap*-deficient embryos display a higher number of nucleated erythrocytes throughout their circulation. The presence of multiple hemorrhages might cause a higher need for oxygen presumably resulting in an increased number of nucleated red blood cells. Under normal conditions, nucleated erythrocytes persist in the blood stream until about E16 when they are finally replaced by mature erythrocytes originating from the liver which becomes the prime fetal hematopoietic organ (Keller et al., 1999). An immediate involvement of PLVAP in hematopoiesis could be excluded by Stan and colleagues by generating mouse lines with a specific deletion of PLVAP in the hematopoietic cell compartments. These mouse lines do not display any phenotype at all. Hematopoiesis is not affected and diaphragms are present (Stan et al., 2012).

In a mixed C57BL/6N/FVB-N genetic background, *Plvap*-deficient mice may survive for at least 4 weeks. Nevertheless, *Plvap*$^{-/-}$ mice in the mixed genetic background show severe growth retardation and metabolic defects. Genetic background-dependent differences of *Plvap*$^{-/-}$ mice in terms of survival and phenotypic manifestations were also observed by Stan and colleagues. They also acknowledge that *Plvap*-deficient animals in a pure C57BL/6J die *in utero* with no survivors beyond P2, whereas *Plvap*-deficient animals in a mixed genetic background survived till 3-4 or 6-7 month of age, depending on the respective background

(Stan et al., 2012). Modifier genes are the most likely reason for the background-dependent differences in the phenotype (Doetschman, 2009; Montagutelli, 2000; Yoshiki and Moriwaki, 2006). It has been shown for numerous genetically modified mouse lines that the genetic background can influence the phenotype dramatically. For instance, deletion of keratin 8 in a pure FVB/N background leads to colorectal epithelial hyperplasia in adults, while on a C57BL/6 background the keratin 8 deficiency causes embryonic lethality, due to abnormal liver development (Baribault et al., 1994, 1993). Therefore, first analysis on a mixed background is advantageous because it gives a first preview on possible background-dependent phenotypes. Another reason might be the different approaches used for the generation of the *Plvap*-deficient mice. While we disrupted *Plvap* gene function by inserting a trapping cassette between exon 1 and 2 of *Plvap,* Stan and colleagues preferred to delete exon 2-5 (Stan et al., 2012).

5.3 Role of PLVAP in Schlemm's canal endothelial cells and ocular capillaries

One aim of my study was to figure out if PLVAP is involved in pore formation in Schlemm's canal endothelial cells. Indeed, immunolabeling confirmed the presence of PLVAP in endothelial cells of several ocular capillaries, including the capillaries of the choriocapillaris, the ciliary body, and the endothelial cells of Schlemm's canal. Furthermore, the examination of ocular capillaries provided the same results as the other vascular beds that were investigated, such as the exocrine pancreas or the peritubular capillaries of the kidney.
Again, diaphragms were absent in fenestrae and caveolae.

Since caveolae with a stomatal diaphragm are considerably more numerous in Schlemm's canal endothelium than diaphragmed minipores, it is likely that diaphragms of caveolae are the primary site of immunolabeling. On the contrary, we also detected immunoreactivity in the continuous endothelium of the ventricular endocardium of the embryonic heart, whose caveolae are supposed to be devoid of diaphragms (Stan et al., 2012). In addition, our data show that PLVAP is expressed in liver sinusoids and glomerular capillaries during embryonic development. This finding can be explained by the fact that fenestrae in liver sinusoids and glomerular capillaries are bridged by diaphragms during embryonic development (Bankston and Pino, 1980), which might be also true for caveolae in the ventricular endocardium of the embryonic heart. Furthermore, we found PLVAP expression to be still present in postnatal liver, but considerable weaker than in tissues that typically show strong expression of PLVAP

such as capillaries of the small intestine or skin. The same results were obtained when postnatal kidneys were stained. PLVAP is expressed in glomerular capillaries but weaker than in the peritubular capillaries of the kidney interstitium (Figure 33), at least until the age of around 3 weeks. The results contradict the opinion that PLVAP is not present in vascular beds that lack diaphragm such as liver sinusoids or glomerular capillaries. It rather implicates PLVAP is expressed in and localized to the surface of endothelial cells beyond embryonic development, even if diaphragms are absent during adulthood. Fenestrae of liver sinusoids are dynamic structures which can be induced or decreased due to drugs, toxins, or diseases (Braet et al., 1998, 1995). In addition, it has been shown that fenestrae formation can take place within 10 min after application of fenestrae-inducing agents, which excludes *de novo* formation of proteins involved in this process (Roberts and Palade, 1995). Rapid pore formation during transcellular leukocyte migration supports this idea. Very likely, proteins including PLVAP are needed at short notice, supporting the idea that PLVAP might be required at or in the membrane of sinusoidal endothelial cells or other endothelial cells with a need for dynamic formation of fenestrae, such as the kidney glomerulus.

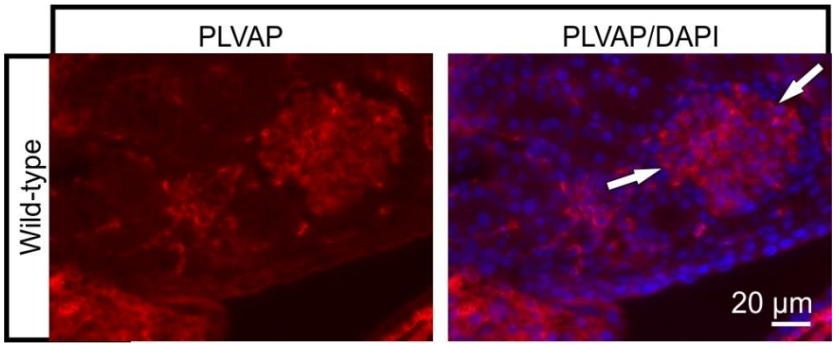

Figure 33: Expression of PLVAP in postnatal kidneys of wild-type animals. PLVAP is expressed in glomerular capillaries of 3-week-old C57BL/6N/FVBN mice. *White arrows* indicate a glomerulus with positive immunoreactivity for PLVAP (*red*).

However, in our *Plvap*-deficient animals the absence of PLVAP did not provoke any alterations in the number of caveolae, similar to the data obtained by an *in vitro* knock-down of *Plvap* (Stan et al., 2004).

5.4 Lack of PLVAP causes a substantial reduction in the number of fenestrae in fenestrated endothelial cells

In fenestrated endothelial vessels, fenestrae are typically bridged by a diaphragm. In *Plvap*-deficient animals, the presence of endothelial fenestrae is rather diminished than abolished, since some fenestrations are still present. The remaining fenestrae without diaphragm are not completely empty, but rather contain some fluffy electron-dense material instead, which might provide residual filter function to regulate and sustain permeability. Possible candidates could be heparan sulfate proteoglycans which have been found on the luminal surfaces of endothelial fenestrae providing anionic charges (Simionescu et al., 1981b, 1981c). The reduced interstitial spaces in the pancreas of *Plvap*-deficient animals might point to the more than likely reduced transendothelial passage of water and solutes caused by the considerable decrease in the number of fenestrations. Also the reduced body size of *Plvap*$^{-/-}$ mice could be attributed to the functional impairment in organs that require fenestrated endothelia for normal function.

The fact that fenestrae in our *Plvap*-deficient animals are not absent, but severely reduced, leads to the assumption that PLVAP is not essential for fenestrae formation. However, PLVAP might be necessary to maintain size, shape, and distribution of fenestrae by anchoring the diaphragms in the rim of the pore, a theory that has been already presented in 1969 (Clementi and Palade, 1969c). Perfusion of rat intestinal capillaries with EDTA, a Ca-complexing agent, resulted in the loss of diaphragms and most importantly fenestrae showed enlarged diameters and were even replaced by wide discontinuities (Clementi and Palade, 1969c). These data are additionally supported by an *in vitro* knockdown of PLVAP by siRNA. This approach caused the loss of diaphragms in fenestrae and beyond that, induced fenestrae with disrupted morphology, enlarged diameters, and reduced fenestrae density (although not significantly) (Ioannidou et al., 2006).
Based on these conclusions and together with the results we obtained with regards to the expression of PLVAP in tissues devoid of structures with a diaphragm, it is reasonable to attribute PLVAP, besides being necessary for the formation of diaphragms, an additional role in maintenance of fenestrae.

Furthermore, in tissues with a substantial need for restricted permeability and high density of fenestrae, open fenestrae due to the loss of the diaphragm might increase the permeability to a level that is too high for normal function. Therefore, it might be reasonable for endothelial cells to counteract by dismantling fenestrae to reestablish barrier function. However, the

basal lamina supporting endothelial cells might act as an additional barrier preventing molecules from passing freely across the cells even when fenestrae are more permeable due to the loss of their diaphragm, a scenario which Clementi and Palade observed during perfusions with EDTA mixed with tracers for electron microscopy. The basement membrane was able to prevent the uncontrolled passage of molecules, despite being altered by EDTA (Clementi and Palade, 1969c).

5.5 PLVAP expression in liver sinusoidal endothelial cells

Despite the common point of view that PLVAP is not expressed in liver sinusoids, we obtained opposite results. As already mentioned, I could show that PLVAP is expressed in sinusoidal endothelial cells during embryonic development and beyond that also in adult liver tissue. That result substantiated the idea of a possible role of PLVAP either in sinusoidal fenestrae formation or maintenance or both.

5.6 The loss of PLVAP in sinusoidal endothelial cells is associated with a lack of fenestrations

Even though liver sinusoids are of the discontinuous type which do not contain diaphragms and lack a basement membrane, sinusoidal endothelial cells also showed a remarkable lack of fenestrae in our *Plvap*-deficient mice. Electron microscopy revealed a pronounced reduction of sinusoidal openings. These results are quite intriguing, supporting the idea that, in addition to being involved in the formation of fenestrae, PLVAP might hold further functions, such as maintenance and/or stabilization of those structures.

Therefore, we conclude that PLVAP is also critically required for fenestrations in sinusoidal endothelial cells of the liver.

The liver plays a major role in several physiological processes, including digestion, metabolism, glycogen storage, detoxification, immune response, and lipid metabolism. Endothelial cell openings in liver sinusoids are pivotal for the liver to accomplish its physiological functions, because they allow the exchange of molecules between the blood and hepatocytes and thus regulate the permeability of sinusoidal endothelial cells.

5.7 The lack of fenestrations leads to a decrease in the permeability of sinusoidal endothelial cells

It has been shown that the induction of fenestrae in sinusoidal endothelial cells increases permeability (Yokomori et al., 2003). In return, the reduction in the amount of fenestrations in *Plvap*$^{-/-}$ mice should influence permeability. Indeed, we were able to show that the reduction in the amount of fenestrations in *Plvap*$^{-/-}$ mice influences permeability negatively. We confirmed that the passage of molecules across sinusoidal endothelial cells is dramatically impaired.

Defenestration or capillarization of liver sinusoids has been associated with liver injury in several studies (Clark et al., 1988; Horn et al., 1987a; Straub et al., 2008; Van Beers et al., 2003; Xu et al., 2003). Hepatotoxins, such as ethanol, carbontetrachloride, dimethylnitrosamine, thioacetamine, and endotoxin, cause a defenestration of sinusoidal endothelial cells, followed by the formation of a basement membrane (Braet and Wisse, 2002; Xu et al., 2004). Furthermore, defenestration of sinusoidal endothelial cells has been linked to the early onset of liver cirrhosis prior accompanied by liver fibrosis (Martinez-Hernandez and Martinez, 1991; Van Beers et al., 2003). Interestingly, this process is thought to be reversible upon removal of the defenestration causing factors (hepatotoxins) but this is only possible before the formation of a basement membrane (Xu et al., 2004). Most likely, liver fibrosis is induced by hepatic stellate cells, fat storing cells which also comprise the majority of retinoids in the body of vertebrates (Blaner et al., 2009). The reduced permeability in defenestrated sinusoidal endothelial cells inhibits the uptake of retinol and thus disturbs retinol metabolism. This is thought to prompt hepatic stellate cells to produce excessive amounts of collagen, which leads to liver fibrosis followed by cirrhosis (Bataller and Brenner, 2005; Blaner et al., 2009; Mederacke et al., 2013; Moreira, 2007).

5.8 Lack of sinusoidal fenestrae in *Plvap*-deficient mice causes hyperlipoproteinemia and steatosis

In *Plvap*-deficient animals, the reduced permeability of the sinusoidal endothelium substantially impairs the passage of lipoproteins between the lumen of liver sinusoids and hepatocytes, a scenario which results in massive hyperlipoproteinemia. Obviously, chylomicron remnants are not able to pass across the sinusoidal endothelial cells due to the lack of open pores. Moreover, VLDL which are formed in the liver are very likely not capable

to leave the space of Disse and do not enter the sinusoidal lumen resulting in the reduction of plasma low density lipoproteins (LDL). VLDL particles do not accumulate in Disse's space of *Plvap*$^{-/-}$ mice, as they are very likely drained via hepatic lymphatics into the blood (Fraser et al., 1995b). In addition, *Plvap*-deficient animals display an excessive accumulation of lipids in their hepatocytes resulting in multivesicular steatosis (Figure 34). In humans, excessive accumulation of lipids in hepatocytes can be induced by alcohol abuse, which is in turn known to cause defenestration of liver sinusoids (Horn et al., 1987b). We attribute the multivesicular steatosis to the induced fatty acid synthesis in hepatocytes due to the inhibited import of essential lipids from circulation, which is in agreement with the decrease of glycogen in hepatocytes of *Plvap*$^{-/-}$ mice.

Based on our results, we conclude that in *Plvap*$^{-/-}$ mice, the lack of fenestrae due to the loss of PLVAP is responsible for both the massive accumulation of chylomicron remnants in the blood and the multivesicular steatosis in hepatocytes which correlates with a decrease in the amount of small plasma lipoproteins.

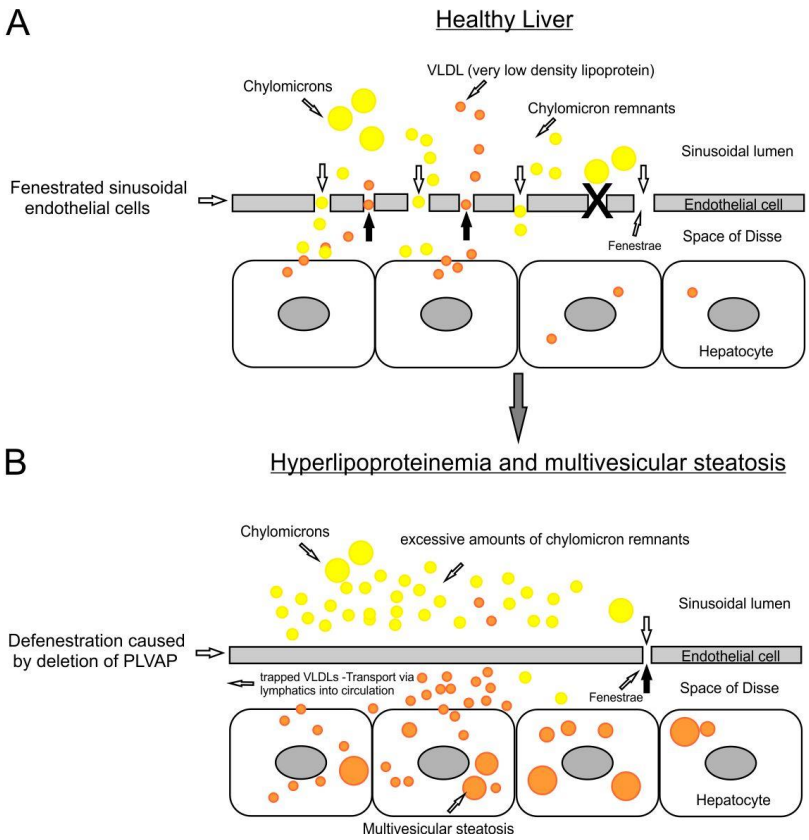

Figure 34: Predicted scenario of hyperlipoproteinemia in *Plvap*-deficient mice. **A** In healthy liver chylomicron remnants are capable of passing through fenestrae to enter the space of Disse, whereas Chylomicrons are excluded due to their size. In turn, VLDL can leave the space of Disse to enter circulation. **B** Sinusoidal endothelial cells in *Plvap*$^{-/-}$ mice lack fenestrae caused by the absence of PLVAP. As a consequence the passage of chylomicron remnants and VLDL is inhibited which results in excessive amounts of lipids in both hepatocytes and sinusoids. (Adapted from Le Couteur et al., 2002)

Furthermore, increased macrophage recruitment with foam cell formation was observed. Foam cells are lipid-laden macrophages/kupffer cells which are known to develop from the uptake of excessive lipids during hyperlipoproteinemia (Sano et al., 2004; Yoshimatsu et al., 2004)

Plvap$^{-/-}$ mice clearly display the typical signs of progressing liver damage including collagen deposition by activated hepatic stellate cells in the space of Disse, and the presence of focal fibrotic and necrotic areas. Moreover, *Plvap*-deficient animals show significantly reduced levels of total protein and albumin in blood plasma samples, a condition named hypoproteinemia which is associated with chronic liver diseases, such as cirrhosis (Blendea et al., 2010; Gatta et al., 2012; Rossing et al., 1988; Weigand, 1977). In addition, alanine transaminase (ALT) and aspartate transaminase (AST), both parameters for liver damage were found to be elevated in the plasma of some animals.

Stan and colleagues reported recently on the phenotype of *Plvap*-deficient mice that were bred in a genetic background (hybrid intercrosses containing a mix of Balb/c, C57Bl/6J and 129Sv/J) different from our animals (Stan et al., 2012). The authors observed similar plasma changes as reported here. Accordingly, *Plvap*$^{-/-}$ (Balb/c, C57Bl/6J, 129Sv/J) mice showed an increase in chylomicron remnants and cholesterol, and a decrease in LDL, HDL, total protein and albumin. The authors argued that the increase in chylomicron remnants might be a sequel to hypoproteinemia, which may cause depletion of endothelial LPL in animals. We regard this possibility as unlikely, as our data clearly show a specific increase in the amounts of chylomicron remnants, while the amounts of chylomicrons were unchanged or decreased in the plasma of *Plvap*$^{-/-}$ mice. We suggest that an analysis of the number of fenestrations and their permeability to macromolecules in the sinusoids of *Plvap*$^{-/-}$ (Balb/c, C57Bl/6J, 129Sv/J) mice might show similar changes as seen in our study.

6 Summary

Plasmalemma vesicle-associated protein (PLVAP), a cationic, endothelial-specific, integral membrane glycoprotein is exclusively localized to stomatal and fenestral diaphragms of caveolae, transendothelial channels and fenestrae. Fenestral and stomatal diaphragms are known to consist of radial fibrils which extend from the peripheral rim of the celllular pore and meet in a central mesh. They act as a permselective barrier, regulating permeability by allowing the passage of water and solutes but inhibiting the transfer of macromolecules across the endothelial barrier. It has been hypothesized that the radial fibrils of diaphragms are built by PLVAP dimers.
To learn about the molecular and biological functions of PLVAP, we generated mutant mice that are deficient in PLVAP and characterized their phenotype.

Depending on the respective genetic background, the deletion of *Plvap* caused either perinatal lethality associated with severe subcutaneous hemorrhages, edema, defects in vascular integrity, and cardiac malformations, or early postnatal death at around 4 weeks of age. Electron microscopy showed the complete absence of diaphragms in caveolae, transendothelial channels, and fenestrae in *Plvap*-deficient animals.
In addition, the lack of PLVAP caused a substantial reduction in the number of fenestrae in fenestrated vascular beds such as the choroid, the peritubular capillaries of the kidney interstitium, or the pancreas. The reduced number of fenestrae caused a restricted transendothelial passage of water and solutes, an effect which correlated with a retardation of postnatal growth.
Intriguingly, the deletion of PLVAP also caused lack of fenestrae in non-diaphragmed liver sinusoidal cells. Consequently, permeability and the passage of chylomicron remnants and other lipoproteins, such as HDL and LDL, was reduced between the lumen of liver sinusoids and the hepatocytes, a scenario that caused hyperlipoproteinemia and resulted in liver injury.

In conclusion, PLVAP was identified as an essential structural component of stomatal and fenestral diaphragms which are completely absent in endothelial cells of *Plvap*-deficient animals. Furthermore, PLVAP/diaphragms are required for the formation of fenestrations, since the loss of diaphragms due to the absence of PLVAP results in a dramatic reduction of fenestrations in both fenestrated and discontinuous vascular beds. This effect is accompanied by major physiological and metabolic changes such as in the liver where fenestrations in sinusoidal endothelial cells are critically required for the passage of lipoproteins.

7 Table of figures

8 List of tables

9 References

Aird, W.C., 2007a. Phenotypic heterogeneity of the endothelium: I. Structure, function, and mechanisms. Circ. Res. 100, 158–173. doi:10.1161/01.RES.0000255691.76142.4a

Aird, W.C., 2007b. Phenotypic heterogeneity of the endothelium: II. Representative vascular beds. Circ. Res. 100, 174–190. doi:10.1161/01.RES.0000255690.03436.ae

Anderson, H.A., Chen, Y., Norkin, L.C., 1996. Bound simian virus 40 translocates to caveolin-enriched membrane domains, and its entry is inhibited by drugs that selectively disrupt caveolae. Mol. Biol. Cell 7, 1825–1834.

Anderson, T.F., 1951. Techniques for the preservation of three-dimensional structure in preparing specimens for the electron microscope. N. Y. Acad. Sci. Trans. 13, 130–134.

Bankston, P.W., Milici, A.J., 1983. A survey of the binding of polycationic ferritin in several fenestrated capillary beds: indication of heterogeneity in the luminal glycocalyx of fenestral diaphragms. Microvasc. Res. 26, 36–48.

Bankston, P.W., Pino, R.M., 1980. The development of the sinusoids of fetal rat liver: morphology of endothelial cells, Kupffer cells, and the transmural migration of blood cells into the sinusoids. Am. J. Anat. 159, 1–15. doi:10.1002/aja.1001590102

Bankston, P.W., Porter, G.A., Milici, A.J., Palade, G.E., 1991. Differential and specific labeling of epithelial and vascular endothelial cells of the rat lung by Lycopersicon esculentum and Griffonia simplicifolia I lectins. Eur. J. Cell Biol. 54, 187–195.

Baribault, H., Penner, J., Iozzo, R.V., Wilson-Heiner, M., 1994. Colorectal hyperplasia and inflammation in keratin 8-deficient FVB/N mice. Genes Dev. 8, 2964–2973.

Baribault, H., Price, J., Miyai, K., Oshima, R.G., 1993. Mid-gestational lethality in mice lacking keratin 8. Genes Dev. 7, 1191–1202. doi:10.1101/gad.7.7a.1191

Bataller, R., Brenner, D.A., 2005. Liver fibrosis. J. Clin. Invest. 115, 209–218. doi:10.1172/JCI24282

Bauer, P.M., Yu, J., Chen, Y., Hickey, R., Bernatchez, P.N., Looft-Wilson, R., Huang, Y., Giordano, F., Stan, R.V., Sessa, W.C., 2005. Endothelial-specific expression of caveolin-1 impairs microvascular permeability and angiogenesis. Proc. Natl. Acad. Sci. U. S. A. 102, 204–209. doi:10.1073/pnas.0406092102

Bearer, E.L., Orci, L., 1985. Endothelial fenestral diaphragms: a quick-freeze, deep-etch study. J. Cell Biol. 100, 418–428.

Beckonert, O., Keun, H.C., Ebbels, T.M.D., Bundy, J., Holmes, E., Lindon, J.C., Nicholson, J.K., 2007. Metabolic profiling, metabolomic and metabonomic procedures for NMR spectroscopy of urine, plasma, serum and tissue extracts. Nat. Protoc. 2, 2692–2703. doi:10.1038/nprot.2007.376

Benninghoff, Drenckhahn, 2003. Anatomie-Makroskopische Anatomie, Histologie, Embryologie, Zellbiologie, 16. Auflage. ed. Urban&Fischer.

Bill, A., Mäepea, O., 1995. Mechanisms and routes of aqueous humor drainage. In: Albert, D.M., Jakobiec, F.A. (Eds.), Principles and Practice of Ophthalmology. WB Saunders Co., Philadelphia PP. 206–226.

Blaner, W.S., O'Byrne, S.M., Wongsiriroj, N., Kluwe, J., D'Ambrosio, D.M., Jiang, H., Schwabe, R.F., Hillman, E.M.C., Piantedosi, R., Libien, J., 2009. Hepatic stellate cell lipid droplets: a specialized lipid droplet for retinoid storage. Biochim. Biophys. Acta 1791, 467–473. doi:10.1016/j.bbalip.2008.11.001

Blendea, M.C., Thompson, M.J., Malkani, S., 2010. Diabetes and Chronic Liver Disease: Etiology and Pitfalls in Monitoring. Clin. Diabetes 28, 139–144. doi:10.2337/diaclin.28.4.139

Braet, F., De Zanger, R., Baekeland, M., Crabbé, E., Van Der Smissen, P., Wisse, E., 1995. Structure and dynamics of the fenestrae-associated cytoskeleton of rat liver sinusoidal endothelial cells. Hepatology 21, 180–189. doi:10.1002/hep.1840210130

Braet, F., De Zanger, R., Jans, D., Spector, I., Wisse, E., 1996. Microfilament-disrupting agent latrunculin A induces and increased number of fenestrae in rat liver sinusoidal endothelial cells: comparison with cytochalasin B. Hepatol. Baltim. Md 24, 627–635. doi:10.1053/jhep.1996.v24.pm0008781335

Braet, F., Spector, I., De Zanger, R., Wisse, E., 1998. A novel structure involved in the formation of liver endothelial cell fenestrae revealed by using the actin inhibitor misakinolide. Proc. Natl. Acad. Sci. U. S. A. 95, 13635–13640.

Braet, F., Wisse, E., 2002. Structural and functional aspects of liver sinusoidal endothelial cell fenestrae: a review. Comp. Hepatol. 1, 1. doi:10.1186/1476-5926-1-1

Brotherton, T.W., Chui, D.H., Gauldie, J., Patterson, M., 1979. Hemoglobin ontogeny during normal mouse fetal development. Proc. Natl. Acad. Sci. U. S. A. 76, 2853–2857.

Bruns, R.R., Palade, G.E., 1968. Studies on blood capillaries. II. Transport of ferritin molecules across the wall of muscle capillaries. J. Cell Biol. 37, 277–299.

Carley, W.W., Milici, A.J., Madri, J.A., 1988. Extracellular matrix specificity for the differentiation of capillary endothelial cells. Exp. Cell Res. 178, 426–434.

Carman, C.V., Springer, T.A., 2004. A transmigratory cup in leukocyte diapedesis both through individual vascular endothelial cells and between them. J. Cell Biol. 167, 377–388. doi:10.1083/jcb.200404129

Carpenter, B., Lin, Y., Stoll, S., Raffai, R.L., McCuskey, R., Wang, R., 2005. VEGF is crucial for the hepatic vascular development required for lipoprotein uptake. Dev. Camb. Engl. 132, 3293–3303. doi:10.1242/dev.01902

Chen, J., Braet, F., Brodsky, S., Weinstein, T., Romanov, V., Noiri, E., Goligorsky, M.S., 2002. VEGF-induced mobilization of caveolae and increase in permeability of endothelial cells. Am. J. Physiol. - Cell Physiol. 282, C1053–C1063. doi:10.1152/ajpcell.00292.2001

Chung, C., Iwakiri, Y., 2013. The lymphatic vascular system in liver diseases: its role in ascites formation. Clin. Mol. Hepatol. 19, 99–104. doi:10.3350/cmh.2013.19.2.99

Cines, D.B., Pollak, E.S., Buck, C.A., Loscalzo, J., Zimmerman, G.A., McEver, R.P., Pober, J.S., Wick, T.M., Konkle, B.A., Schwartz, B.S., Barnathan, E.S., McCrae, K.R., Hug, B.A., Schmidt, A.M., Stern, D.M., 1998. Endothelial cells in physiology and in the pathophysiology of vascular disorders. Blood 91, 3527–3561.

Clark, S., Bramwell Cook, H., Oxner, R.G., Angus, H., George, P., Fraser, R., 1988. DEFENESTRATION OF HEPATIC SINUSOIDS AS A CAUSE OF HYPERLIPOPROTEINAEMIA IN ALCOHOLICS. The Lancet 332, 1225–1227. doi:10.1016/S0140-6736(88)90813-6

Clark, T.G., Conway, S.J., Scott, I.C., Labosky, P.A., Winnier, G., Bundy, J., Hogan, B.L., Greenspan, D.S., 1999. The mammalian Tolloid-like 1 gene, Tll1, is necessary for normal septation and positioning of the heart. Dev. Camb. Engl. 126, 2631–2642.

Clementi, Palade, 1969a. Intestinal capillaries. I. Permeability to peroxidase and ferritin. J. Cell Biol. 41, 33–58.

Clementi, Palade, 1969b. INTESTINAL CAPILLARIES. J. Cell Biol. 42, 706–714.

Clementi, Palade, 1969c. INTESTINAL CAPILLARIES. J. Cell Biol. 42, 706–714.

Cohen, D., Fisher, E., 2013. Lipoprotein Metabolism, Dyslipidemia, and Nonalcoholic Fatty Liver Disease. Semin. Liver Dis. 33, 380–388. doi:10.1055/s-0033-1358519

DeLeve, L.D., 2007. Hepatic microvasculature in liver injury. Semin. Liver Dis. 27, 390–400. doi:10.1055/s-2007-991515

Doetschman, T., 2009. Influence of Genetic Background on Genetically Engineered Mouse Phenotypes. Methods Mol. Biol. Clifton NJ 530, 423–433. doi:10.1007/978-1-59745-471-1_23

Donnelly, K.L., Smith, C.I., Schwarzenberg, S.J., Jessurun, J., Boldt, M.D., Parks, E.J., 2005. Sources of fatty acids stored in liver and secreted via lipoproteins in patients with nonalcoholic fatty liver disease. J. Clin. Invest. 115, 1343–1351. doi:10.1172/JCI23621

Drab, M., Verkade, P., Elger, M., Kasper, M., Lohn, M., Lauterbach, B., Menne, J., Lindschau, C., Mende, F., Luft, F.C., Schedl, A., Haller, H., Kurzchalia, T.V., 2001. Loss of caveolae, vascular dysfunction, and pulmonary defects in caveolin-1 gene-disrupted mice. Science 293, 2449–2452. doi:10.1126/science.1062688

Dumont, D.J., Gradwohl, G., Fong, G.H., Puri, M.C., Gertsenstein, M., Auerbach, A., Breitman, M.L., 1994. Dominant-negative and targeted null mutations in the endothelial receptor tyrosine kinase, tek, reveal a critical role in vasculogenesis of the embryo. Genes Dev. 8, 1897–1909.

Dvorak, A.M., Feng, D., 2001. The Vesiculo–Vacuolar Organelle (VVO): A New Endothelial Cell Permeability Organelle. J. Histochem. Cytochem. 49, 419–431. doi:10.1177/002215540104900401

Ebner, K., 2009. Die Lokalisation des Membranproteins PV-1 in den Gefäßen des Auges (Dissertation). Universität Regensburg.

Engelhardt, B., Wolburg, H., 2004. Mini-review: Transendothelial migration of leukocytes: through the front door or around the side of the house? Eur. J. Immunol. 34, 2955–2963. doi:10.1002/eji.200425327

Engelman, J.A., Zhang, X., Galbiati, F., Volonte, D., Sotgia, F., Pestell, R.G., Minetti, C., Scherer, P.E., Okamoto, T., Lisanti, M.P., 1998. Molecular genetics of the caveolin gene family: implications for human cancers, diabetes, Alzheimer disease, and muscular dystrophy. Am. J. Hum. Genet. 63, 1578–1587.

Esser, S., Wolburg, K., Wolburg, H., Breier, G., Kurzchalia, T., Risau, W., 1998a. Vascular endothelial growth factor induces endothelial fenestrations in vitro. J. Cell Biol. 140, 947–959.

Esser, S., Wolburg, K., Wolburg, H., Breier, G., Kurzchalia, T., Risau, W., 1998b. Vascular endothelial growth factor induces endothelial fenestrations in vitro. J. Cell Biol. 140, 947–959.

Feng, D., Nagy, J.A., Dvorak, H.F., Dvorak, A.M., 2002. Ultrastructural studies define soluble macromolecular, particulate, and cellular transendothelial cell pathways in venules, lymphatic vessels, and tumor-associated microvessels in man and animals. Microsc. Res. Tech. 57, 289–326. doi:10.1002/jemt.10087

Fisher, E.A., Feig, J.E., Hewing, B., Hazen, S.L., Smith, J.D., 2012. High-density lipoprotein function, dysfunction, and reverse cholesterol transport. Arterioscler. Thromb. Vasc. Biol. 32, 2813–2820. doi:10.1161/ATVBAHA.112.300133

Fra, A.M., Williamson, E., Simons, K., Parton, R.G., 1995. De novo formation of caveolae in lymphocytes by expression of VIP21-caveolin. Proc. Natl. Acad. Sci. 92, 8655–8659.

Frank, P.G., 2010. Endothelial Caveolae and Caveolin-1 as Key Regulators of Atherosclerosis. Am. J. Pathol. 177, 544–546. doi:10.2353/ajpath.2010.100247

Frank, P.G., Woodman, S.E., Park, D.S., Lisanti, M.P., 2003a. Caveolin, Caveolae, and Endothelial Cell Function. Arterioscler. Thromb. Vasc. Biol. 23, 1161–1168. doi:10.1161/01.ATV.0000070546.16946.3A

Frank, P.G., Woodman, S.E., Park, D.S., Lisanti, M.P., 2003b. Caveolin, Caveolae, and Endothelial Cell Function. Arterioscler. Thromb. Vasc. Biol. 23, 1161–1168. doi:10.1161/01.ATV.0000070546.16946.3A

Fraser, R., Dobbs, B.R., Rogers, G.W., 1995a. Lipoproteins and the liver sieve: the role of the fenestrated sinusoidal endothelium in lipoprotein metabolism, atherosclerosis, and cirrhosis. Hepatol. Baltim. Md 21, 863–874.

Fraser, R., Dobbs, B.R., Rogers, G.W., 1995b. Lipoproteins and the liver sieve: the role of the fenestrated sinusoidal endothelium in lipoprotein metabolism, atherosclerosis, and cirrhosis. Hepatol. Baltim. Md 21, 863–874.

Freund, J., Kalbitzer, H.R., 1995. Physiological buffers for NMR spectroscopy. J. Biomol. NMR 5, 321–322. doi:10.1007/BF00211760

Friederici, 1968a. The tridimensional ultrastructure of fenestrated capillaries. J. Ultrastruct. Res. 23, 444–456.

Friederici, 1968b. The tridimensional ultrastructure of fenestrated capillaries. J. Ultrastruct. Res. 23, 444–456. doi:10.1016/S0022-5320(68)80109-1

Friederici, 1969. On the diaphragm across fenestrae of capillary endothelium. J. Ultrastruct. Res. 27, 373–375.

Furuya, S., 1990. Ultrastructure and formation of diaphragmed fenestrae in cultured endothelial cells of bovine adrenal medulla. Cell Tissue Res. 261, 97–105.

Gatmaitan, Z., Varticovski, L., Ling, L., Mikkelsen, R., Steffan, A.M., Arias, I.M., 1996. Studies on fenestral contraction in rat liver endothelial cells in culture. Am. J. Pathol. 148, 2027–2041.

Gatta, A., Verardo, A., Bolognesi, M., 2012. Hypoalbuminemia. Intern. Emerg. Med. 7 Suppl 3, S193–199. doi:10.1007/s11739-012-0802-0

Gerber, H.P., Hillan, K.J., Ryan, A.M., Kowalski, J., Keller, G.A., Rangell, L., Wright, B.D., Radtke, F., Aguet, M., Ferrara, N., 1999. VEGF is required for growth and survival in neonatal mice. Dev. Camb. Engl. 126, 1149–1159.

Ghitescu, L., Fixman, A., 1984. Surface charge distribution on the endothelial cell of liver sinusoids. J. Cell Biol. 99, 639–647.

Glenney, J.R., Jr, 1992. The sequence of human caveolin reveals identity with VIP21, a component of transport vesicles. FEBS Lett. 314, 45–48.

Gumbleton, M., Abulrob, A.G., Campbell, L., 2000. Caveolae: An Alternative Membrane Transport Compartment. Pharm. Res. 17, 1035–1048. doi:10.1023/A:1026464526074

Guo, J., Friedman, S.L., 2007. Hepatic fibrogenesis. Semin. Liver Dis. 27, 413–426. doi:10.1055/s-2007-991517

Hallmann, R., Mayer, D.N., Berg, E.L., Broermann, R., Butcher, E.C., 1995. Novel mouse endothelial cell surface marker is suppressed during differentiation of the blood brain barrier. Dev. Dyn. Off. Publ. Am. Assoc. Anat. 202, 325–332. doi:10.1002/aja.1002020402

Hehlgans, S., Cordes, N., 2011. Caveolin-1: an essential modulator of cancer cell radio-and chemoresistance. Am. J. Cancer Res. 1, 521–530.

Hellerbrand, C., 2013. Hepatic stellate cells--the pericytes in the liver. Pflüg. Arch. Eur. J. Physiol. 465, 775–778. doi:10.1007/s00424-012-1209-5

Herrnberger, L., Ebner, K., Junglas, B., Tamm, E.R., 2012a. The role of plasmalemma vesicle-associated protein (PLVAP) in endothelial cells of

Schlemm's canal and ocular capillaries. Exp. Eye Res. 105, 27–33. doi:10.1016/j.exer.2012.09.011

Herrnberger, L., Seitz, R., Kuespert, S., Bösl, M.R., Fuchshofer, R., Tamm, E.R., 2012b. Lack of endothelial diaphragms in fenestrae and caveolae of mutant Plvap-deficient mice. Histochem. Cell Biol. 138, 709–724. doi:10.1007/s00418-012-0987-3

Hnasko, R., Carter, J.M., Medina, F., Frank, P.G., Lisanti, M.P., 2006. PV-1 labels trans-cellular openings in mouse endothelial cells and is negatively regulated by VEGF. Cell Cycle Georget. Tex 5, 2021–2028.

Hofman, P., Blaauwgeers, H.G., Tolentino, M.J., Adamis, A.P., Nunes Cardozo, B.J., Vrensen, G.F., Schlingemann, R.O., 2000. VEGF-A induced hyperpermeability of blood-retinal barrier endothelium in vivo is predominantly associated with pinocytotic vesicular transport and not with formation of fenestrations. Vascular endothelial growth factor-A. Curr. Eye Res. 21, 637–645.

Horn, T., Christoffersen, P., Henriksen, J.H., 1987a. Alcoholic liver injury: defenestration in noncirrhotic livers--a scanning electron microscopic study. Hepatol. Baltim. Md 7, 77–82.

Horn, T., Christoffersen, P., Henriksen, J.H., 1987b. Alcoholic liver injury: defenestration in noncirrhotic livers--a scanning electron microscopic study. Hepatol. Baltim. Md 7, 77–82.

Huber, F., Kremer, W., Kalbitzer, H.R., 2005. Process for the Determination of Lipoproteins in Body Fluids. WO/2005/119285.

Ichimura, K., Stan, R.V., Kurihara, H., Sakai, T., 2008. Glomerular endothelial cells form diaphragms during development and pathologic conditions. J. Am. Soc. Nephrol. JASN 19, 1463–1471. doi:10.1681/ASN.2007101138

Inomata, H., Bill, A., Smelser, G.K., 1972. Aqueous humor pathways through the trabecular meshwork and into Schlemm's canal in the cynomolgus monkey (Macaca irus). An electron microscopic study. Am. J. Ophthalmol. 73, 760–789.

Ioannidou, S., Deinhardt, K., Miotla, J., Bradley, J., Cheung, E., Samuelsson, S., Ng, Y.-S., Shima, D.T., 2006. An in vitro assay reveals a role for the diaphragm protein PV-1 in endothelial fenestra morphogenesis. Proc. Natl. Acad. Sci. U. S. A. 103, 16770–16775. doi:10.1073/pnas.0603501103

Jenne, C.N., Kubes, P., 2013. Immune surveillance by the liver. Nat. Immunol. 14, 996–1006. doi:10.1038/ni.2691

Johnson, M., 2006. “What controls aqueous humour outflow resistance?” Exp. Eye Res. 82, 545–557. doi:10.1016/j.exer.2005.10.011

Jonas, A., Phillips, M., 2008. Lipoprotein structure In: Vance DE, Vance JE, eds. Biochemistry of lipids, lipoproteins and membranes. Amsterdam, The Netherlands: Elsevier, 485–506.

Kawano, Y., Cohen, D.E., 2013. Mechanisms of hepatic triglyceride accumulation in non-alcoholic fatty liver disease. J. Gastroenterol. 48, 434–441. doi:10.1007/s00535-013-0758-5

Keller, G., Lacaud, G., Robertson, S., 1999. Development of the hematopoietic system in the mouse. Exp. Hematol. 27, 777–787.

Keuschnigg, J., Henttinen, T., Auvinen, K., Karikoski, M., Salmi, M., Jalkanen, S., 2009. The prototype endothelial marker PAL-E is a leukocyte trafficking molecule. Blood 114, 478–484. doi:10.1182/blood-2008-11-188763

Kohn, S., Nagy, J.A., Dvorak, H.F., Dvorak, A.M., 1992. Pathways of macromolecular tracer transport across venules and small veins. Structural basis for the hyperpermeability of tumor blood vessels. Lab. Investig. J. Tech. Methods Pathol. 67, 596–607.

Komarova, Y., Malik, A.B., 2010. Regulation of endothelial permeability via paracellular and transcellular transport pathways. Annu. Rev. Physiol. 72, 463–493. doi:10.1146/annurev-physiol-021909-135833

Le Couteur, D.G., Fraser, R., Cogger, V.C., McLean, A.J., 2002. Hepatic pseudocapillarisation and atherosclerosis in ageing. The Lancet 359, 1612–1615. doi:10.1016/S0140-6736(02)08524-0

Lee, S., Choi, I., Hong, Y.-K., 2010. Heterogeneity and plasticity of lymphatic endothelial cells. Semin. Thromb. Hemost. 36, 352–361. doi:10.1055/s-0030-1253457

Levick, J.R., Smaje, L.H., 1987. An analysis of the permeability of a fenestra. Microvasc. Res. 33, 233–256.

Ley, K., Laudanna, C., Cybulsky, M.I., Nourshargh, S., 2007. Getting to the site of inflammation: the leukocyte adhesion cascade updated. Nat. Rev. Immunol. 7, 678–689. doi:10.1038/nri2156

Lisanti, M.P., Scherer, P.E., Tang, Z., Sargiacomo, M., 1994. Caveolae, caveolin and caveolin-rich membrane domains: a signalling hypothesis. Trends Cell Biol. 4, 231–235.

Liu, J., Wang, X.B., Park, D.S., Lisanti, M.P., 2002. Caveolin-1 Expression Enhances Endothelial Capillary Tubule Formation. J. Biol. Chem. 277, 10661–10668. doi:10.1074/jbc.M110354200

Lombardi, T., Montesano, R., Furie, M.B., Silverstein, S.C., Orci, L., 1986. Endothelial diaphragmed fenestrae: in vitro modulation by phorbol myristate acetate. J. Cell Biol. 102, 1965–1970.

Lombardi, T., Montesano, R., Furie, M.B., Silverstein, S.C., Orci, L., 1988. In vitro modulation of endothelial fenestrae: opposing effects of retinoic acid and transforming growth factor beta. J. Cell Sci. 91 (Pt 2), 313–318.

Maniatis, N.A., Brovkovych, V., Allen, S.E., John, T.A., Shajahan, A.N., Tiruppathi, C., Vogel, S.M., Skidgel, R.A., Malik, A.B., Minshall, R.D., 2006. Novel mechanism of endothelial nitric oxide synthase activation mediated by caveolae internalization in endothelial cells. Circ. Res. 99, 870–877. doi:10.1161/01.RES.0000245187.08026.47

Mansbach, C.M., Siddiqi, S.A., 2010. The biogenesis of chylomicrons. Annu. Rev. Physiol. 72, 315–333. doi:10.1146/annurev-physiol-021909-135801

Martinez-Hernandez, A., Martinez, J., 1991. The role of capillarization in hepatic failure: studies in carbon tetrachloride-induced cirrhosis. Hepatol. Baltim. Md 14, 864–874.

McCuskey, R.S., 2008. The hepatic microvascular system in health and its response to toxicants. Anat. Rec. Hoboken NJ 2007 291, 661–671. doi:10.1002/ar.20663

McGuire, R.F., Bissell, D.M., Boyles, J., Roll, F.J., 1992. Role of extracellular matrix in regulating fenestrations of sinusoidal endothelial cells isolated from normal rat liver. Hepatol. Baltim. Md 15, 989–997.

Mederacke, I., Hsu, C.C., Troeger, J.S., Huebener, P., Mu, X., Dapito, D.H., Pradere, J.-P., Schwabe, R.F., 2013. Fate tracing reveals hepatic stellate cells as dominant contributors to liver fibrosis independent of its aetiology. Nat. Commun. 4. doi:10.1038/ncomms3823

Mehta, D., Malik, A.B., 2006. Signaling mechanisms regulating endothelial permeability. Physiol. Rev. 86, 279–367. doi:10.1152/physrev.00012.2005

Milici, A.J., L'Hernault, N., Palade, G.E., 1985. Surface densities of diaphragmed fenestrae and transendothelial channels in different murine capillary beds. Circ. Res. 56, 709–717.

Millán, J., Hewlett, L., Glyn, M., Toomre, D., Clark, P., Ridley, A.J., 2006. Lymphocyte transcellular migration occurs through recruitment of endothelial ICAM-1 to caveola- and F-actin-rich domains. Nat. Cell Biol. 8, 113–123. doi:10.1038/ncb1356

Minshall, R.D., Tiruppathi, C., Vogel, S.M., Malik, A.B., 2002. Vesicle formation and trafficking in endothelial cells and regulation of endothelial barrier function. Histochem. Cell Biol. 117, 105–112. doi:10.1007/s00418-001-0367-x

Montagutelli, X., 2000. Effect of the Genetic Background on the Phenotype of Mouse Mutations. J. Am. Soc. Nephrol. 11, S101–S105.

Montesano, R., Roth, J., Robert, A., Orci, L., 1982. Non-coated membrane invaginations are involved in binding and internalization of cholera and tetanus toxins. Nature 296, 651–653. doi:10.1038/296651a0

Moreira, R.K., 2007. Hepatic stellate cells and liver fibrosis. Arch. Pathol. Lab. Med. 131, 1728–1734. doi:10.1043/1543-2165(2007)131[1728:HSCALF]2.0.CO;2

Muller, W.A., 2011. Mechanisms of Leukocyte Transendothelial Migration. Annu. Rev. Pathol. 6, 323–344. doi:10.1146/annurev-pathol-011110-130224

Naito, M., Wisse, D.E., 1978. Filtration effect of endothelial fenestrations on chylomicron transport in neonatal rat liver sinusoids. Cell Tissue Res. 190, 371–382. doi:10.1007/BF00219553

Nasser, M.W., Datta, J., Nuovo, G., Kutay, H., Motiwala, T., Majumder, S., Wang, B., Suster, S., Jacob, S.T., Ghoshal, K., 2008. Down-regulation of micro-RNA-1 (miR-1) in lung cancer. Suppression of tumorigenic property of lung cancer cells and their sensitization to doxorubicin-induced apoptosis by miR-1. J. Biol. Chem. 283, 33394–33405. doi:10.1074/jbc.M804788200

Navarro, A., Anand-Apte, B., Parat, M.-O., 2004. A role for caveolae in cell migration. FASEB J. Off. Publ. Fed. Am. Soc. Exp. Biol. 18, 1801–1811. doi:10.1096/fj.04-2516rev

Niemelä, H., Elima, K., Henttinen, T., Irjala, H., Salmi, M., Jalkanen, S., 2005. Molecular identification of PAL-E, a widely used endothelial-cell marker. Blood 106, 3405–3409. doi:10.1182/blood-2005-01-0254

Palade, G., Simionescu, M., Simionescu, N., 1981. Differentiated microdomains on the luminal surface of the capillary endothelium. Biorheology 18, 563–568.

Patan, S., 1998. TIE1 and TIE2 receptor tyrosine kinases inversely regulate embryonic angiogenesis by the mechanism of intussusceptive microvascular growth. Microvasc. Res. 56, 1–21. doi:10.1006/mvre.1998.2081

Pavlides, S., Gutierrez-Pajares, J.L., Danilo, C., Lisanti, M.P., Frank, P.G., 2012. Atherosclerosis, caveolae and caveolin-1. Adv. Exp. Med. Biol. 729, 127–144. doi:10.1007/978-1-4614-1222-9_9

Pelkmans, L., Helenius, A., 2002. Endocytosis via caveolae. Traffic Cph. Den. 3, 311–320.

Pelta, M.D., Morris, G.A., Stchedroff, M.J., Hammond, S.J., 2002. A one-shot sequence for high-resolution diffusion-ordered spectroscopy. Magn. Reson. Chem. 40, S147–S152. doi:10.1002/mrc.1107

Peng, X., Wu, X., Druso, J.E., Wei, H., Park, A.Y.-J., Kraus, M.S., Alcaraz, A., Chen, J., Chien, S., Cerione, R.A., Guan, J.-L., 2008. Cardiac developmental defects and eccentric right ventricular hypertrophy in cardiomyocyte focal adhesion kinase (FAK) conditional knockout mice. Proc. Natl. Acad. Sci. U. S. A. 105, 6638–6643. doi:10.1073/pnas.0802319105

Petersen, A.-K., Stark, K., Musameh, M.D., Nelson, C.P., Römisch-Margl, W., Kremer, W., Raffler, J., Krug, S., Skurk, T., Rist, M.J., Daniel, H., Hauner, H., Adamski, J., Tomaszewski, M., Döring, A., Peters, A., Wichmann, H.-E., Kaess, B.M., Kalbitzer, H.R., Huber, F., Pfahlert, V., Samani, N.J., Kronenberg, F., Dieplinger, H., Illig, T., Hengstenberg, C., Suhre, K., Gieger, C., Kastenmüller, G., 2012. Genetic associations with lipoprotein subfractions provide information on their biological nature. Hum. Mol. Genet. 21, 1433–1443. doi:10.1093/hmg/ddr580

Predescu, S.A., Predescu, D.N., Palade, G.E., 1997. Plasmalemmal vesicles function as transcytotic carriers for small proteins in the continuous endothelium. Am. J. Physiol. 272, H937–949.

Puri, M.C., Rossant, J., Alitalo, K., Bernstein, A., Partanen, J., 1995. The receptor tyrosine kinase TIE is required for integrity and survival of vascular endothelial cells. EMBO J. 14, 5884–5891.

Ranger, A.M., Grusby, M.J., Hodge, M.R., Gravallese, E.M., de la Brousse, F.C., Hoey, T., Mickanin, C., Baldwin, H.S., Glimcher, L.H., 1998. The transcription factor NF-ATc is essential for cardiac valve formation. Nature 392, 186–190. doi:10.1038/32426

Razani, B., Engelman, J.A., Wang, X.B., Schubert, W., Zhang, X.L., Marks, C.B., Macaluso, F., Russell, R.G., Li, M., Pestell, R.G., Di Vizio, D., Hou, H., Jr, Kneitz, B., Lagaud, G., Christ, G.J., Edelmann, W., Lisanti, M.P., 2001. Caveolin-1 null mice are viable but show evidence of hyperproliferative and vascular abnormalities. J. Biol. Chem. 276, 38121–38138. doi:10.1074/jbc.M105408200

Reeves, W.H., Kanwar, Y.S., Farquhar, M.G., 1980. Assembly of the glomerular filtration surface. Differentiation of anionic sites in glomerular capillaries of newborn rat kidney. J. Cell Biol. 85, 735–753.

Renkin, E.M., 1977. Multiple pathways of capillary permeability. Circ. Res. 41, 735–743.

Richardson, K.C., Jarett, L., Finke, E.H., 2009. Embedding in Epoxy Resins for Ultrathin Sectioning in Electron Microscopy [WWW Document]. URL http://informahealthcare.com/doi/abs/10.3109/10520296009114754 (accessed 9.6.13).

Roberts, W.G., Palade, G.E., 1995. Increased microvascular permeability and endothelial fenestration induced by vascular endothelial growth factor. J. Cell Sci. 108 (Pt 6), 2369–2379.

Roberts, W.G., Palade, G.E., 2000. Endothelial fenestrae and fenestral diaphragms. Rissau W Rubanyi GM Eds Morphog. Endothel. Hardwood Acad. Publ. Amst. pp.23–41.

Rossing, T.H., Boixeda, D., Maffeo, N., Fencl, V., 1988. Hyperventilation with hypoproteinemia. J. Lab. Clin. Med. 112, 553–559.

Rothberg, K.G., Heuser, J.E., Donzell, W.C., Ying, Y.S., Glenney, J.R., Anderson, R.G., 1992. Caveolin, a protein component of caveolae membrane coats. Cell 68, 673–682.

Sano, J., Shirakura, S., Oda, S., Hara, T., Ishihara, T., 2004. Foam cells generated by a combination of hyperglycemia and hyperlipemia in rats. Pathol. Int. 54, 904–913. doi:10.1111/j.1440-1827.2004.01778.x

Sarin, H., 2010. Physiologic upper limits of pore size of different blood capillary types and another perspective on the dual pore theory of microvascular permeability. J. Angiogenesis Res. 2, 14. doi:10.1186/2040-2384-2-14

Sato, T.N., Tozawa, Y., Deutsch, U., Wolburg-Buchholz, K., Fujiwara, Y., Gendron-Maguire, M., Gridley, T., Wolburg, H., Risau, W., Qin, Y., 1995. Distinct roles of the receptor tyrosine kinases Tie-1 and Tie-2 in blood vessel formation. Nature 376, 70–74. doi:10.1038/376070a0

Schaffner, F., Poper, H., 1963. Capillarization of hepatic sinusoids in man. Gastroenterology 184, 239–242. doi:10.1001/jama.1963.03700140159106

Scherer, P.E., Lisanti, M.P., Baldini, G., Sargiacomo, M., Mastick, C.C., Lodish, H.F., 1994. Induction of caveolin during adipogenesis and association of GLUT4 with caveolin-rich vesicles. J. Cell Biol. 127, 1233–1243.

Scherer, P.E., Okamoto, T., Chun, M., Nishimoto, I., Lodish, H.F., Lisanti, M.P., 1996. Identification, sequence, and expression of caveolin-2 defines a caveolin gene family. Proc. Natl. Acad. Sci. 93, 131–135.

Schubert, W., Frank, P.G., Razani, B., Park, D.S., Chow, C.-W., Lisanti, M.P., 2001. Caveolae-deficient Endothelial Cells Show Defects in the Uptake and Transport of Albumin in Vivo. J. Biol. Chem. 276, 48619–48622. doi:10.1074/jbc.C100613200

Schuppan, D., Kim, Y.O., 2013. Evolving therapies for liver fibrosis. J. Clin. Invest. 123, 1887–1901. doi:10.1172/JCI66028

Senetta, R., Stella, G., Pozzi, E., Sturli, N., Massi, D., Cassoni, P., 2013. Caveolin-1 as a promoter of tumour spreading: when, how, where and why. J. Cell. Mol. Med. 17, 325–336. doi:10.1111/jcmm.12030

Shearer, G.C., Kaysen, G.A., 2006. Endothelial bound lipoprotein lipase (LpL) depletion in hypoalbuminemia results from decreased endothelial binding, not decreased secretion. Kidney Int. 70, 647–653. doi:10.1038/sj.ki.5000318

Shin, J.S., Gao, Z., Abraham, S.N., 2000. Involvement of cellular caveolae in bacterial entry into mast cells. Science 289, 785–788.

Simionescu, M., Palade, G., Simionescu, N., Silbert, J., 1981a. Differentiated microdomains on the luminal surface of the capillary endothelium. Biorheology 18, 563–8.

Simionescu, M., Simionescu, N., Palade, G., 1981b. Differentiated microdomains on the luminal surface of the capillary endothelium. I. Preferential distribution of anionic sites. J. Cell Biol. 90, 605–613.

Simionescu, M., Simionescu, N., Palade, G.E., 1974. MORPHOMETRIC DATA ON THE ENDOTHELIUM OF BLOOD CAPILLARIES. J. Cell Biol. 60, 128–152.

Simionescu, M., Simionescu, N., Palade, G.E., 1982. Preferential distribution of anionic sites on the basement membrane and the abluminal aspect of the endothelium in fenestrated capillaries. J. Cell Biol. 95, 425–434.

Simionescu, M., Simionescu, N., Palade, G.E., 1984. Partial chemical characterization of the anionic sites in the basal lamina of fenestrated capillaries. Microvasc. Res. 28, 352–367.

Simionescu, M., Simionescu, N., Silbert, J., Palade, G., 1981c. Differentiated microdomains on the luminal surface of the capillary endothelium. II. Partial characterization of their anionic sites. J. Cell Biol. 90, 614–621.

Simionescu, N., Siminoescu, M., Palade, G.E., 1975. Permeability of muscle capillaries to small heme-peptides. Evidence for the existence of patent transendothelial channels. J. Cell Biol. 64, 586–607.

Skarnes, W.C., Rosen, B., West, A.P., Koutsourakis, M., Bushell, W., Iyer, V., Mujica, A.O., Thomas, M., Harrow, J., Cox, T., Jackson, D., Severin, J., Biggs, P., Fu, J., Nefedov, M., de Jong, P.J., Stewart, A.F., Bradley, A., 2011. A conditional knockout resource for the genome-wide study of mouse gene function. Nature 474, 337–342. doi:10.1038/nature10163

Sonveaux, P., Martinive, P., DeWever, J., Batova, Z., Daneau, G., Pelat, M., Ghisdal, P., Grégoire, V., Dessy, C., Balligand, J.-L., Feron, O., 2004. Caveolin-1 expression is critical for vascular endothelial growth factor-induced ischemic hindlimb collateralization and nitric oxide-mediated angiogenesis. Circ. Res. 95, 154–161. doi:10.1161/01.RES.0000136344.27825.72

Sörensson, J., Fierlbeck, W., Heider, T., Schwarz, K., Park, D.S., Mundel, P., Lisanti, M., Ballermann, B.J., 2002. Glomerular endothelial fenestrae in vivo are not formed from caveolae. J. Am. Soc. Nephrol. JASN 13, 2639–2647.

Stan, R.V., 2000. Channels across Endothelial Cells [WWW Document]. URL http://www.ncbi.nlm.nih.gov/books/NBK6260/ (accessed 1.21.14).

Stan, R.V., 2005. Structure of caveolae. Biochim. Biophys. Acta 1746, 334–348. doi:10.1016/j.bbamcr.2005.08.008

Stan, R.V., 2007. Endothelial stomatal and fenestral diaphragms in normal vessels and angiogenesis. J. Cell. Mol. Med. 11, 621–643. doi:10.1111/j.1582-4934.2007.00075.x

Stan, R.V., Ghitescu, L., Jacobson, B.S., Palade, G.E., 1999a. Isolation, cloning, and localization of rat PV-1, a novel endothelial caveolar protein. J. Cell Biol. 145, 1189–1198.

Stan, R.V., Kubitza, M., Palade, G.E., 1999b. PV-1 is a component of the fenestral and stomatal diaphragms in fenestrated endothelia. Proc. Natl. Acad. Sci. U. S. A. 96, 13203–13207.

Stan, R.V., Roberts, W.G., Predescu, D., Ihida, K., Saucan, L., Ghitescu, L., Palade, G.E., 1997. Immunoisolation and partial characterization of endothelial plasmalemmal vesicles (caveolae). Mol. Biol. Cell 8, 595–605.

Stan, R.V., Tkachenko, E., Niesman, I.R., 2004. PV1 Is a Key Structural Component for the Formation of the Stomatal and Fenestral Diaphragms. Mol. Biol. Cell 15, 3615–3630. doi:10.1091/mbc.E03-08-0593

Stan, R.V., Tse, D., Deharvengt, S.J., Smits, N.C., Xu, Y., Luciano, M.R., McGarry, C.L., Buitendijk, M., Nemani, K.V., Elgueta, R., Kobayashi, T., Shipman, S.L., Moodie, K.L., Daghlian, C.P., Ernst, P.A., Lee, H.-K., Suriawinata, A.A., Schned, A.R., Longnecker, D.S., Fiering, S.N., Noelle, R.J., Gimi, B., Shworak, N.W., Carrière, C., 2012. The diaphragms of fenestrated endothelia: gatekeepers of vascular permeability and blood composition. Dev. Cell 23, 1203–1218. doi:10.1016/j.devcel.2012.11.003

Steffan, A.M., Gendrault, J.L., Kirn, A., 1987. Increase in the number of fenestrae in mouse endothelial liver cells by altering the cytoskeleton with cytochalasin B. Hepatol. Baltim. Md 7, 1230–1238.

Straub, A.C., Clark, K.A., Ross, M.A., Chandra, A.G., Li, S., Gao, X., Pagano, P.J., Stolz, D.B., Barchowsky, A., 2008. Arsenic-stimulated liver sinusoidal capillarization in mice requires NADPH oxidase–generated superoxide. J. Clin. Invest. 118, 3980–3989. doi:10.1172/JCI35092

Sumpio, B.E., Riley, J.T., Dardik, A., 2002. Cells in focus: endothelial cell. Int. J. Biochem. Cell Biol. 34, 1508–1512.

Svistounov, D., Warren, A., McNerney, G.P., Owen, D.M., Zencak, D., Zykova, S.N., Crane, H., Huser, T., Quinn, R.J., Smedsrød, B., Le Couteur, D.G., Cogger, V.C., 2012. The Relationship between Fenestrations, Sieve Plates and Rafts in Liver Sinusoidal Endothelial Cells. PLoS ONE 7, e46134. doi:10.1371/journal.pone.0046134

Tamm, E.R., 2009a. The trabecular meshwork outflow pathways: structural and functional aspects. Exp. Eye Res. 88, 648–655. doi:10.1016/j.exer.2009.02.007

Tamm, E.R., 2009b. The trabecular meshwork outflow pathways: structural and functional aspects. Exp. Eye Res. 88, 648–655. doi:10.1016/j.exer.2009.02.007

Tamm, E.R., 2010. The Role of the Ciliary Body in Aqueous Humor Dynamics Structural Aspects, in: Darlene A. Dartt (Ed.), Encyclopedia of the Eye. Academic Press, Oxford, pp. 179–186.

Tamm, E.R., Lütjen-Drecoll, E., 1996. Ciliary body. Microsc. Res. Tech. 33, 390–439. doi:10.1002/(SICI)1097-0029(19960401)33:5<390::AID-JEMT2>3.0.CO;2-S

Tang, Z., Scherer, P.E., Okamoto, T., Song, K., Chu, C., Kohtz, D.S., Nishimoto, I., Lodish, H.F., Lisanti, M.P., 1996. Molecular Cloning of Caveolin-3, a Novel Member of the Caveolin Gene Family Expressed Predominantly in Muscle. J. Biol. Chem. 271, 2255–2261. doi:10.1074/jbc.271.4.2255

Tkachenko, E., Tse, D., Sideleva, O., Deharvengt, S.J., Luciano, M.R., Xu, Y., McGarry, C.L., Chidlow, J., Pilch, P.F., Sessa, W.C., Toomre, D.K., Stan, R.V., 2012. Caveolae, fenestrae and transendothelial channels retain PV1 on the surface of endothelial cells. PloS One 7, e32655. doi:10.1371/journal.pone.0032655

Tse, D., Stan, R.V., 2010. Morphological heterogeneity of endothelium. Semin. Thromb. Hemost. 36, 236–245. doi:10.1055/s-0030-1253447

Tuma, P.L., Hubbard, A.L., 2003. Transcytosis: Crossing Cellular Barriers. Physiol. Rev. 83, 871–932. doi:10.1152/physrev.00001.2003

Van Beers, B.E., Materne, R., Annet, L., Hermoye, L., Sempoux, C., Peeters, F., Smith, A.M., Jamart, J., Horsmans, Y., 2003. Capillarization of the sinusoids in liver fibrosis: noninvasive assessment with contrast-enhanced MRI in the rabbit. Magn. Reson. Med. Off. J. Soc. Magn. Reson. Med. Soc. Magn. Reson. Med. 49, 692–699. doi:10.1002/mrm.10420

Vasile, E., Hong, Q., Dvorak, H.F., Dvorak, A.M., 1999. Caveolae and Vesiculo-Vacuolar Organelles in Bovine Capillary Endothelial Cells Cultured with VPF/VEGF on Floating Matrigel-collagen Gels. J. Histochem. Cytochem. 47, 159–167. doi:10.1177/002215549904700205

Verma, S., Buchanan, M.R., Anderson, T.J., 2003. Endothelial Function Testing as a Biomarker of Vascular Disease. Circulation 108, 2054–2059. doi:10.1161/01.CIR.0000089191.72957.ED

Vogel, U., Sandvig, K., Deurs, B. van, 1998. Expression of caveolin-1 and polarized formation of invaginated caveolae in Caco-2 and MDCK II cells. J. Cell Sci. 111, 825–832.

Warren, A., Cogger, V.C., Arias, I.M., McCuskey, R.S., Le Couteur, D.G., 2010. Liver sinusoidal endothelial fenestrations in caveolin-1 knockout mice. Microcirc. N. Y. N 1994 17, 32–38. doi:10.1111/j.1549-8719.2009.00004.x

Weigand, K., 1977. [The regulation of serum albumin in physiological and pathological conditions (author's transl)]. Klin. Wochenschr. 55, 295–305.

Willnow, T.E., 1997. Mechanisms of hepatic chylomicron remnant clearance. Diabet. Med. J. Br. Diabet. Assoc. 14 Suppl 3, S75–80. doi:10.1002/(SICI)1096-9136(199708)14:3+<S75::AID-DIA449>3.0.CO;2-9

Willnow, T.E., Armstrong, S.A., Hammer, R.E., Herz, J., 1995. Functional expression of low density lipoprotein receptor-related protein is controlled by receptor-associated protein in vivo. Proc. Natl. Acad. Sci. U. S. A. 92, 4537–4541.

Wisse, E., Braet, F., Luo, D., Zanger, R.D., Jans, D., Crabbe, E., Vermoesen, A.N., 1996. Structure and Function of Sinusoidal Lining Cells in the Liver. Toxicol. Pathol. 24, 100–111. doi:10.1177/019262339602400114

Wisse, E., de Zanger, R.B., Charels, K., van der Smissen, P., McCuskey, R.S., 1985. The liver sieve: Considerations concerning the structure and function of endothelial fenestrae, the sinusoidal wall and the space of disse. Hepatology 5, 683–692. doi:10.1002/hep.1840050427

Wisse, E., Jacobs, F., Topal, B., Frederik, P., De Geest, B., 2008. The size of endothelial fenestrae in human liver sinusoids: implications for hepatocyte-directed gene transfer. Gene Ther. 15, 1193–1199. doi:10.1038/gt.2008.60

Wu, G., Markowitz, G.S., Li, L., D'Agati, V.D., Factor, S.M., Geng, L., Tibara, S., Tuchman, J., Cai, Y., Park, J.H., van Adelsberg, J., Hou, H., Jr, Kucherlapati, R., Edelmann, W., Somlo, S., 2000. Cardiac defects and renal failure in mice with targeted mutations in Pkd2. Nat. Genet. 24, 75–78. doi:10.1038/71724

Xu, B., Broome, U., Uzunel, M., Nava, S., Ge, X., Kumagai-Braesch, M., Hultenby, K., Christensson, B., Ericzon, B.-G., Holgersson, J., Sumitran-Holgersson, S., 2003. Capillarization of hepatic sinusoid by liver endothelial cell-reactive autoantibodies in patients with cirrhosis and chronic hepatitis. Am. J. Pathol. 163, 1275–1289. doi:10.1016/S0002-9440(10)63487-6

Xu, G.-F., Wang, X.-Y., Ge, G.-L., Li, P.-T., Jia, X., Tian, D.-L., Jiang, L.-D., Yang, J.-X., 2004. Dynamic changes of capillarization and peri-sinusoid fibrosis in alcoholic liver diseases. World J. Gastroenterol. WJG 10, 238–243.

Yokomori, H., Oda, M., Yoshimura, K., Nagai, T., Ogi, M., Nomura, M., Ishii, H., 2003. Vascular endothelial growth factor increases fenestral permeability in hepatic sinusoidal endothelial cells. Liver Int. Off. J. Int. Assoc. Study Liver 23, 467–475.

Yoshiki, A., Moriwaki, K., 2006. Mouse Phenome Research: Implications of Genetic Background. ILAR J. 47, 94–102. doi:10.1093/ilar.47.2.94

Yoshimatsu, M., Terasaki, Y., Sakashita, N., Kiyota, E., Sato, H., van der Laan, L.J.W., Takeya, M., 2004. Induction of macrophage scavenger receptor MARCO in nonalcoholic steatohepatitis indicates possible involvement of endotoxin in its pathogenic process. Int. J. Exp. Pathol. 85, 335–343. doi:10.1111/j.0959-9673.2004.00401.x

Zhao, Y.-Y., Liu, Y., Stan, R.-V., Fan, L., Gu, Y., Dalton, N., Chu, P.-H., Peterson, K., Ross, J., Jr, Chien, K.R., 2002. Defects in caveolin-1 cause dilated cardiomyopathy and pulmonary hypertension in knockout mice. Proc. Natl. Acad. Sci. U. S. A. 99, 11375–11380. doi:10.1073/pnas.172360799

10 Abbreviations

ALT	Alanine transaminase
AP	Aqueous plexus
AST	Aspartate transaminase
α-SMA	α-smooth muscle-actin
B-pore	Border pore
bp	Base pair
CB	Ciliary body
cDNA	Complementary deoxyribonucleic acid
Ch	Choroid
Chylo	Chylomicron
CM	Ciliary muscle
DAPI	4',6-diamino-2-phenylindol
DNA	Deoxribonucleic acid
dNTP	Deoyribonucleotide
E.	Embryonal day
ECM	Extracellular matrix
EGTA	Ethylene glycol tetraacetic acid
ES	Embryonic stem cells
FITC-dextran	Fluorescein isothiocyanate-dextran
GAPDH	Glycerinaldehyde-3-phosphate dehydrogenase
GNB2L	Guanine nucleotide binding protein, beta polypeptide 2-like
GV	Giant vacuole
He	Hepatocyte
He	Heart
HRP	horseredish peroxidase
HUVEC	Human umbilical vein endothelial cells
H&E	Hematoxylin and Eosin
I-pore	intracellular pore
ICP-MS	Inductively coupled plasma mass spectrometry
In	Intestine
Is	Islet
HSC	hepatic stellate cell
HDL	High density lipoprotein
LDL	Low density lipoprotein

LDLR	Low density lipoprotein receptor
LRP	Low density lipoprotein receptor-related protein
LPL	Lipoprotein lipase
Lu	Lumen
Lu	Lung
MECA-32	Mouse panendothelial cell antigen-32
mRNA	Messenger ribonucleic acid
OCT	Optimal cooling temperature
P.	Postnatal day
Page	Polyacrylamide gel electrophoresis
PAS	Periodic acid schiff
PBS	Phosphate buffered saline
PCR	Polymerase chain reaction
PFA	Paraformaldehyde
PLVAP	Plasmalemma vesicle-associated protein
PPD	P-phenylendiamine
PT	proximal tubulus
Re	Retina
RNA	Ribonucleic acid
RPE	Retinal pigment epithelium
RT-PCR	Real-time reverse transcription PCR
Sc	Sclera
Sc	Spinal chord
SC	Schlemm's canal
SD	Standard deviation
SD	Stomatal diaphragm
SDS	Sodium dodecyl sulfate
SEM	Scanning electron microscopy
Sk	Skin
Ss	Scleral spur
St	Sternum
TBS	Tris buffered saline
TEM	Transmission electron microscopy
TM	Trabecular meshwork
Tr	Thrombocyte
VEGF	Vascular endothelial growth factor
VLDL	Very low density lipoprotein

11 Acknowledgements-Danksagung

Zu allererst möchte ich mich bei Prof. Dr. Ernst Tamm bedanken, der es mir ermöglichte meine Arbeit an seinem Lehrstuhl durchzuführen. Danke für die tolle Unterstützung, für die Bereitschaft mich und mein Projekt auch in unerwartete Richtungen gehen zu lassen, für die unzähligen Stunden, die du für mich und meine Korrekturen investiert hat (trotz Urlaub mit der Familie) und für die Auslandsaufenthalte und Kongresse, an denen ich teilnehmen durfte.

Frau Prof. Dr. Charlotte Wagner möchte ich herzlich für die Übernahme des Zweitgutachtens danken.

Herrn Prof. Dr. Achim Göpferich für die Kooperation und die Bereitschaft mich in meinem Kolloquium zu prüfen.

Mein zusätzlicher Dank gilt allen Personen, die meine Arbeit durch Kooperationen oder auch einfach nur durch Hilfsbereitschaft unterstützt haben, wie zum Beispiel, Robert Hennig, Achim Göpferich, Werner Kremer, Hans Robert Kalbitzer, Claus Hellerbrand, Ruth Schewior, Roswitha Seitz und Sabrina Küspert.

Angelika, Elke, Silvia und Eva, euch danke ich für eure Unterstützung im Laboralltag und für eure Geduld. Ohne euch würde im Labor nichts funktionieren!
Besonders möchte ich mich bei dir, liebe Margit, bedanken. Danke für die endlosen Stunden, die du mit mir am EM verbracht hast und für deine Geduld hinsichtlich meiner Sprunghaftigkeit und meiner vielen Richtungswechsel...Auge...Herz...Niere...nein doch wieder Auge...oder doch Leber?.... jetzt bräuchte ich doch wieder EM vom Herz...oder so ähnlich...Vielen Dank!

Den Doktoranden, den medizinischen Doktoranden, den Masterstudenten und den Postdocs möchte ich für das tolle Klima, die tolle Zusammenarbeit, die Freundschaft und das Zusammensein auch außerhalb der Arbeit danken. Besonders erwähnen möchte ich Rosi und Susi für die schönen Mädchenabende, Patrick für den gemeinsamen Weg durch das Studium und die Doktorarbeit und für die Freundschaft, Rudi für die sportlichen Aktivitäten (Joggen rocks!) und die Betreuung im Kurs. Aber auch allen anderen möchte ich natürlich danken! Ihr seid eine tolle Gruppe und ein außergewöhnlicher Lehrstuhl!

Ganz besonders will ich mich bei meinem Freund Chris bedanken, der mir in stressigen Phasen immer den Rücken freihält, mich erträgt, sich immer geduldig meine Sorgen und meinen Ärger anhört und einfach immer für mich da ist. Ich danke Dir!

Und zu guter Letzt danke ich natürlich meiner Familie. Ohne euch wäre diese Arbeit und mein ganzer bisheriger Weg nicht möglich gewesen. Ich danke euch für euer Vertrauen und für eure Zuversicht, dafür dass ihr mich niemals unter Druck gesetzt habt, mich immer habt machen lassen und immer für mich da gewesen seid! Ihr seid die besten Eltern und die beste Familie, die man sich nur wünschen kann!